THE UNIVERSITY *of* EDINBURGH

Statistical Mechanics of non-Markovian Exclusion Processes

Robert Concannon

Doctor of Philosophy
The University of Edinburgh
2013

Lay summary

A common and fruitful approach in physics is to simplify a problem down by keeping only the aspects of it which are expected to be important. These "minimal models" are usually significantly easier to solve, and they allow us to see which components of the full problem are required to reproduce the behaviour seen. Once we understand the minimal model, we can progressively make the model fit reality better using what we know as a baseline.

The Asymmetric Exclusion Process is a very important model in statistical mechanics because of its range of well understood properties. It is a minimal model of traffic flow that has been used to study a range of real systems, including protein transcription from mRNA, intracellular motors, and why buses all come at once. A concrete example of the exclusion process is a circle of lily pads, which can have a maximum of one frog on them at a time. The frogs can jump to next lily pad around the circle provided there is not already a frog occupying it, and do so with a certain probability every second. The vast majority of the exclusion processes that have been studied require that the probability of hopping does not change with time. In this thesis we extend what has gone before by allowing the probability that the hop will happen to be dependent on how long the frog has been stationary.

We run into a few challenges if frogs are allowed to choose extremely large times between hops, even if these "falling asleep" events are very unlikely. Firstly, we cannot use the usual analytical techniques for investigating the exclusion process because of the time dependence of the hop probability, so we simulate it and attempt to explain the behaviour seen from first principles. In the simulations we find traffic jams whereby all frogs in the circle are stuck behind one frog which has fallen asleep. We show that the traffic jams become more important as the circle size and number of frogs increases, however the simulations where the traffic jams are dominant require very large amounts of time to run. We create a short-cut in the simulations and use this to see that traffic jams only ever partially break up, and that the next jam forms from the remnants of the previous one. We can understand this interaction of traffic jams mathematically, and we use that understanding to predict what happens when the number of lily pads becomes very large.

Using our exclusion process as the baseline, we work out what happens when we allow frogs to hop in both directions around the circle. We find that unless frogs are equally likely to go forwards as backwards, there will be traffic jams behind sleeping frogs nearly all the time. We also use it to investigate a couple of other related physical systems which have previously been restricted to a single particle (frog). We find that if frogs only start choosing hop times once the target lily pad is empty we have a situation where traffic jams completely break apart once the sleeping frog wakes up, and the traffic jams are only present for a finite fraction of the time.

Abstract

The Totally Asymmetric Simple Exclusion Process (TASEP) is often considered one of the fundamental models of non-equilibrium statistical mechanics, due to its well understood steady state and the fact that it can exhibit condensation, phase separation and phase transitions in one spatial dimension. As a minimal model of traffic flow it has enjoyed many applications, including the transcription of proteins by ribosomal motors moving along an mRNA track, the transport of cargo between cells and more human-scale traffic flow problems such as the dynamics of bus routes. It consists of a one-dimensional lattice of sites filled with a number of particles constrained to move in a particular direction, which move to adjacent sites probabilistically and interact by mutual exclusion. The study of non-Markovian interacting particle systems is in its infancy, due in part to a lack of a framework for addressing them analytically. In this thesis we extend the TASEP to allow the rate of transition between sites to depend on how long the particle in question has been stationary by using non-Poissonian waiting time distributions. We discover that if the waiting time distribution has infinite variance, a dynamic condensation effect occurs whereby every particle on the system comes to rest in a single traffic jam. As the lattice size increases, so do the characteristic condensate lifetimes and the probability that a condensate will interact with the preceding one by forming out of its remnants. This implies that the thermodynamic limit depends on the dynamics of such spatially complete condensates.

As the characteristic condensate lifetimes increase, the standard continuous time Monte Carlo simulation method results in an increasingly large fraction of failed moves. This is computationally costly and led to a limit on the sizes of lattice we could simulate. We integrate out the failed moves to create a rejection-free algorithm which allows us to see the interacting condensates more clearly. We find that if condensates do not fully dissolve, the condensate lifetime ages and saturates to a particular value. An unforeseen consequence of this new technique, is that it also allowed us to gain a mathematical understanding of the ageing of condensates, and its dependence on system size. Using this we can see that the fraction of time spent in the spatially complete condensate tends to one in the thermodynamic limit.

A random walker in a random force field has to escape potential wells of random depth, which gives rise to a power law waiting time distribution. We use the non-Markovian TASEP to investigate this model with a number of interacting particles. We find that if the potential well is re-sampled after every failed move, then this system is equivalent to the non-Markovian TASEP. If the potential well is only re-sampled after a successful move, then we restore particle-hole symmetry, allow condensates to completely dissolve, and the thermodynamic limit spends a finite fraction of time in the spatially complete state. We then generalised the non-Markovian TASEP to allow for particles to move in both directions. We find that the full condensation effect remains robust except for the case of perfect symmetry.

Declaration

I declare that this thesis was composed by myself, that the work contained herein is my own except where explicitly stated otherwise in the text, and that this work has not been submitted for any other degree or professional qualification except as specified.

(*Robert Concannon, September 2013*)

Acknowledgements

This thesis, and the work it represents, would not have been possible without the guidance, assistance and support of many people.

Firstly I wish to thank my primary supervisor, Richard Blythe, for regular meetings full of humour, good advice and constructive criticism, and his unflinching belief that the light at end of the tunnel was not a train. My thanks also go out to my second supervisor, Martin Evans, who was always ready to field odd questions, the postgraduate secretary Jane Patterson for being persistently lovely, and to Donald Grigor of the physics computing support team for not shouting at me. I also need to thank EPCC for the use of their facilities, and EPSRC for providing my funding.

Sometimes the best teachers are your peers, and I am fortunate to have shared a department with a large number of very friendly and clever people. My time in Edinburgh would have been quite bereft without their conversation, camaraderie and cake. Special thanks go to Kym Eden who has helped immensely with everything to do with my simulations, and for being an intelligent sounding-board, who never sounded bored, for the rest.

I am grateful to my non-physicist friends for their company, especially my erstwhile flatmate, Gemma, for being a delight to live with. Last, but by no means least, my family and my other half, Trisha, have my undying thanks for their continual love, support and help in all things. I could not have been here without them.

Contents

List of Figures

Chapter 1

Introduction

A system is a collection of interacting entities forming a complex whole, and the study of systems of interacting physical entities has long been the domain of the sciences. Classical and quantum mechanics allows us to make predictions of the future state of a system given the knowledge of its initial state [83]. For a small number of degrees of freedom, such as a system with few particles in it, this is fine. With an increasing number of degrees of freedom, both classical and quantum mechanics become more analytically intractable and it becomes harder for us to find precise data on the initial state. Statistical mechanics allows us to make predictions of the expected average quantities of a system given incomplete knowledge of its initial state and/or its environment, and as such has much applicability when considering real world problems. The central idea of statistical mechanics is to follow the behaviour of a large collection of systems similar to the one we are considering, called an ensemble. More precicely an ensemble is the collection of all possible histories of the system in question. With the knowledge of the average behaviour of systems in our ensemble, we can predict what is expected to happen to a particular system [72].

A lot of interesting systems, indeed all living systems, are not in equilibrium, as they irreversibly exchange particles, heat or volume with their environment [13], or have transition rates between sites that do not satisfy detailed balance (see chapter 2). Non-equilibrium statistical mechanics is concerned with the dynamics of such systems and approaches them as stochastic processes, which is to say the system evolves in time by moving randomly between states. Probability theory is the mathematics that underpins the study of stochastic processes and does not require that the systems in question are physical ones composed of particles,

merely that there are entities, be they cars, investors, bacteria, genetic material etc., that obey rules probabilistically. Stochastic processes with many interacting agents can exhibit highly interesting collective behaviour such as traffic jams, stock market crashes and population extinction [64], that are emergent properties of the underlying dynamics [6]. This range of applicability has led to statistical mechanics being extensively studied and applied to problems in the real world.

A straightforward way to create a non-equilibrium interacting particle system is to induce a current through it. This could be achieved by attaching it to reservoirs of particles at different chemical potentials for instance [73]. These are known as driven diffusive systems and unlike their equilibrium counterparts, they can exhibit non-trivial dynamics, such as phase separation and phase transitions even in one dimension [33]. One of the reasons we are interested in driven diffusive systems is the existence of condensation. Condensation is an emergent phenomenon whereby a macroscopic fraction of the particles occupy a microscopic region of phase space. This could imply a particular configuration of adjacent particles with mutual exclusion, or particles without mutual exclusion being at the same location. Bose-Einstein condensation is one of the most famous examples of condensation in real systems, and occurs where a macroscopically large number of non-interacting bosons enter the ground state [5]. Condensation also appears in the "rich-get-richer" idea in economics, which leads to the accumulation of a large amount of wealth by a small number of individuals [17], [10]. Condensation in driven diffusive systems often means an interruption of the proper flow, which makes them qualitatively interesting and easy to identify. They have been used extensively, for example, as models of traffic jams [32] [63][53], gelation on networks [28] and aggregation of particles in shaken granular gasses [85].

A standard way to approach non-equilibrium statistical mechanics is to assume that the immediate future of the system is entirely dependent on its current state, and not its history. This is known as the Markov assumption, and all systems which can be described by a Poisson process obey it. Poisson processes are abundant in nature as any system that can be described by characteristic rates fits in this category, for example, radioactive decay and the arrival of calls to a switchboard [37]. The Markov property allows us to simplify the equations for the evolution of the probability distributions of the system down to the master equation. In some cases the master equation is analytically solvable for the steady states [13].

In cases where a process is Markovian but very complicated, we can integrate

out degrees of freedom to make the system easier to analyse. Non-Markovian processes have history dependence, which means we cannot write down the master equation. We must find a way to characterise the behaviour of each model without the machinery that helps with the already analytically tricky Markovian problems. Few non-Markovian models have yielded many analytic results and those were single particle systems, even examples which seem as simple as the random acceleration process, discussed below, require much work.

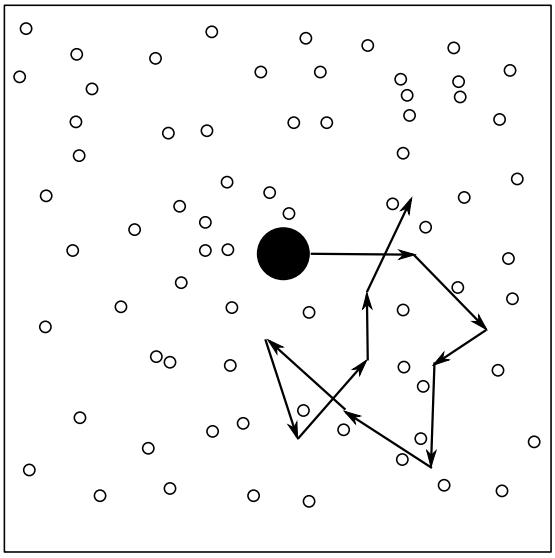

Figure 1.1 *A cartoon of Brownian motion of a tracer particle in a bath of particles. Track of the tracer particle illustrated with arrows.*

We will look at two examples of the potential pitfalls involved in integrating out degrees of freedom. Firstly we investigate Brownian motion, which is cartooned in figure 1.1. In a bath of interacting particles, Brownian motion is the seemingly random movement of a particular tracer particle. The effect was first observed by Robert Brown, when tracking the motion of pollen grains in water. Albert Einstein showed that the seemingly random motion was due to other particles in the bath colliding with the tracer [22]. Since Newton's laws require the instantaneous position and velocity of every particle, modelling systems directly is both Markovian, and becomes exceptionally computationally difficult when we have many particles. We could simplify the problem by integrating out the interactions of all the particles of the bath, with each other, the environment and the tracer. In order to properly account for correlations in space and time that are built up by repeatedly colliding with nearby particles, we would need to keep track of which particles the tracer collided with, and when. This implies that we have broken the Markovian property. A sufficient stochastic description

of the tracer ignores correlations in time by simply replacing all interactions with a random velocity. Written mathematically this is $\dot{x} = \eta$, where x is the particle's position and η is a random variable. We use a Gaussian white noise for the random variable η as it is uncorrelated in time, and with no bias in any particular direction. If we were to simulate this in discrete time we would update the particle's position by using the following update rule: $x_i = x_{i-1} + \Delta\eta$ where Δ is the timestep and i is the index of the next time increment. To find the next particle location we need only its current location, which satisfies the Markov assumption. This model results in the observed wandering tracer path, and so is known as the random walk.

Our second example of the perils of integrating out degrees of freedom is the random acceleration model. We can write this as $\ddot{x} = \eta$ (see [59] and references therein). In the random acceleration model, particles have a current position and velocity. The discrete time update rule for this is

$$\begin{pmatrix} x_i \\ v_i \end{pmatrix} = \begin{pmatrix} x_{i-1} + \Delta v_{i-1} \\ v_{i-1} + \Delta\eta \end{pmatrix}$$

which contains only the current state, and is therefore Markovian. If, however, we were to integrate out the degree of freedom associated with the velocity, particles would only have one state variable, the current position. The discrete time update rule would then be $x_i = 2x_{i-1} - x_{i-2} + \Delta^2\eta$ using $v_i = v_{i-1} + \Delta\eta$ and $v_i = \frac{x_i - x_{i-1}}{\Delta}$. This requires more knowledge of the particles trajectory, and is therefore non-Markovian.

In this thesis we will investigate the Totally Asymmetric Simple Exclusion Process, or *TASEP*, which is a conceptually simple traffic flow model. It is also considered one of the paradigmatic models of interacting particles in non-equilibrium statistical mechanics. It consists of a one dimensional lattice of sites which can either be occupied by a single particle, or empty. Particles may only move if the space in front of them is empty, and they are constrained to move in one direction. The TASEP on a ring is cartooned in figure 1.2. The steady state of the TASEP is well understood and there have been many generalisations and extensions which allow it to more closely the imitate real traffic flow. Interestingly for us, the standard Markovian TASEP on a ring does not exhibit condensation, whereas we will see that our non-Markovian TASEP does.

Due to the analytical difficulties of non-Markovian processes, only two papers exist, to our knowledge, that address the effects of the TASEP ceasing to be

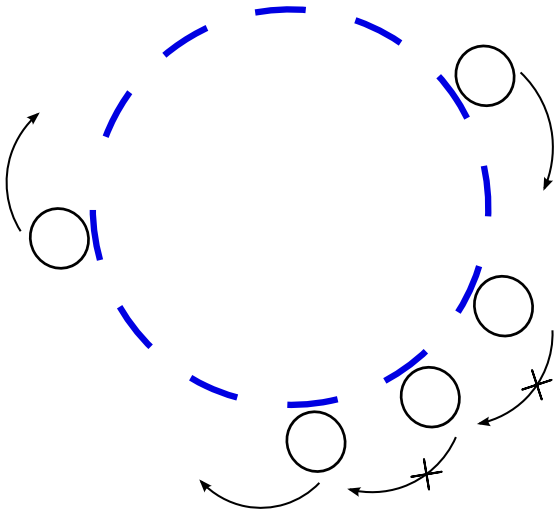

Figure 1.2 *A cartoon of the TASEP with periodic boundary conditions. Particles: circles, allowed moves: arrows, prohibited moves: arrows with crosses through them.*

Markovian. The first paper [46] found an interesting condensation effect in the Zero Range Process (ZRP), which is a related model to the TASEP. We note that making the ZRP non-Markovian increased the critical density above which condensation is observed. The second [42] found no qualitative difference to the basic Markovian TASEP when the the waiting time distribution was not an exponential decay but had an exponentially decaying tail, i.e. the process was non-Poissonian. In this thesis we will show that although an exponentially tailed waiting time distribution does not qualitatively affect the non-Markovian TASEP, we can induce condensation by using a different class of waiting time distribution. We will show how to understand the formation and behaviour of condensates both qualitatively and quantitatively. We will demonstrate that condensates persist as the size of the system becomes large, and how this effects the behaviour of the system in the thermodynamic limit. We will also investigate how strongly the observed condensation depends on the specific details of the model, in particular, the complete asymmetry. Finally we will apply our understanding of this model to related physical systems.

1.1 Thesis outline

In chapter 2 I provide an overview of the relevant results and applications of the Markovian TASEP, and examine the two papers [46] and [42] that address the non-Markovian TASEP.

A non-Markovian TASEP with a single particle is an example of a semi-Markov process and the sequence of move events is a renewal process. In chapter 3 I investigate the mathematics of semi-Markov and renewal processes to see how relevant they will be, and whether any of the techniques used to solve them could be useful to the study of the non-Markovian TASEP. A recurring theme in both processes is the sum of a number of random variables, which I find easiest to access by convolution theorem. Chapter 5 also requires convolution theorem, so the remainder of chapter 3 is spent discussing Laplace transforms and their application to the sum of random variables.

In chapter 4 we use a continuous time Monte Carlo method to simulate the non-Markovian TASEP with a power law waiting time distribution of the form $p_1(t) = (\gamma - 1)t^{-\gamma}\Theta[t-1]$, where $\Theta[t-1]$ is the Heaviside Theta function ensuring $t \geq 1$. For the range $2 < \gamma < 3$, we observe a condensation effect whereby every particle on the lattice is blocked by a single particle. We attempt to understand the behaviour of the condensate, and therefore the system, in the thermodynamic limit, and show that a simple minded model predicts the wrong behaviour.

In chapter 5 we attempt to compute the probability that a particle will move at time W given that it is blocked for a time T, which we call the blocked waiting time distribution $p(W;T)$. We use this to construct a rejection-free algorithm for the non-Markovian TASEP, which we compare with the standard Monte Carlo method in a number of ways, in order to ensure that their results are compatible.

In chapter 6 we return to the non-Markovian TASEP using the rejection-free algorithm and $p(W;T)$ to understand how consecutive condensates interact. We claim that this is the key to understanding how the non-Markovian TASEP behaves in the thermodynamic limit.

In the final results chapter, chapter 7, we use a multi-particle version of the trap model to investigate a few different physical mechanisms which are related to the non-Markovian TASEP, to see if they also exhibit our understood condensation effect. We will also relax the asymmetry constraint, which restricts particles to move in one direction, to investigate the robustness of condensation to different levels of asymmetry.

Chapter 2

Interacting particle systems

Statistical mechanics concerns itself with the net behaviour of large collections of agents, which can commonly be modelled as stochastic systems of interacting particles. A straightforward way to create a non-equilibrium interacting particle system is to induce a current of particles through it [73], and as discussed in chapter 1, we are interested in the condensation effects which they exhibit.

2.1 Markov processes

There exist a number of analytical methods for investigating the behaviour of a stochastic process. It will therefore be useful to recap some of the basic definitions and results concerning their dynamics.

At any instant the state of a system can be specified by a set of numbers, in thermodynamics for instance, these could be the macroscopic state variables, pressure, temperature and volume. Microscopically, these would be the locations and speeds of all the particles in the system.

A process is one in which the state of the system evolves with time. In a stochastic process, a system makes transitions randomly between the states. In principle the probability of transition between any pair of states could be dependent on a number of things, including the particular current state occupied, the target state, how long the system has been in the current state, and the previous states occupied. A way of simplifying this very general description to allow analytical equations is to make the Markovian assumption [49]. If the

probability of transition between two states is independent of any previous states it occupied and the time elapsed since it last transitioned, then it satisfies the Markov assumption. This is a very strong condition, but it is so useful that it has become the standard assumption made when investigating stochastic processes. It is also a common assumption because there are a large number of systems that can usefully be characterised by a process that is only dependent on its current state, and not its history, for instance random walkers, queuing systems [36], and population dynamics [45].

The Markov assumption allows us to write down the Master equation. $p(i,t)$ is the probability that the system is in state i at time t,

$$\frac{\partial p(i,t)}{\partial t} = \sum_j w_{ji} p(j,t) - \sum_j w_{ij} p(i,t) \tag{2.1}$$

which can be written

$$\frac{\partial \underline{P}(t)}{\partial t} = \boldsymbol{M}\underline{P}(t)$$

where $\underline{P}(t)$ is the state vector, $\boldsymbol{M}$ is the Markov matrix and w_{ji} is the transition rate from state j to state i. The steady state is when $\frac{\mathrm{d}p(i,t)}{\mathrm{d}t} = 0$, and one condition for this is detailed balance, $w_{ji}p(j,t) = w_{ij}p(i,t)$, i.e. the probability flux out of a particular state is the same as that into it. Detailed balance always leads to a steady state, but the converse is not necessarily true.

2.2 The Asymmetric Simple Exclusion Process (ASEP)

One of the paradigmatic models of driven diffusive systems is the Asymmetric Simple Exclusion Process (ASEP). It is important because a lot of traffic flow models can be cartooned as a number of indistinguishable particles whose positions are mutually exclusive. The ASEP appeared in mathematics literature in 1965 as a model of diffusion with collisions between particles [13] and has enjoyed a long career investigating topics such as biopolymerisation [57], traffic flow [58] and biomotors [43]. The ASEP consists of N hopping particles on a discrete one dimensional lattice of size L, see Figure 2.1, where the density $\rho = \frac{N}{L} < 1$. The particles interact by mutual exclusion, and therefore each site can either be occupied, or unoccupied. In this case the state of the system could

be described by the configuration $\mathcal{C} = \{\tau_1, \tau_2, ..., \tau_L\}$ where τ_i is one if the site is occupied, zero if it is not, and is known as the occupation number of site i. We will relax the Markovian assumption later in this thesis, but for now we will discuss the Markovian ASEP. Here the particles are biased to hop in one direction with rate p and in the other with rate q where $p > q$. If the rate q is set to zero, then the particles are restricted to move in one direction only. This simplification is called the Totally Asymmetric Simple Exclusion Process, or *TASEP*.

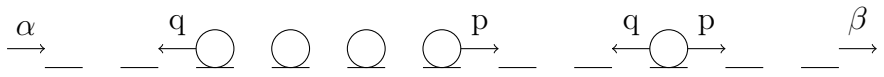

Figure 2.1 *A cartoon of the ASEP with open boundary. conditions*

If the system has periodic boundaries, when a particle moves off the end of the lattice it reappears on the other end. This can more colloquially referred to as an ASEP on a ring, as the lattice can be thought of as a chain of sites around the circumference of a circle. The ASEP with periodic boundary conditions has steady states that are analytically solvable by looking at the terms in the Master equation [13]. The steady state is when $\frac{\partial p(i,t)}{\partial t} = 0$. We note that only configurations which are one move away from the particular configuration i have $w_{ji} \neq 0$, so we can restrict j to these configurations. We further split j to configurations, d, which can move to i by a particle moving downstream (i.e. to the right) with rate $w_{ji} = q$ and configurations, u, where a particle moves upstream (i.e. to the left) with rate $w_{ji} = p$.

$$0 = \sum_{j,\mathrm{u}} pp(j,t) - \sum_{j,\mathrm{u}} pp(i,t) + \sum_{j,\mathrm{d}} qp(j,t) - \sum_{j,\mathrm{d}} qp(i,t)$$

Collecting like terms in p, q we can see that the steady state can be realised when

$$\sum_{j,\mathrm{u}} p(j,t) = \sum_{j,\mathrm{u}} p(i,t)$$

This is a more general condition than detailed balance, known as dynamic reversibility [54]. It is satisfied when $p(j,t) = p(i,t)$ for all j, and because i was an arbitrary choice this holds for all i, so all configurations are equally likely. This allows the steady state flux of particles past a point to be derived. A similar argument can be made to show that the probability that a particular site is occupied is also constant, and therefore equal to ρ. Particles are indistinguishable, as are holes, so there are $\binom{L}{N}$ ways of arranging them, where $\binom{L}{N} = \frac{L!}{(L-N)!N!}$ is the binomial coefficient. This implies that the probability of any particular state

is $\frac{1}{\binom{L}{N}}$.

We can derive the radial distribution function, or position correlation function, $g(r)$, from fact that all configurations are equally likely, where $g(r)$ is the probability that there is a particle occupying site r, given that there is a particle occupying site zero. Since the probability that a particular site is occupied is constant, $g(r)$ will be a step function

$$g(r) = \begin{cases} 1 & \text{for } r < 1 \\ \frac{N-1}{L-1} & \text{for } r \geq 1 \end{cases} \tag{2.2}$$

Consider by contrast the case of a lattice containing a condensate composed of every particle on the lattice, which we refer to as a spatially complete condensate. We can see intuitively that there should be a radial distribution function which is not flat, as there is a larger probability of finding particles adjacent to each-other. We can compute the form of $g(r)$ easily for a periodic system. A particle is chosen at random, and it defines the zero position. Since the lattice is periodic, there will be some particles at the left hand end of the lattice and, unless the leftmost particle was chosen, there will also be particles at the right hand end of the lattice, as cartooned in figure 2.2. The probability $g(r)$ can be split into

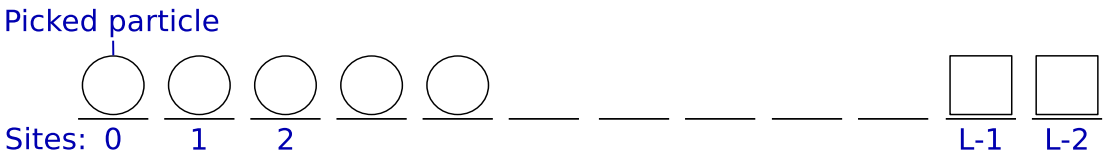

Figure 2.2 *A periodic lattice with a spatially complete condensate. Particles downstream of the chosen particle represented as circles, upstream particles represented as squares.*

two contributions; the probability that a particle occupies position r given that it is downstream of the zero particle, and the probability that it occupies r given that it is upstream. Since the lattice is discrete, positions will be referred to with a subscript. Taking the downstream particles first we see that $g_{0,\text{downstream}} = 1$ as the chosen particle defines the zero position. Site 1 will be filled unless the picked particle was the rightmost particle in the condensate, which happens with probability $\frac{1}{N}$. Similarly site 2 will be occupied unless either of the two rightmost

particles was picked.

$$\begin{aligned} g_{0,\text{downstream}} &= 1 \\ g_{1,\text{downstream}} &= 1 - \frac{1}{N} \\ g_{2,\text{downstream}} &= 1 - \frac{2}{N} \\ g_{i\leq N-1,\text{downstream}} &= 1 - \frac{i}{N} \\ g_{i,\text{downstream}} &= \frac{N-i}{N}\Theta[N-i] \end{aligned}$$

where that the probability $g_{i,\text{downstream}}$ is ensured to be positive by the Heaviside Theta function $\Theta[x]$ which is defined as

$$\Theta[x] \equiv \begin{cases} 0 & \text{for } x < 0 \\ 1 & \text{for } x \geq 0 \end{cases}$$

Taking $i \to L - i$ gives $g_{i,\text{upstream}}$ because of the symmetry of the problem.

$$g_{i,\text{upstream}} = \frac{N-L+i}{N}\Theta[N-L+i]$$

g_r is the probability that there is a particle at site r given that there is one at zero, regardless of whether that particle is upstream or downstream, so

$$\begin{aligned} g_i &= g_{i,\text{downstream}} + g_{i,\text{upstream}} \\ &= \frac{N-i}{N}\Theta[N-i] + \frac{N-L+i}{N}\Theta[N-L+i] \end{aligned} \tag{2.3}$$

We can see that the presence of condensates in the system can be distinguished by the shape of the radial distribution function $g(r)$. The flatness of $g(r)$ implies that we expect a lack of condensates in the system if all configurations are equally likely. Conversely, if we see condensates on the system, this is a good indicator that we cannot safely assume that all states are equally likely.

Using the fact that all configurations are equally likely in the steady state of the TASEP with periodic boundaries we can compute the flux of particle around the system, J [24]. Since $g(r)$ is flat, the occupation probability for a particular site is ρ, and is independent of its neighbours. A particle can only move from a site if that site is occupied and its downstream neighbour is unoccupied. The probability that this will be the case is $\rho(1-\rho)$. The average rate at which

particles move over a site is the rate at which particles leave a site multiplied by the probability that the particle can move.

$$J = p\rho(1-\rho) \tag{2.4}$$

For low densities, increasing the density will increase the flux and for higher densities increasing density reduces the flux, as the flow is restricted by the number of available places to move into. This change occurs continuously and we see no phase transition. The symmetric shape is also indicative of particle hole symmetry.

Mean field theory is a method of simplifying calculations by ignoring correlations between sites $\langle p(i)p(i+1)\rangle = \langle p(i)\rangle\langle p(i+1)\rangle$. This implies that the mutual exclusion condition can be taken into account by the product of the probabilities that the site in question is occupied and the target site is unoccupied, rather than the joint probability, which can be very useful when solving the TASEP analytically. Mean field theory allows the probability of a particular configuration in the stationary state to be written in a factorised form, which facilitates its solution [13]. The mean field assumption can be relaxed somewhat by keeping more correlations, such as the two point correlation functions, but it is still a mean field theory as correlations are being ignored at some level. It should be noted that this would not be a safe assumption to make if there were condensation effects seen in the system, as this would lead to a probability of particles being adjacent to each other which would be greater than that predicted by the probability that any individual site is occupied, as discussed previously.

A common aim is to obtain certain properties of the system, such as the flux, which become independent of the number of particles in the system, as N tends to infinity. This is known as the thermodynamic limit. The variable of interest in the flux is the density ρ, which can be kept constant for $N \to \infty$ if $L \to \infty$ such that $\rho = \frac{N}{L}$; which is the thermodynamic limit for the ASEP. As pointed out in [56], the thermodynamic limit is important as there is often a differing of timescales between microscopic and macroscopic dynamics. This leads to microscopic models which "can be rather crude, [or] even blatantly wrong" and still exhibit the correct macroscopic behaviour.

The relaxation of the system to the steady state is a shorter timescale effect that can be investigated using the Bethe ansatz. The Markov matrix which describes the TASEP on a ring can be mapped to a non-Hermitian Hamiltonian,

and the Bethe ansatz assists in finding their eigenvalues and eigenvectors. This gives the result that the density has a relaxation time of order $L^{\frac{3}{2}}$ and the current a relaxation time of order L^1 [61].

2.3 Extensions of the ASEP

The ASEP is often claimed to be a paradigmatic model of driven diffusive systems. In this section I aim to demonstrate why this is true by giving a brief outline of some of the many variations and extensions of the ASEP, and to showcase the variety of different applications of the ASEP to physical problems.

One of the commonly used variants, is the ASEP with open boundary conditions. This is an important example as it exhibits phase transitions in one dimension, which from the point of view of one dimensional equilibrium systems is an unexpected result [33]. It also allows the ASEP to be applied when the system does not have a conserved number of particles. In the open boundary condition case this allows the *upstream* end site to have a rate at which particles attach to it, α, and the *downstream* end site to have a rate of detachment from it, β, as in figure 2.1. This corresponds to allowing the ends of the lattice to sit in baths of particles. We can consider the flux J, which is defined as the number of particles which make the transition between two sites per unit time. In the TASEP, the behaviour of J with respect to the transition rates can be understood intuitively by considering the bottlenecks in the system. If the entrance rate α is the limiting process then the lattice will be under-full, and the system will be in the "low-density phase". If the exit rate is the limiting process then particles will pile up on the lattice waiting to get off, and the system will be in the "high-density phase". If the transition along the lattice is the limiting process, then particles will be added to the lattice soon after the entrance site becomes free, and will be removed from the exit site soon after it becomes occupied. The limiting factor being the availability of holes to move into implies the flux will be highest in this regime and the system is said to be in the "maximal-current phase". If the transition rate between sites $p = 1$ then the phase diagram is as shown in figure 2.3 [13].

The average of the occupation number at a particular point is the local density at that point, and the local density as a function of the position on the lattice is a density profile. In the thermodynamic limit $N \to \infty$, $L \to \infty$ such that $\rho = \frac{N}{L}$, we can assume the non-uniform density varies slowly on the microscopic

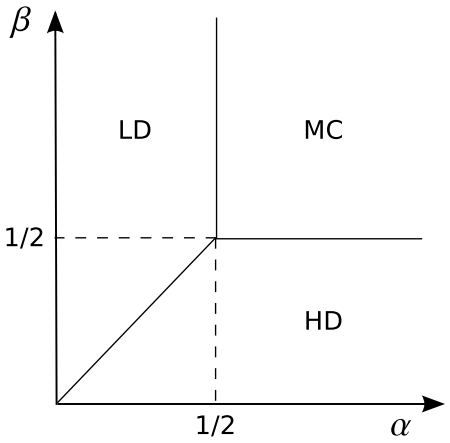

Figure 2.3 *Phase diagram for the TASEP with open boundary conditions. $p = 1$, entrance rate α, exit rate β, MC = maximal-current phase, HD = high-density phase, LD = low-density phase*

scale [56], and so we can look instead at the continuous position variable x. The equation for the evolution of $\rho(x,t)$ in time in the steady state is

$$\frac{\partial \rho(x,t)}{\partial t} + \frac{a}{\tau}(2p-1)\frac{\partial \rho(x,t)(1-\rho(x,t))}{\partial x} = 0 \tag{2.5}$$

where a is the lattice spacing (a microscopic length scale), τ is a microscopic time which defines the timescale of the transition rate $\frac{p}{\tau}$. This is the Burgers equation with zero viscosity. This implies that in the thermodynamic limit, the ASEP is the discrete version of the Burgers equation ([60] and references therein) which is known to contain shocks, which is to say that the density profile of the ASEP develops discontinuities, as cartooned in figure 2.4. This is due to the fact that low density regions travel faster than high density regions and so catch up with them to form the shocks [13]. In the low-density regime ($\beta > \alpha$ and $\alpha < \frac{1}{2}$) the shock propagates to the end of the lattice and the system takes the density associated with the entrance boundary. In the high-density regime ($\alpha > \beta$ and $\beta < \frac{1}{2}$) the shock moves to the entrance boundary, and the system has the density associated with the exit boundary. In the maximal-current phase there are no shocks in the system. At the phase boundary the shock moves around the lattice as a random walker once it is far from the boundaries.

The shape of the shocks can be analytically investigated by the introduction of a second species of particle which acts as a marker for the discontinuity in the density. Consider the TASEP with open boundaries as described, but now with two species or "classes" of particle. The first species of particle has the mutual exclusion property such that it cannot exchange places with another first class

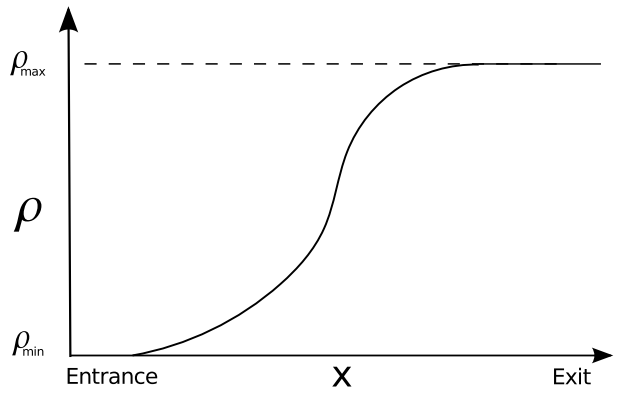

Figure 2.4 *Cartoon of the density profile around a shock in the ASEP with open boundaries*

particle, but it can exchange places with second class particle or hole, whereas second class particles can only exchange places with holes, as illustrated in figure 2.5. Consider the case where there is only one second class particle. The exclusion rules imply that if there are holes downstream of the second class particle, and first class particles upstream, the second class particle cannot move and will be forced to sit on the density discontinuity if one exists. The value of the local density on the hole side of the second class particle can be shown to fall off as order $x^{-\frac{1}{2}}$ where x is the distance from the second class particle [26].

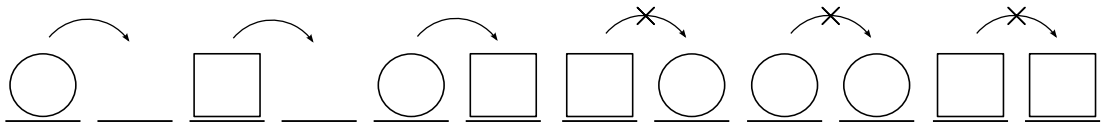

Figure 2.5 *Exclusion conditions for two species model. First class particles: circles, second class particles: squares.*

The presence of shocks in the ASEP with open boundaries implies that there are correlations between adjacent sites, and mean field approaches are approximations. The exact solution is computed with the matrix-product method. The matrix-product method assumes that there is a steady state of the system whereby $P(\mathcal{C}) = \prod_{i=1}^{L} f_i(\tau_i)$, where f_i are scalar factors which may be dependent on the site, labelled i. Since the scalar factors depend only on the current site, this method ignores correlations between sites, which we have argued to be important for condensation. A generalised form of this is matrix-product form, where the factors f_i are replaced with matrices X_{τ_i}. Since the matrices need not commute, this allows for correlations to be taken into account. This resulting product of matrices can be operated on by vectors to the right and left to get a scalar probability. For an overview of matrix-product methods,

and the situations that satisfy the matrix-product assumption, see for instance [13]. This method has been used to analytically solve many variations on the ASEP, including models with an arbitrary number of species [67]. There have also been extensions of the ASEP with multiple interacting lanes of traffic, which can display qualitatively different phase diagrams [52].

A couple of symmetries in the system have been preserved so far in this discussion; the symmetry between particles, and the symmetry between sites. These symmetries can be broken, to give new phase transitions. Firstly the symmetry between particles can be broken allowing disorder in the hopping rates, i.e. by assigning particles different speeds. For the TASEP on a ring with randomly chosen particle hopping probabilities, two phases are seen [55]. At high density particle speeds are limited by the number of holes in the lattice, and differences in particle speed become irrelevant. For low densities there is a jamming transition where a macroscopic number of particles form a queue behind the slowest particle. The symmetry between sites can be broken by introducing disorder in the sites, i.e. allowing them to have randomly chosen transition rates to neighbouring sites. Phase separation into regions of different local density is observed [84].

Traffic flow models in one physical dimension, such as the ASEP find a natural application in the study of molecular motors. "Motor proteins are molecular machines that convert the chemical energy derived from the hydrolysis of ATP into mechanical work used to power cellular motility" [48]. They are of particular interest when studying driven diffusive systems in one physical dimension due to the fact that they move along cystoskeletal filaments and can exhibit mutual exclusion. A particular example of a motor protein is the ribosomal motor, which is a protein which synthesises other proteins as it moves along the codons of an mRNA strand [8]. Molecular motors are proteins which have a finite length which is greater than the size of a single codon, can detach themselves from the mRNA before the end of the lattice, and move through a complicated mechano-chemical process, and so they have inspired a number of extensions to the ASEP as discussed so far.

For the TASEP on a ring with movers of length l, the fact that all configurations are equally likely can be used to find the probability that a system has a particular flux [76]. The mean flux in the steady state, J, can be found to

be

$$J = \frac{\rho}{l} \frac{1-\rho}{1-\rho+\frac{\rho}{l}-1/N}$$

This shows that there is no longer particle hole symmetry and that the maximum flux is reduced.

Attachment and detachment can be modelled by adding and removing movers from each site with certain probabilities. In the open boundary TASEP it was found that in the region close to the onset of the maximal current phase, where the boundary and bulk effects are competing there can exist a coexistence phase where high and low densities are separated by a shock. Unlike the shock in the open boundary TASEP without attachment and detachment, the shock is localised in space and doesn't move about the lattice randomly [65].

Since molecular motors use complicated chemistry to move, this has been modelled by the introduction of interstitial places, which I call stages, between the sites on the lattice, see figure 2.6. The model described in [43] was inspired by the cycle of actions performed by a ribosomal motor before it makes a transition to the next codon on an m-RNA strand. A simple two place version was used in [68]. For the TASEP on a ring with finite length particles of size l, with a complicated seven stage structure, mean field theory was used to find the mean flux in the steady state [7]

$$J = \frac{\omega\rho(1-\rho l)}{(1+\rho-\rho l)+\Omega(1-\rho l)}$$

where ω is the smallest rate in the system and Ω is an effective rate which is a combination of the other rates. This complicated structure quantitatively adjusts the flux, but no qualitative difference was seen beyond that reported for finite length particles alone.

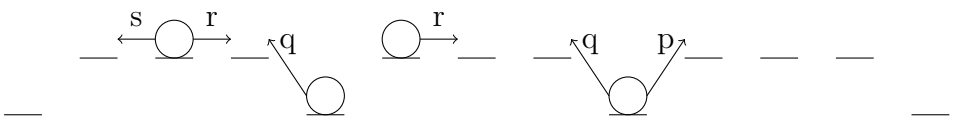

Figure 2.6 *A cartoon of the ASEP with interstitial places.*

2.4 The Zero Range Process (ZRP)

We now turn to the study of the Zero Range Process (ZRP) because it is another paradigmatic model of driven diffusive systems which can be mapped exactly, under conditions discussed below, to the ASEP. The ZRP is a simple model of shaken granular gases, which consists of a discrete lattice of sites each of which can contain many indistinguishable hopping particles and was first introduced by Spitzer in 1970 [80]. It is a Markovian model which allows for both mutual exclusion and a longer range attraction/repulsion between adjacent particles. The inclusion of the attraction/repulsion between adjacent particles is a useful extension to the ASEP for the study of condensation effects, gelation in networks and the tendency of buses to come all at once (see [33] and references therein) for instance.

With periodic boundary conditions and hopping restricted to adjacent sites the ZRP can be uniquely mapped to the ASEP up to translations of the ASEP lattice [33]. To map between the ZRP and the ASEP we identify particles in the ZRP as the spaces to the right of a particle in the ASEP and the sites on the ZRP as the particles of the ASEP. This mapping is shown diagrammatically in Figure 2.7. It can be seen that a particle moving right in the ZRP corresponds to a particle moving left in the ASEP. In the case of open boundary conditions, the number of sites in the ZRP is conserved but the number of particles is not. This corresponds to the conservation of number of particles in the ASEP but not the number of sites, which means that the mapping cannot be used for open boundaries. It can also be seen that if particles in the ZRP are allowed to move to non-adjacent sites the mapping to an ASEP is broken.

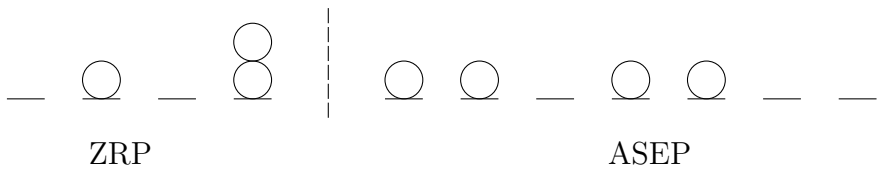

Figure 2.7 *Mapping between the ZRP and the ASEP*

If the transition rate of a particle in the ZRP is dependent on the number of particles on its exit site, when mapped to the ASEP it corresponds to the transition rate of particles being dependent on their distance from the particle to their right. The ZRP can then be interpreted as a model of long range interactions between particles in the ASEP, and therefore is used as a model of condensation

effects.

In a similar manner to before, we can encode the state of the system in a configuration $\mathcal{C} = \{n_1, n_2, ..., n_L\}$ where n_i is the number of particles occupying site i (c.f. the occupation numbers τ_i of the ASEP). The probability of finding the steady state of the system in a configuration $\mathcal{C}$ can be written as the product of functions which only depend on a single site,

$$P(\mathcal{C}) \sim \prod_{i=1}^{L} f(n_i)$$

as shown in [33], where f is a scalar function, as above. The fact that the steady state can be factorised in this way, allows the calculation of all of the properties of the steady state [33].

Interesting condensation effects occur for specific choices of intersite hop rates $u(n)$ [33][41]. For example, if the hop rate from a site with n particles decays more slowly than $u(n) \sim 1 + \frac{b}{n}$, where $b = 2$. b is known as the static exponent of the ZRP and plays the role of the inverse temperature [41]. If $u(n)$ has an asymptotic value $\beta > 0$ as $n \to \infty$, and the system has a density higher than the critical density, macroscopic numbers of particles condense onto a single site [33]. The rest of the particles fill the remaining sites and are known as *background fluid* [44]. If the transition probability tends to zero as $n \to \infty$, i.e. $\beta = 0$, then there is no critical density and there is always phase separation between the macroscopic site and the background fluid. It can be shown that ([33]) the presence of disorder in the sites, i.e. the presence of slow sites affects the condensation. In the case where there is a single defect site, it acts as a sink for particles and the condensate will form on it.

The dynamics of these condensates has been of some interest because of examples of moving condensates in real world systems, such as traffic jams. For finite size systems, the motion of the condensate is entirely non-local, which is to say that it jumps randomly about the lattice. Stochastic effects imply that the condensate has fluctuations in its size which could lead to it becoming unstable with respect to other condensates forming on the lattice. The condensate spends a large amount of time, τ on one site, before disappearing and reappearing elsewhere. The formation time of a condensate is much less than τ, and τ grows as the system size M to the power b (the static exponent) [41]. This shows that in the thermodynamic limit we expect a single condensate containing a macroscopic number of particles which does not move.

The update rule can be modified to model the increasing speed of aggregation of particles seen in differential sedimentation, gravitational clustering and droplet formation (see [87] and references therein). This is achieved by allowing for an increased rate of exchange of particles between neighbouring condensates. If the exit site has m particles and the target site has n particles an update rule of the form $u(m,n) \sim (mn)^\gamma$ with $\gamma > 2$ shows very fast condensate formation. In the case of totally asymmetric hopping, it also has the property that the condensate moves along the lattice with speed $\nu \sim L^\gamma$ where L is the size of the lattice. Using extreme value theory it is shown [87] that the time to form the condensate has the form $(\log L)^{1-\gamma}$ and so is instantaneous in the $L \to \infty$ limit.

2.5 Non-Markovian ZRP

In this section we see the relaxation of the Markovian assumption in the Zero Range Process by Hirschberg et al [46] and [47]. Condensates observed in real life can move, traffic jams for instance, and we will see that making the ZRP non-Markovian in a particular way gives rise to a novel moving condensate. This section raises the interesting question of the effect of breaking the Markov assumption in the ASEP, which we will discuss in more depth in the rest of this thesis.

In the ZRP with nearest neighbour hopping a moving condensate can be made by breaking the Markov property in a particular way [46]. As with the model described above, the non-Markovian ZRP consists of a discrete lattice of L boxes filled with N particles. In this modification each site also has an internal clock, which measures the amount of time elapsed since a particle last moved onto that site τ (note that this is not the same as the occupation numbers of the ASEP τ_i, as the occupation numbers in the ZRP are denoted n_i). The internal clocks increment stochastically with a rate c. The hop rates between sites can now depend on both the number of particles at that site, and the site's internal clock. When a particle hops into a new site, it resets that site's internal clock, which makes the jump process non-Markovian as the history of the system is taken into account. If we consider the jump process and the clock increments together we have defined a Markovian process, as it is a stochastic system with transitions between states governed by the exponential distribution. This is a good example of integrating out the degrees of freedom contained in a part of the system, the clock increments, to make a non-Markovian process when you consider only a

subsystem, the hopping, as explored further in section 2.7. Importantly for us, the resetting of the target sites internal clock in the ZRP maps exactly to the hopping particles internal clock being reset in the ASEP. An illustration of this can be seen in Figure 2.8.

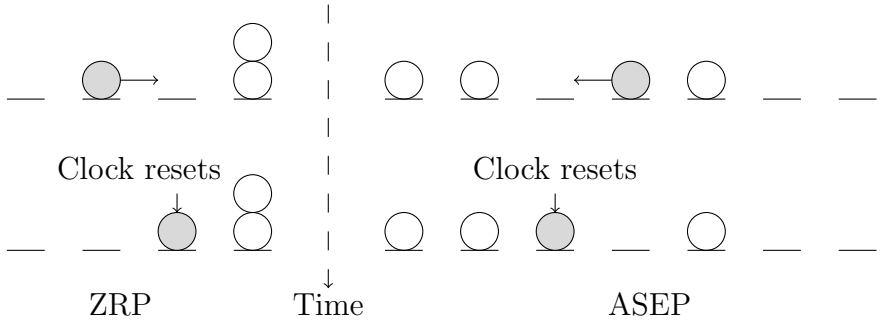

Figure 2.8 *Mapping between the ZRP and the ASEP when a particle hops. ZRP particle hops to the right corresponds to a space in the ASEP hopping right, or equivalently, an ASEP particle hopping left. The ZRP target site clock resets, which is the third site and corresponds to the third ASEP particle's clock resetting.*

Hirschberg et al [46] write down the Master equation for the full model with random target sites. This allows them to get rid of inter-site correlation, factorise the Master equation, solve it for the stationary states and match it to the stationary states of the unaltered ZRP. As a specific example they set the transition rate for a site, $u(n, \tau)$ as in Equation 2.6. They find that the non-Markovian effects on the hopping process increases the critical density needed for condensation in the system to occur when the hop rates are chosen to ensure a condensate above the critical density as before $u(n) = \gamma(1 + \frac{b}{n^\sigma})$.

$$u(n,\tau) = \begin{cases} 0 & \tau = 0 \qquad \text{“off state”} \\ u(n) & \tau \geqslant 1 \qquad \text{“on state”} \end{cases} \tag{2.6}$$

Next they consider fully asymmetric nearest neighbour hopping with periodic boundary conditions and, as they can no longer factorise their Master equation, they study the behaviour they see in simulations. Beyond the critical density, a condensate always exists as usual however they notice that the condensate drifts around the system. Instead of one site being macroscopically occupied, the condensate spans two adjacent sites. They observe that the condensate at the rear fills up the condensate at the front until it drops down occupation numbers similar to the background fluid. At this point the front condensate can come out of the off state for long enough to start moving particles. It will then fill up

the site in front of it, and so the condensate moves around the ring. They call this motion *slinky* motion. These observe these effects analytically when they measure the time averaged occupation probability distribution, and they notice they are distinct from the distribution in the ZRP case.

We see when we map this time dependency back to the ASEP, resetting the target site time in the ZRP is equivalent to resetting the time of the moved particle in the ASEP. This raises the interesting question of how breaking the Markov property affects the ASEP, and what condensation effects may occur.

2.6 Simulating interacting particle systems

We are interested in breaking the Markov assumption in the ASEP, as discussed above. This implies that techniques which require the Markov assumption may not be used, so we expect writing down and solving a master equation to be difficult, if not impossible. One of the standard techniques of investigating stochastic process, especially where analytic progress is difficult, is to simulate it.

To fully specify a stochastic model that we wish to simulate, we must also state the update scheme we are using. These split into two types, discrete and continuous time. In the literature we see that random sequential updating, parallel updating and ordered sequential updating are common discrete time update schemes. In random sequential updates, at each timestep an event is chosen at random and executed if it is allowed. In the ASEP this corresponds to choosing a particle at random, and attempting to move with probability p, where p is the probability of making the transition between the current and target sites per unit time. Due to the fact that in traffic flow all particles are moving simultaneously, parallel updates are often used [32]. Here all movers attempt to move simultaneously. In the TASEP this corresponds to all particles attempting to hop forward simultaneously with their particular p, which may depend on the current site, target site, the particle in question and possibly the time since the particle last attempted to move. The mutual exclusion principle is applied before particles move, so only particles which are unblocked at the start of the update are allowed to move. Since the backwards hopping probability is zero in the TASEP there is no conflict between particles trying to occupy the same location. In ordered sequential dynamics there is a particular predefined order of performing the update, which in the ASEP corresponds to updating the sites in a particular order at each timestep.

This thesis will be mostly restricted to considering the behaviour of stochastic processes in continuous time, and to simulate continuous time we use the same modified continuous time Monte Carlo method [74] as in [42] which we call the *waiting time update*. Each event is assigned a time to next occurrence from the particular waiting time distribution associated with that event. The event with the shortest time is implemented, and a new time is assigned to it which is the sum of its current time and a new time drawn from the relevant waiting time distribution (figure 2.9). In the ASEP this corresponds to a each particle having a clock which counts down to its next attempted move, where the time is drawn from the relevant waiting time distribution. All clocks progress until the next event occurs, that particle moves if allowed, its clock is reset and a new time to next attempted move is drawn.

There are a number of different choices of update rules that can be made. A particular update scheme defines the dynamics of the system, and different update schemes may lead to processes which look similar but are not identical. It is noted in [32] that a process described by different update rules may exhibit qualitatively similar behaviour, but that particular numerical values, of critical points for instance, may change. Their example is the TASEP on a ring with disorder in particle hopping rates, where the critical density between the two phases (section 2.3) is higher for ordered sequential updates where the direction of update is opposite to the particle flow, and lowest for random sequential updates.

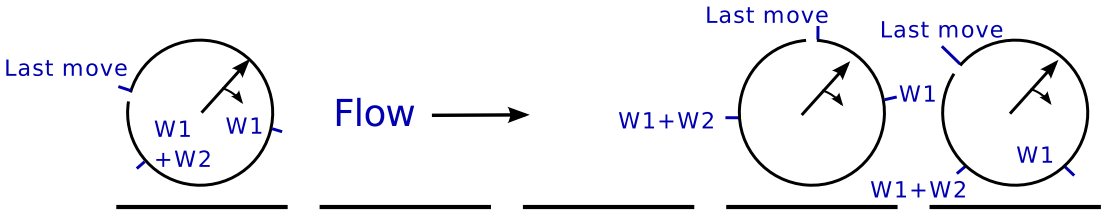

Figure 2.9 *Illustration of the waiting time update*

The useful thing about the waiting time update is it allows Markovian and non-Markovian effects to be investigated without changing the update scheme of the simulation. The Markov assumption implies that there is a constant probability per unit time of a particular event occurring, where this probability is possibly dependent on the current state of the system, and its target state. Non-Markovian systems can have events which are also dependent on time. In the ASEP for instance, the probability that a particle makes a particular transition could be dependent on its current site, its target site and how long it was since it last moved. The only waiting time distribution which generates events with a constant

probability of success per unit time is the exponential decay $p(t) = \lambda \exp[-\lambda t]$ where λ is the rate. This is due to the fact that the exponential decay has the *memoryless property*. A distribution with this property satisfies the relation

$$P(X > x + y | X > y) = P(X > x) \tag{2.7}$$

The probability that a random variable drawn from the exponential decay of rate λ is larger than x is $\exp[-x\lambda]$, i.e the probability that the event in question occurs after x. We quickly verify that the exponential decay has the memoryless property.

$$\frac{\exp[-\lambda(x+y)]}{\exp[-y\lambda]} = \exp[-x\lambda]$$

as required. Considering the random variable drawn from the distribution to be the time of first success of an event, we see that if an event has not occurred up to time y, then the probability that it will also not occur in $2y$ is the same as the probability that it survived y in the first instance. This is equivalent to saying that the event has a constant probability per unit time of occurring, and is required for a Markov process. Any other waiting time distribution will not have this property, and will therefore make the simulation non-Markovian.

2.7 Integrating out degrees of freedom

In thermodynamics we are comfortable with the idea that we could ignore the degrees of freedom associated with the environment of the system and replace their effect with a noise term. In statistical mechanics however, often the cost of integrating out unwanted degrees of freedom is the breaking of the Markov property. We discussed the example of the random acceleration model in the previous chapter and the non-Markovian ZRP is also an example of this because, if the stochastic incrementation of time is taken into account in the master equation, the process is fully Markovian. When considering purely the translation along the lattice, the transition rates become time dependent, and this is non-Markovian.

We want to consider the effect of breaking the Markov assumption in the ASEP, however from the point of view of applications, stochastically increasing discrete time can be seen as somewhat artificial. A non-Markovian ASEP arises naturally when integrating out the stages from the interstitial place model.

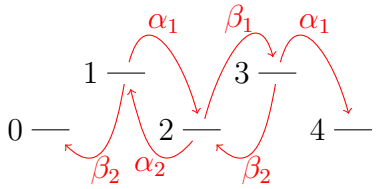

Figure 2.10 *A diagram of the interstitial place model, stages 1 and 3 between sites 0, 2 and 4. Transitions with their respective rates shown in red.*

The TASEP with interstitial places was used to model molecular motors as described in section 2.3. As an illustration of reducing the number of degrees of freedom to generate non-Markovian effects, we can use a single interstitial place (which for notation purposes I call a stage). The lattice contains L sites, L stages and N particles. To move between sites, a particle must cross the stage between them. The transition rates between sites and stages are shown in figure 2.10. We want the probability that a particle makes a transition between two adjacent sites without entering another, for instance a trajectory, χ, occurs which will take a particle from site 2 to site 4 and does not enter site 0. Given that it starts at site 2, it can make l loops $2 \to 1 \to 2$ and r loops $2 \to 3 \to 2$ before moving $2 \to 3 \to 4$.

Consider a pair of processes X, Y which occur with rates x, y. The probability that the first event, which is X, occurs at time t is the product of the probability that the first success of the Poisson process X occurs at t with the probability that Y hasn't had a success yet. This is $P_X(t) = x \exp[-xt] \exp[-yt]$. We want the probability that the first success after time $t = 0$ is X, which is $P_X(t)$ integrated over t.

$$P(X) = x \int_{t=0}^{\infty} \exp[-(x+y)t] \mathrm{d}t = \frac{x}{x+y}$$

The probability that particle takes a particular trajectory χ in a particular order of loops is

$$P(\chi_{\text{particular}}) = (a_1 a_2)^l (b_1 b_2)^r a_1 b_1$$

where $a_1 = \frac{\alpha_1}{\alpha_1+\beta_2}$, $a_2 = \frac{\alpha_2}{\alpha_2+\beta_1}$, $b_1 = \frac{\beta_1}{\alpha_2+\beta_1}$, $b_2 = \frac{\beta_2}{\alpha_1+\beta_2}$, l is the number of loops made to the left, and r is the number of loops made to the right as described above. There are $\binom{l+r}{r}$ ways of ordering r loops out of $l+r$ options, where $\binom{l+r}{r}$ is the binomial coefficient as before. The probability of trajectory χ where the

order of loops is irrelevant is

$$P(l,r) = \binom{l+r}{r}(a_1a_2)^l(b_1b_2)^r(a_1b_1)$$

The probability that trajectory χ takes a time t will be the convolution (see appendix A) of the time to first success of each step. The Laplace transform will be discussed at length in chapter 3 but for now it is sufficient to say that the Laplace transform of some function $f(t)$ is

$$\mathcal{L}[f(t)] \equiv \mathcal{L}[f(t),t,s] \equiv \tilde{f}(s) \equiv \int_0^\infty \exp[-st]f(t)\mathrm{d}t \tag{2.8}$$

and that the Laplace transform of a convolution of two functions is the product of their individual Laplace transforms. In this thesis I use the notation $\mathcal{L}[f(t),t,s]$ to make clear which variables are involved in the transform. The Laplace transform of $\lambda\exp[-\lambda t]$ is $\frac{\lambda}{s+\lambda}$, so the Laplace transform of the pdf of the time to arrive at the end of trajectory χ is $P(s|\chi)$. Using the change of variable $n = l + r$,

$$P(s|\chi) = \left(\frac{\alpha_2}{s+\alpha_2}\frac{\alpha_1}{s+\alpha_1}\right)^l\left(\frac{\beta_1}{s+\beta_1}\frac{\beta_2}{s+\beta_2}\right)^r\frac{\alpha_1}{s+\alpha_1}\frac{\beta_1}{s+\beta_1}$$

There are $\binom{l+r}{r}$ ways of arranging r loops out of $n = l+r$ choices, so the Laplace transform of the pdf of the time to arrive at the end of a trajectory with l left steps and r right steps is

$$P(s,l,r) = \binom{l+r}{r}\left(\frac{a_1a_2\alpha_2\alpha_1}{(s+\alpha_1)(s+\alpha_2)}\right)^l\left(\frac{b_1b_2\beta_1\beta_2}{(s+\beta_1)(s+\beta_2)}\right)^r\frac{a_1b_1\alpha_1\beta_1}{(s+\alpha_1)(s+\beta_1)}$$
$$P(s,n,r) = \binom{n}{r}\left(\frac{a_1a_2\alpha_2\alpha_1}{(s+\alpha_1)(s+\alpha_2)}\right)^{n-r}\left(\frac{b_1b_2\beta_1\beta_2}{(s+\beta_1)(s+\beta_2)}\right)^r\frac{a_1b_1\alpha_1\beta_1}{(s+\alpha_1)(s+\beta_1)}$$

We now need to sum out the different paths using $P(s) = \sum_{n=0}^\infty\sum_{r=0}^\infty P(s,n,r)$. We note the binomial form of $P(s,n,r)$ so we use $(x+y)^n = \sum_{r=0}^\infty\binom{n}{r}x^ry^{n-r}$

$$P(s) = \frac{a_1b_1\alpha_1\beta_1}{(s+\alpha_1)(s+\beta_1)}\sum_{n=0}^\infty\left(\frac{a_1a_2\alpha_2\alpha_1}{(s+\alpha_1)(s+\alpha_2)} + \frac{b_1b_2\beta_1\beta_2}{(s+\beta_1)(s+\beta_2)}\right)^n$$
$$= \frac{a_1b_1\alpha_1\beta_1}{(s+\alpha_1)(s+\beta_1)}\frac{1}{1-\left(\frac{a_1a_2\alpha_2\alpha_1}{(s+\alpha_1)(s+\alpha_2)} + \frac{b_1b_2\beta_1\beta_2}{(s+\beta_1)(s+\beta_2)}\right)}$$

provided

$$\left| \frac{a_1 a_2 \alpha_2 \alpha_1}{(s+\alpha_1)(s+\alpha_2)} + \frac{b_1 b_2 \beta_1 \beta_2}{(s+\beta_1)(s+\beta_2)} \right| < 1$$

which is true for $\Re\{s\} > 0$. Rearranging $P(s)$ gives

$$P(s) = \frac{a_1 b_1 \alpha_1 \beta_1 (s+\alpha_2)(s+\beta_2)}{(s+\alpha_1)(s+\alpha_2)(s+\beta_1)(s+\beta_2) - a_1 a_2 \alpha_2 \alpha_1 (s+\beta_1)(s+\beta_2) + b_1 b_2 \beta_1 \beta_2 (s+\alpha_1)(s+\alpha_2)}$$

If the four roots of the denominator r_1, r_2, r_3, r_4 are distinct $P(s)$ can be simplified, and then partial fractions used.

$$\begin{aligned} P(s) &= \frac{a_1 b_1 \alpha_1 \beta_1 (s+\alpha_2)(s+\beta_2)}{(s-r_1)(s-r_2)(s-r_3)(s-r_4)} \\ &= \frac{A}{s-r_1} + \frac{B}{s-r_2} + \frac{C}{s-r_3} + \frac{D}{s-r_4} \end{aligned}$$

where A, B, C, D are constants which depend on $\alpha_1, \alpha_2, \beta_1, \beta_2$. The Laplace transform of $\exp[at]$ is $\frac{1}{s-a}$, and the inverse Laplace transform of $P(s)$ gives $P(t)$

$$P(t) = A \exp[r_1 t] + B \exp[r_2 t] + C \exp[r_3 t] + D \exp[r_4 t]$$

which is a valid probability distribution if all the roots r_1, r_2, r_3, r_4 are negative.

We see that we could reduce the number of events available to the system by integrating out the interstitial places, and we could simulate this by using the waiting time update explained in section 2.6. This simulation would be non-Markovian as the sum of exponential decays is not an exponential decay itself. In preliminary simulations of this system for the TASEP on a ring we found no qualitative difference to the flux density plot from the basic TASEP on a ring. We attribute this to the fact that in the long time limit of $P(t)$ the dominant term is a single exponential decay, it has finite mean and variance and central limit theorem applies. This is to say that large deviations from the mean are exponentially suppressed. For condensation effects to occur we need particles to stop for long enough for particles behind them to catch up, which implies that the first particle must have picked a time which, on average, must be much larger than the mean. If condensation effects do not occur, then mean field theory is a good approximation, and the same flux relations as for the basic TASEP on a ring can be computed. We are aware of only one example in the literature which investigates a non-Markovian ASEP directly.

2.8 A non-Markovian ASEP

In [42] is the only example, to my knowledge, of a non-Markovian ASEP in the literature. It is claimed that the waiting time between moves of a ribosome along an mRNA strand can be well fitted by either an exponential distribution, or a difference of exponentials. The model they use is a TASEP to model the interaction between a number of ribosomes, with open boundary conditions to model the generation of proteins as the ribosome moves along codons. Ribosomes are complicated molecular machines which are larger than a single codon, and each ribosome occupies a number of sites l. The degradation of mRNA, i.e. the lattice itself, occurs with rate λ, and the particular instance of the simulation is stopped once the mRNA has decayed. Each of these are effects that had been previously examined, however they also used a waiting time update with a waiting time distribution which is gamma-distributed $P(\tau) = \frac{\tau^{n-1}k^n}{\Gamma(n)} \exp[-k\tau]$. The various rates and gamma distribution shape parameters are taken from experiments. The aim of the work was to find the protein copy number E, which is the number of ribosomes which leave the end of the lattice before the mRNA decays. They compare their results with the predicted geometric distribution of E using the theory by Berg [9], and find consistency with the geometric distribution, with some deviations at small E. They state that the lattice model is too complicated to find the distribution of E analytically, so they solve a much simpler model neglecting all spatial effects to show that it predicts a geometric distribution that fits well with the geometric distribution from their simulations.

2.9 Chapter summary

In this chapter we have explored the literature surrounding driven diffusive processes, which are systems that are driven far from equilibrium by having a current in them. We saw that they can have steady states, and found that even in one dimension they can have phase transitions and other interesting effects, including condensation, that their equilibrium counterparts cannot show. The ASEP and the ZRP have the status of being paradigmatic models of driven diffusive systems due to their analytic tractability, their relation to each other and their range of applications. In attempting to create a moving condensate in the ZRP to investigate traffic flow problems [46], non-Markovian effects were introduced. Both Poissonian and non-Poissonian waiting times can be used in

the waiting time update scheme, which therefore can be used to investigate both Markovian and non-Markovian processes. The investigation of non-Markovian effects in the ASEP and ZRP is in its infancy, and we examined the two known examples of this from the literature. In the next chapter we will explore some of the mathematical framework required to investigate Markovian and non-Markovian stochastic processes in continuous time.

Chapter 3

Renewal and semi-Markov processes in continuous time

In the previous chapter we discussed non-Markovian stochastic processes, in particular the non-Markovian ASEP and ZRP. These are an extension to the underlying Markov process where each particle has a transition rate which is dependent on the time since their last attempted move. We noted that in principle such a non-Markovian process can be cast in the form of a Markov process with more dimensions. In the ASEP this would correspond to each particle having a discrete current position variable and a continuous waiting time variable. In principle a master equation could be written down, though it would be very complicated and extraordinarily difficult, if not impossible, to solve analytically. There do exist more simple examples of non-Markovian processes with a single particle which can be studied.

The semi-Markov process has a pair of variables, a state variable and a variable which records the time since the last change of state. The transition time between states is a random variable drawn from a waiting time distribution. This corresponds exactly to the non-Markovian ASEP described in section 2.8 with a single particle, where the states of the system are the sites. The renewal process is framed more simply in terms of the statistics of recurrent events, where the time between each occurrence is a random variable drawn from a waiting time distribution. As discussed before, using a non-Poissonian waiting time distribution breaks the Markov property, but the framework of renewal and semi-Markov processes does not require it. In the first part of this chapter I present an elementary overview of the semi-Markov and the renewal process as

they do not tend to be included in undergraduate physics degrees.

We will see that one of the most frequently occurring questions when investigating renewal or semi-Markov processes is the sum of a number of random variables. I approach this by using Laplace transforms due to the convolution theorem (see appendix A, and for more examples of where Laplace transforms are used in probability theory, see chapter XIV of Feller [36]), and so I examine all of the useful results concerning Laplace transforms and complex variable calculus that we will need in the remainder of the thesis. We will consider a number of examples of the sum of random variables with both Poissonian and non-Poissonian distributions, to see their challenges and limitations.

3.1 Renewal processes

A renewal process is one where events, often called renewals, occur in succession and the times between each event are governed by the same probability distribution [49], as cartooned in figure 3.1. This has obvious applications when considering the motion of a single particle in the non-Markovian ASEP described in section 2.8, and the techniques used to investigate renewal processes will appear again in chapter 5. There are various names for the time between renewal events including dwell time, renewal time and lifetime, but I will refer to them as waiting times, and their probability distribution as the waiting time distribution $p_1(T)$. As we require successive events to occur in the proper order, we must set $T \geq 0$. If the waiting time distribution is memoryless, i.e. Poissonian, renewal processes are a special case of Markov processes, however the basic framework below does not require the Markov assumption.

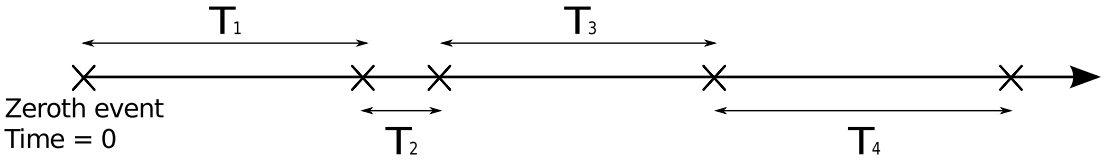

Figure 3.1 *A cartoon of the renewal process, where the time between each renewal, shown by a cross, is a random variable T drawn from the waiting time distribution $p_1(T)$*

If the times between each event are $T_1, T_2, ..., T_n$, the time of the occurrence of the n$^{\text{th}}$ event is $S_n = \sum_{i=1}^{n} T_i$. The probability that S_n takes values between $t, t + \mathrm{d}t$ is given by the pdf $\mathcal{S}_n(t)$, which is the distribution of the sum of n

independent identically distributed (i.i.d) random variables drawn from a common distribution. This corresponds to a convolution of the distribution with itself n times, which we discuss further in section 3.4. The analysis of the sum of i.i.d random variables often occurs in the study of stochastic processes and is one of the primary reasons renewal process are so well studied.

An obvious question to ask is; what is the probability that an event will occur at time t, $U(t)$. The probability that the final event of a sequence of i recurrent events occurs at t is equivalent to $\mathcal{S}_i(t)$. The probability that the final event of a sequence of zero events occurs at t is zero unless $t = 0$, so it can be included without harm.

$$U(t) = \mathcal{S}_0(t) + \mathcal{S}_1(t) + \mathcal{S}_2(t) + ... \tag{3.1}$$

$$= \sum_{i=0}^{\infty} \mathcal{S}_i(t) \tag{3.2}$$

Due to $T > 0$, $U(t < 0) = 0$, and the zero time is defined at the zeroth event, so $U(0) = 1$. The "renewal argument" can be used to construct an equation containing only U and p_1 by noticing the following recursion. An event can occur at time t in two ways; it could be the first event that occurred at that time with probability $p_1(t)$, or there could be some number of other events which occurred before t, the last of which occurred at time t', $U(t')$, and the next event waits for $t - t'$ with probability $p_1(t - t')$.

$$U(t) = p_1(t) + [p_1 \star U](t) \tag{3.3}$$

$$\equiv p_1(t) + \int_0^t p_1(u)U(t-u)\mathrm{d}u$$

This is an example of a renewal equation, the solutions of which are found using renewal theory [36]. Alternatively the convolution can be replaced with a product in Laplace transform space due to convolution theorem, $\tilde{U}(s)$ found algebraically and then $U(t)$ found by inverting the Laplace transform. For clarity we repeat the definition of the Laplace transform here. The Laplace transform of some function $f(t)$ is

$$\mathcal{L}[f(t)] \equiv \mathcal{L}[f(t), t, s] \equiv \tilde{f}(s) \equiv \int_0^{\infty} \exp[-st] f(t)\mathrm{d}t \tag{3.4}$$

and the Laplace transform of a convolution of two functions is the product of their individual Laplace transforms (see appendix A). In this thesis I use the

notation $\mathcal{L}[f(t), t, s]$ to make clear which variables are involved in the transform. We will see an example of a renewal argument in chapter 5 when we look at the following renewal process problem. What is the probability that the first renewal after time T takes the value $T + W$, where $W > 0$?

Renewal theory can be used to investigate self-renewing aggregates (when a machine component fails it is replaced with a like component, and all components have a common failure time distribution), counters (once a detector triggers, it has a recharge time before it can trigger again) and reveal the waiting time paradox, all of which are examples discussed in [36]. To illustrate the waiting time paradox consider the following example from Feller [36]. A machine has a particular component which only operates for a certain time before breaking, where that time has a probability distribution $p(t)$. On breaking it is immediately replaced with a similar component with the same operation time distribution $p(t)$. The operation time of a particular component is tested at some particular time, for instance when the engineer gets round to it on the scheduled maintenance day. The expected value of the total operation time of the tested component will be larger than the expectation of $p(t)$ as it is more likely for a particular time which is independent of the process to fall in a longer operation time interval than a shorter one.

3.2 Semi-Markov processes

A semi-Markov process is an extension of a Markov process where the transition rates between states are dependent on the time since the last transition. As we have already noted, the non-Markovian ASEP (described in section 2.8) with a single particle corresponds exactly to a semi-Markov process. In this section we hope to gain some understanding of the difficulties involved in the analytic solution of even very simple semi-Markov processes, and thereby motivate the numerical approach we will take in the next chapter.

We define our notation, following [50]. p_{ij} is the probability that the system makes the transition from its current state i to its target state j. There are L available states, so $i, j \in [1, L]$. These are the Markovian transition probabilities and satisfy $p_{ij} \geq 0 \ \forall i, j$, and $\sum_{j=1}^{L} p_{ij} = 1 \ \forall i$. When the system enters state i it chooses a target site j using p_{ij} and then waits before it attempts to make the transition for a time chosen from the holding time distribution $h_{ij}(t)$. We can define waiting time distribution for the state i, which is the distribution of times

spent in state i independent of the target state, and is a weighted sum of the holding time distributions $w_i(t) = \sum_{j=1}^{L} p_{ij} h_{ij}(t)$.

As discussed in chapter 2, considered as presented the semi-Markov process is non-Markovian, but it can be mapped to a Markov process with an extra degree of freedom. A semi-Markov process with physical states can be converted to a fully Markovian process with the same physical states, and a counter measuring the time since the system transitioned into its current state. In discrete time at each timestep a particle may make a transition between the states with a probability that is dependent on the counter and the states in question. If it does not make that transition the counter increments by a timestep. The fact that the transition rates between states is still independent of the history of the system allows this mapping and gives the semi-Markov process its name.

We are often interested in the probability that the system will be in the state j at time t given that it transitioned into state i at time zero. This is referred to as the interval transition probability $\phi_{ij}(t)$ [50]. Implicitly this allows any number of transitions between states, provided that the system ends up being in j at t given that it started in i at $t = 0$. This also does not require that the system transitions into state j at time t, but also allows for transitions to j before t provided that it is still there at t.

In computing $\phi_{ij}(t)$ there are two possibilities to consider; either the system has made no transitions before t, or it has made some number of transitions. In the case where there are no transitions before t the contribution to $\phi_{ij}(t)$ will be zero if $i \neq j$. If $i = j$ the probability that the system is still in site i at t is $S_i(t)$, where $S_i(t) \equiv \int_t^\infty w_i(t')\mathrm{d}t'$. This is the probability that the holding time for the target site was larger than t, and is commonly known as the survival probability as the system "survives" in state i at least until time t.

In the case where there have been some sequence of transitions before t it helps to think of the first transition into state k at time τ, and then by some sequence of transitions ends up in state j some time $t - \tau$ later. Recognising that we have to use the same function as we are trying to compute, the probability that this occurs can be written $h_{ik}(\tau)\phi_{kj}(t-\tau)$. Since we do not care when the system made the intervening transition into state k we integrate it out $\int_{\tau=0}^{t} h_{ik}(\tau)\phi_{kj}(t-\tau)$, which takes the form of a convolution. Putting all this together, $\phi_{ij}(t)$ has a contribution from the zero transitions case, and L contributions from the other

(as there are L possible choices of the intermediate state k).

$$\phi_{ij}(t) = S_i(t)\delta_{ij} + \sum_{k=1}^{L} p_{ik} \int_{\tau=0}^{t} h_{ik}(\tau)\phi_{kj}(t-\tau)\mathrm{d}\tau \tag{3.5}$$

$$= S_i(t)\delta_{ij} + \int_{\tau=0}^{t} \sum_{k=1}^{L} p_{ik}h_{ik}(\tau)\phi_{kj}(t-\tau)\mathrm{d}\tau \tag{3.6}$$

This is similar to the renewal equation of section 3.1 in that it gives the function $\phi_{ij}(t)$ in terms of convolutions of itself with the holding time distributions. It can be re-expressed in matrix form using the definitions; $\Phi(t)$ has elements $\phi_{ij}(t)$, $S(t)$ is a diagonal matrix containing elements $S_i(t)$, P has elements p_{ij}, $H(t)$ has elements $h_{ij}(t)$. We define congruent matrix multiplication [50] with box notation $A \,\square\, B$ so that $[A \,\square\, B]_{ij} = a_{ij}b_{ij}$. We also note the standard matrix multiplication $(AB)_{ij} = \sum_k a_{ik}b_{kj}$. We can now define the "core matrix" $C(t) = P \,\square\, H(t)$.

$$\Phi(t) = S(t) + \int_{\tau=0}^{t} \left(P \,\square\, H(\tau)\right) \Phi(t-\tau)\mathrm{d}\tau \tag{3.7}$$

$$= S(t) + \int_{\tau=0}^{t} C(t)\Phi(t-\tau)\mathrm{d}\tau$$

This is in the form of a convolution, which we can tidy up by taking the Laplace transform of equation 3.5 and using the convolution theorem (appendix A). δ_{ij} and P are matrices of constants, and so are unaffected by the transformation.

$$\tilde{\phi_{ij}}(s) = \tilde{S_{ij}}(s)\delta_{ij} + \sum_{k=1}^{L} p_{ik}\tilde{h}_{ik}(s)\tilde{\phi_{kj}}(s)$$

This can also be expressed in matrix form, and we see

$$\tilde{\Phi}(s) = \tilde{S}(s) + \left(P \,\square\, \tilde{H}(s)\right) \tilde{\Phi}(s) \tag{3.8}$$

$$\tilde{\Phi}(s) = \tilde{S}(s) + \tilde{C}(s)\tilde{\Phi}(s)$$

We see that the Laplace transform of a matrix is a matrix composed of the Laplace transforms of each of its elements and $\tilde{C}(s) \equiv P \,\square\, \tilde{H}(s)$. This can then be solved by multiplying from the left by the inverse of the matrix $\left(I - \tilde{C}(s)\right)$, where I is

the identity matrix.

$$\begin{aligned} \tilde{\Phi}(s) &= \tilde{S}(s) + \tilde{C}(s)\tilde{\Phi}(s) \\ \left(I - \tilde{C}(s)\right)\tilde{\Phi}(s) &= \tilde{S}(s) \\ \tilde{\Phi}(s) &= \left(I - \tilde{C}(s)\right)^{-1}\tilde{S}(s) \end{aligned}$$

Once this has been done, the inverse Laplace transform must be taken to get the form of $\Phi(t)$. For large systems this will be difficult to achieve analytically in principle, however I will present a small example in section 3.4.2.

In the language of the renewal process, $\Phi(t)$ is the probability that the sum of the holding times for the intervening states between the initial i and the final j is less than t and that adding on the next holding time gives a random number which is larger than t. We see that the sum of random variables is a common theme in both the renewal process and in the semi-Markov process, and for that reason we will investigate it more thoroughly in the remainder of this chapter.

3.3 Laplace transforms

The difference between Markov processes and non-Markov processes in continuous time is whether or not a Poissonian or non-Poissonian waiting time distribution is used (sections 2.6 and 2.7). As has been discussed previously (sections 2.7, 3.1 and 3.2), we often wish to consider the sum of independent identically distributed (i.i.d) random variables drawn from a common probability distribution, which will usually require Laplace transforms and convolution theorem (appendix A). In the rest of this chapter we discuss using Laplace transforms to investigate the sum of i.i.d random variables in both the Poissonian and non-Poissonian cases, but first we must discuss Laplace transforms more directly.

The Laplace transform, or the exponential transform [50], of the function $f(t)$ taking t to the complex variable s is denoted

$$\mathcal{L}[f(t)] \equiv \mathcal{L}[f(t), t, s] \equiv \tilde{f}(s) \equiv \int_0^\infty \exp[-st] f(t) \mathrm{d}t \tag{3.9}$$

In applications, negative times, radius or height are often un-physical, which makes integrating over only the positive half of the variable a sensible thing to

do. For the Laplace transform to be defined we require

$$\int_0^\infty \exp[-st]|f(t)|\mathrm{d}t < \infty$$

and $f(x)$ to be of "exponential order" [3].

The difficulty in using Laplace transforms lies in reversing the process to get back to real space. The inverse transform uses the Bromwich inversion integral.

$$f(t) = \frac{1}{2\pi i}\int_{c-i\infty}^{c+i\infty} \exp[st]\tilde{f}(s)\mathrm{d}s \tag{3.10}$$

To demonstrate that this is indeed the inverse, we change the order of integration, make the substitution $s = c + iv$ and use the integral form of the Dirac delta function

$$2\pi\delta(t) = \int_{-\infty}^{\infty} \exp[-iut]\mathrm{d}u$$

like so

$$\begin{aligned}
f(t) &= \frac{1}{2\pi i}\int_{s=c-i\infty}^{c+i\infty} \exp[st]\int_{u=0}^{\infty}\exp[-su]f(u)\mathrm{d}u\mathrm{d}s \\
&= \frac{1}{2\pi i}\int_{s=c-i\infty}^{c+i\infty}\int_{u=0}^{\infty}\exp[s(t-u)]f(u)\mathrm{d}u\mathrm{d}s \\
&= \frac{1}{2\pi i}\int_{u=0}^{\infty} f(u)\int_{v=-\infty}^{\infty}\exp[(c+iv)(t-u)]i\mathrm{d}v\mathrm{d}u \\
&= \frac{1}{2\pi}\int_{u=0}^{\infty} f(u)\exp[c(t-u)]2\pi\delta(t-u)\mathrm{d}u \\
&= f(t)
\end{aligned}$$

There are a few ways to take the full analytic Laplace inverse. The first is to take a lot of Laplace transforms of basic functions, and recognise the inverse Laplace transform when you see it (as in section 2.7). The most straightforward way to do this, apart from by using a mathematics program such as Mathematica, is to use a table of known inverse Laplace transforms, [70] for instance. The second way is to use contour integration as described in [3]. I will present an example of Laplace inversion for a function with a branch point, but no isolated singularities, in section B.1.

3.3.1 Asymptotic results

Full analytic inversion of a Laplace transform is often unnecessary, as we only need an approximation of the Laplace transform in a particular limit. Consider a function $f(t)$ and its Laplace transform $\tilde{f}(s)$. The limits $t \to 0$ and $t \to \infty$ of $f(t)$ can be investigated directly with the initial and final value theorems. An interesting derivation of these results using inequalities can be found in [19], however the common way these are shown is by using the first law of calculus, taking the Laplace transform of a differential and using integration by parts.

$$\begin{aligned}\mathcal{L}\left[\frac{\mathrm{d}f(t)}{\mathrm{d}t}\right] &= \int_0^\infty \exp[-st]\frac{\mathrm{d}f(t)}{\mathrm{d}t}\mathrm{d}t \\ &= [\exp[-st]f(t)]_0^\infty + s\tilde{f}(s) \\ &= s\tilde{f}(s) - f(0)\end{aligned}$$

assuming that $\exp[-st]f(t) \to 0$ as $t \to \infty$. Taking the limit $s \to \infty$

$$\lim_{s\to\infty} \mathcal{L}\left[\frac{\mathrm{d}f(t)}{\mathrm{d}t}\right] = 0$$

assuming that $\lim_{s\to\infty} \exp[-st]\frac{\mathrm{d}f(t)}{\mathrm{d}t} \to 0$. This then gives the initial value theorem

$$\lim_{s\to\infty} s\tilde{f}(s) = \lim_{t\to 0} f(t)$$

Taking the limit $s \to 0$

$$\begin{aligned}\lim_{s\to 0}\mathcal{L}\left[\frac{\mathrm{d}f(t)}{\mathrm{d}t}\right] &= \int_0^\infty \frac{\mathrm{d}f(t)}{\mathrm{d}t}\mathrm{d}t \\ &= f(\infty) - f(0)\end{aligned}$$

which gives the final value theorem

$$\lim_{s\to 0} s\tilde{f}(s) = \lim_{t\to\infty} f(t)$$

It should be noted that final value theorem can give spurious results for the limit, if that limit does not exist. Being aware of the singularities and branch points of the function gives us a way to obtain asymptotic forms for the inversion and avoid this problem. Assuming there are no branch points we can get the asymptotic form of $f(t)$ for $t \to \infty$ by noticing that the singularity with the least

negative $\Re[s]$ will have the smallest damping effect from $\exp[s_j t]$, and therefore be dominant at $t \to \infty$.

$$\lim_{t\to\infty} f(t) \approx \exp[s_1 t] C_{-1} \tag{3.11}$$

where s_1 is the singularity with the least negative real part, and C_{-1} is the coefficient of the first inverse term in the Laurent expansion of $f(t)$ at s_1 (see appendix B). It is possible to get pairs of singularities with the least smallest $\Re[s]$, and these are indicative of an oscillatory function, for example

$$\begin{aligned}\mathcal{L}[\sin(t), t, s] &= \frac{1}{1+s^2} \\ &= \frac{1}{(1+is)(1-is)}\end{aligned}$$

When a function has a branch point, then the same contour integral can be done as in section B.1 with contributions from the singularities.

3.3.2 Series expansion of Laplace transforms

If we could get the series expansion for the Laplace transform about the point we are interested in, we could invert each term individually. Various examples of such methods are given in [19]. In section 3.3.1 we noted that the final value theorem needs the limit $s \to 0$ of the Laplace transform, which leads us neatly to the Taylor series expansion. If the Laplace transform is analytic and all the moments of the probability distribution exist we can write the expansion of the Laplace transform about $s \to 0$ as a Taylor series.

$$\begin{aligned}g(s) &= \int_{t=0}^{\infty} \exp(-st) p(t) \mathrm{d}t \\ &= \sum_{n=0}^{\infty} \frac{s^n}{n!} \left.\frac{\mathrm{d^n} g(s)}{\mathrm{d}s^n}\right|_{s\to 0} \\ &= \sum_{n=0}^{\infty} \frac{s^n}{n!} \left.\int_{t=0}^{\infty} (-t)^n \exp(-st) p(t) \mathrm{d}t\right|_{s\to 0} \\ &= \sum_{n=0}^{\infty} \frac{(-1)^n s^n}{n!} \int_{t=0}^{\infty} (t)^n p(t) \mathrm{d}t \\ &= \sum_{n=0}^{\infty} \frac{(-1)^n s^n}{n!} \mu_n\end{aligned}$$

where μ_n is the nth moment of $p(t)$, $\mu_n = \int_0^\infty t^n p(t)\mathrm{d}t$.

An example which will be useful later in the thesis is the Taylor expansion of a function with a heavy tail and some infinite moments [34]. The Taylor series works up to the last finite moment (μ_{N-1}), and the next term that must be included is the singular term which comes from the first diverging moment (μ_N) We have to be quite careful at this point not to apply the Taylor series where it is not applicable. We do this by ignoring the prefactors for now and simply asking the power of the term we must include. Following the same logic as the Taylor series, the powers of s we have is

$$s^N \left.\frac{\mathrm{d}^\mathrm{N} g(s)}{\mathrm{d}s^N}\right|_{s\to 0} = s^N \left.\int_{t=0}^{\infty} (-t)^N \exp(-st)p(t)\mathrm{d}t\right|_{s\to 0}$$

Making a change of variable $y = st$

$$\begin{aligned} s^N \int_{t=0}^{\infty} (-t)^N \exp(-st)p(t)\mathrm{d}t &= (-1)^N s^N \int_{y=0}^{\infty} \left(\frac{y}{s}\right)^N \exp(-y)p\left(\frac{y}{s}\right)\frac{\mathrm{d}y}{s} \\ &= (-1)^N s^{-1} \int_{y=0}^{\infty} y^N \exp(-y)p\left(\frac{y}{s}\right)\mathrm{d}y \end{aligned}$$

We note that as $s \to 0$ the argument in $p(t)$ becomes very large, so we use the tail of the distribution $p(t \to \infty) \approx At^{-\gamma}$

$$(-1)^N s^{-1} \left.\int_{y=0}^{\infty} y^N \exp(-y)A\left(\frac{y}{s}\right)^{-\gamma}\mathrm{d}y\right|_{s\to 0} = (-1)^N A s^{\gamma-1}\Gamma[N+1-\gamma]$$

Where $\Gamma[x]$ is the Gamma function. Note that this gives us the condition $N > \gamma$. So we can write

$$g(s) = \sum_{n=0}^{\mathrm{Int}[\gamma]} \frac{(-1)^n s^n}{n!}\mu_n + bs^{\gamma-1} + ...$$

We then find out what this constant is by taking the N^{th} derivative of this expansion, and taking the limit $s \to 0$ and matching powers of s with the full

form using the integral we have just done.

$$\begin{aligned}
\frac{\mathrm{d}^{\mathrm{N}}g(s)}{\mathrm{d}s^N} &= \int_{t=0}^{\infty}(-t)^N \exp(-st)p(t)\mathrm{d}t \\
bs^{\gamma-1-N}\prod_{n=1}^{N}(\gamma-n) &= (-1)^N A s^{\gamma-1-N}\Gamma[N+1-\gamma] \\
b &= \frac{(-1)^N A\Gamma[N+1-\gamma]}{\prod_{n=1}^{N}(\gamma-n)} \\
&= \frac{(-1)^N A\Gamma[N+1-\gamma]\Gamma[\gamma-N]}{\Gamma[\gamma]} \\
&= A\Gamma[1-\gamma]
\end{aligned}$$

For demonstration purposes, we will transform the Pareto distribution $p(t) = (\gamma-1)t^{-\gamma}\Theta[t-1]$ where $2 < \gamma < 3$ and the Heaviside theta is used to ensure $t \geq 1$ for normalisation purposes. The zeroth moment is

$$\int_0^{\infty} p(t)\mathrm{d}t = 1$$

and the first moment $\langle t\rangle = \frac{\gamma-1}{\gamma-2}$, and the rest are infinite. We can identify $A = \gamma - 1$ and therefore

$$\tilde{p}(s) \approx 1 - \frac{s(\gamma-1)}{\gamma-2} + (\gamma-1)\Gamma[1-\gamma]s^{\gamma-1}$$

We can invert each term back individually. The delta functions only exist at zero, and so can be safely ignored in the large t approximation.

$$\begin{aligned}
\mathcal{L}^{-1}[1,s,t] &= \delta(t) \\
\mathcal{L}^{-1}[s,s,t] &= \delta'(t) \\
\mathcal{L}^{-1}[s^{\gamma-1},s,t] &= \frac{t^{-\gamma}}{\Gamma[1-\gamma]} \\
p(t\to\infty) &\approx (\gamma-1)t^{-\gamma}
\end{aligned}$$

3.4 The sum of random variables

In this section we apply the Laplace transform to some questions posed earlier in the chapter. The pdf of the sum of two random variables is their convolution (appendix A). Using the same notation as section 3.1, we draw n random variables

$T_1, T_2, ..., T_n$ from the pdf p_1. The sum of these variables is a new random variable $S_n = \sum_{i=1}^{n} T_i$. The probability that S_n takes values between $t, t+\mathrm{d}t$ is given by the pdf $\mathcal{S}_n(t)$, and is the convolution of p_1 with itself $n-1$ times. Using convolution theorem (appendix A) we write that the Laplace transform of $\mathcal{S}_n(t)$ is the Laplace transform of p_1 to the n^{th} power. The notation for the convolution of $f(t)$ with itself $n-1$ times $= [f \star^{n-1} f](t)$ under the condition that $S_1(t) = p_1(t)$. This allows us to write down $\mathcal{S}_n(t) = [p_1 \star^{n-1} p_1](t)$. In real space this is difficult to evaluate but the Laplace transform is more compact $\tilde{\mathcal{S}_n}(s) = \tilde{p_1}^n(s)$. To find $\mathcal{S}_n(t)$ from $\tilde{\mathcal{S}_n}(s)$ we must invert the Laplace transform.

3.4.1 The sum of i.i.d random variables from a Poisson distribution

The Laplace transform of the Poissonian pdf $p(t) = \lambda \exp[-\lambda t]$ is $\frac{\lambda}{s+\lambda}$, and therefore $\tilde{\mathcal{S}_n}(s) = \frac{\lambda^n}{(s+\lambda)^n}$. This is a function with a pole of order n at $s = -\lambda$ and no branch points, which implies that the inverse Laplace transformation can be done using the Cauchy Residue Theorem as in section B.

$$\tilde{\mathcal{S}_n}(s) = \frac{\lambda^n}{(s+\lambda)^n}$$
$$\mathcal{S}_n(t) = \text{Residue of } \frac{\exp[st]\lambda^n}{(s+\lambda)^n} \text{ at } s = -\lambda$$

We can apply the Taylor series to the function $\exp[st]$ about $s = -\lambda$ to get the Laurent series expansion of the function $\frac{\exp[st]\lambda^n}{(s+\lambda)^n}$.

$$\frac{\lambda^n}{(s+\lambda)^n}\left(\exp[-\lambda t] + (s+\lambda)t\exp[-\lambda t] + ... + \frac{(s+\lambda)^{n-1}t^{n-1}}{(n-1)!}\exp[-\lambda t] + ...\right)$$
$$= \frac{\lambda^n \exp[-\lambda t]}{(s+\lambda)^n} + \frac{\lambda^n t \exp[-\lambda t]}{(s+\lambda)^{n-1}} + ... + \frac{\lambda^n t^{n-1}\exp[-\lambda t]}{(n-1)!(s+\lambda)} + ...$$

The coefficient of the $(s+\lambda)^{-1}$ term is the residue of the function, and is therefore $\frac{\lambda^n t^{n-1}\exp[-\lambda t]}{(n-1)!}$. This gives the distribution of the sum of n i.i.d random variables drawn from the Poissonian distribution to be the Gamma distribution [4]

$$\mathcal{S}_n(t) = \frac{\lambda^n t^{n-1}\exp[-\lambda t]}{(n-1)!} \tag{3.12}$$

3.4.2 Example semi-Markov process with a Poisson waiting time distribution

As has been noted in section 3.2 the interval transition probability distribution $\Phi(t)$ of a semi-Markov process is the probability distribution of the sum of random variables (the holding times) for the intervening states between the initial i and the final j taking a value less than t and that adding on the next holding time gives a random number which is larger than t. This is a sum of random variables under a number of constraints. A semi-Markov process with a Poissonian waiting time distribution is a properly Markovian process as the transition rate between states is time independent. It is however an illuminating example of the difficulties involved in solving even Markovian problems in continuous time.

Consider a system with two states as illustrated in figure 3.2.

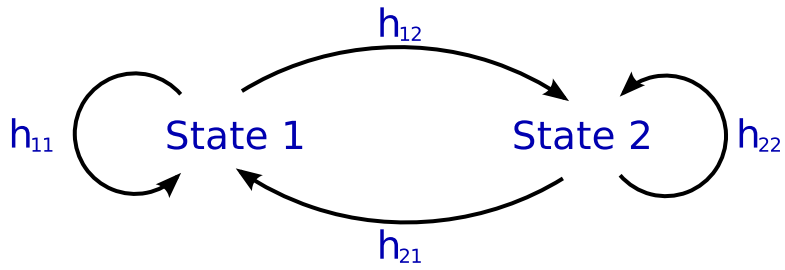

Figure 3.2 *Example two state process. Holding time distribution matrix H shown term-by-term.*

This can be described by the following matrices, where (p, q) are the transition probabilities (h_{12}, h_{21}) respectively, and (a, b, c, d) are the rates of the transitions $(h_{11}, h_{12}, h_{21}, h_{22})$ respectively.

$$P = \begin{pmatrix} p & 1-p \\ 1-q & q \end{pmatrix}$$

$$H(t) = \begin{pmatrix} a\exp[-at] & b\exp[-bt] \\ c\exp[-ct] & d\exp[-dt] \end{pmatrix}$$

$$W(t) = \begin{pmatrix} ap\exp[-at] + b(1-p)\exp[-bt] & 0 \\ 0 & dq\exp[-dt] + c(1-q)\exp[-ct] \end{pmatrix}$$

$$S(t) = \begin{pmatrix} p\exp[-at] + (1-p)\exp[-bt] & 0 \\ 0 & q\exp[-dt] + (1-q)\exp[-ct] \end{pmatrix}$$

Next the transform of the matrices is needed.

$$\int_0^\infty \exp[-st]\exp[-\lambda t]\mathrm{d}t = \frac{1}{s+\lambda}$$

$$\tilde{H}(s) = \begin{pmatrix} \frac{a}{s+a} & \frac{b}{s+b} \\ \frac{c}{s+c} & \frac{d}{s+d} \end{pmatrix}$$

$$\tilde{S}(s) = \begin{pmatrix} \frac{p}{s+a} + \frac{1-p}{s+b} & 0 \\ 0 & \frac{q}{s+d} + \frac{1-q}{s+c} \end{pmatrix}$$

$$= \begin{pmatrix} \frac{s+a(1-p)+pb}{(s+a)(s+b)} & 0 \\ 0 & \frac{s+d(1-q)+qc}{(s+c)(s+d)} \end{pmatrix}$$

$$\tilde{C}(s) \equiv P \,\square\, \tilde{H}(s)$$

$$= \begin{pmatrix} \frac{pa}{s+a} & \frac{(1-p)b}{s+b} \\ \frac{(1-q)c}{s+c} & \frac{qd}{s+d} \end{pmatrix}$$

The inverse of $\left(I - \tilde{C}(s)\right)$ gives $\tilde{\Phi}(s)$

$$I - \tilde{C}(s) = \begin{pmatrix} 1 - \frac{pa}{s+a} & -\frac{(1-p)b}{s+b} \\ -\frac{(1-q)c}{s+c} & 1 - \frac{qd}{s+d} \end{pmatrix}$$

$$|I - \tilde{C}(s)|^{-1}$$

$$= \frac{(a+s)(b+s)(c+s)(d+s)}{(s+a(1-p))(s+d(1-q))(b+s)(c+s) - b(1-p)c(1-q)(a+s)(d+s)}$$

$$\left(I - \tilde{C}(s)\right)^{-1} = |I - \tilde{C}(s)|^{-1} \begin{pmatrix} \frac{s+d(1-q)}{s+d} & \frac{(1-p)b}{s+b} \\ \frac{(1-q)c}{s+c} & \frac{s+a(1-p)}{s+a} \end{pmatrix}$$

$$\tilde{\Phi}(s) = |I - \tilde{C}(s)|^{-1} \begin{pmatrix} \frac{s+d(1-q)}{s+d} & \frac{(1-p)b}{s+b} \\ \frac{(1-q)c}{s+c} & \frac{s+a(1-p)}{s+a} \end{pmatrix} \begin{pmatrix} \frac{s+a(1-p)+pb}{(s+a)(s+b)} & 0 \\ 0 & \frac{s+d(1-q)+qc}{(s+c)(s+d)} \end{pmatrix}$$

$$= |I - \tilde{C}(s)|^{-1} \begin{pmatrix} \frac{(s+d(1-q))(s+a(1-p)+pb)}{(s+a)(s+b)(s+d)} & \frac{b(1-p)(s+d(1-q)+qc)}{(s+b)(s+c)(s+d)} \\ \frac{c(1-q)(s+a(1-p)+pb)}{(s+a)(s+b)(s+c)} & \frac{(s+a(1-p))(s+d(1-q)+qc)}{(s+a)(s+c)(s+d)} \end{pmatrix}$$

We notice that each matrix element is a cubic or lower order polynomial divided by the same quartic polynomial, $\tilde{\Phi}_4$, for each element. We also notice that the constant term cancels so we can pull out a factor of s and leave another cubic $\tilde{\Phi}_3$

$$\tilde{\Phi}_4 = (s + a(1-p))(s + d(1-q))(b+s)(c+s) - b(1-p)c(1-q)(a+s)(d+s)$$

$$\tilde{\Phi}_4 = s\tilde{\Phi}_3$$

If the three roots of $\tilde{\Phi}_3$ are denoted s_1, s_2, s_3 then $\tilde{\Phi}_4 = s(s-s_1)(s-s_2)(s-s_3)$. Each matrix element can then be split up using partial fractions. If the roots are non-degenerate, each term will become four fractions of the form $\frac{\text{constant}}{s-s_j}$. In this

case each term of $\tilde{\Phi}(s)$ can be written

$$\tilde{\phi}_{ij}(s) = \frac{c_{ij0}}{s} + \frac{c_{ij1}}{s - s_1} + \frac{c_{ij2}}{s - s_2} + \frac{c_{ij3}}{s - s_3}$$

where c_{ijk} are the constants which arise from the partial fractions. To invert the Laplace transform we recognise the form of the exponential.

$$\phi_{ij}(t) = c_{ij0} + c_{ij1} \exp[s_1 t] + c_{ij2} \exp[s_2 t] + c_{ij3} \exp[s_3 t]$$

We know that $\phi_{ij}(t)$ is the probability that if the system transitioned into state i at time $t = 0$ that it is in state j at time t. This implies that all the roots s_1, s_2, s_3 must have negative real parts in order that the probability remains less than one, and that $\lim_{t\to\infty} \phi_{ij}(t) = c_{ij0}$.

This example demonstrates that even for a pair of states, the solution of the interval probability distribution is complicated. I believe it is worthwhile quoting Ronald Howard's conclusions about the continuous time semi-Markov process from pg. 763 of [50]. "However, as we realise from even the simple examples we have considered, the possibility of using exponential transform analysis [i.e. Laplace transforms] for the solution of even very small Markovian models is slim." For more complicated models, such as the non-Markovian ASEP, we will approach them in a different way to avoid these difficulties.

3.4.3 The sum of i.i.d random variables from a non-Poisson distribution

We can prove using Laplace transforms that the sum of n i.i.d. random variables with a common distribution function $p_1(t)$ tends to n times the mean of $p_1(t)$, $\langle t \rangle$ as $n \to \infty$, if $\langle t \rangle$ is finite. This is the weak law of large numbers [36] and is a result which does not require that the distribution in question be Poissonian. Suppose random numbers $X_1, X_2, ...$ are drawn from the probability distribution with finite mean $\langle t \rangle$. The Laplace transform of the distribution is $\tilde{p}_1(s)$. The distribution of the sum of n such numbers is $\mathcal{S}_n$, and the distribution of the average of those numbers is $\mathcal{A}_n$. We know that $\mathcal{L}[\mathcal{S}_n(y), y, s] = \tilde{p}_1^n(s)$. Using the

fundamental rule of calculus we can relate $\mathcal{S}_n$ to $\mathcal{A}_n$.

$$\begin{aligned}\mathcal{A}_n(x)\mathrm{d}x &= \mathcal{S}_n(y)\mathrm{d}y \\ x &= \frac{y}{n} \\ \mathcal{A}_n(x) &= n\mathcal{S}_n(nx)\end{aligned}$$

We now want the Laplace transform $\mathcal{A}_n$ in terms of $\tilde{p}_1(s)$. We use the change of variable $y = nx$

$$\begin{aligned}\tilde{\mathcal{A}}_n(s) &= \mathcal{L}\left[\mathcal{A}_n(x), x, s\right] \\ &= n\mathcal{L}\left[\mathcal{S}_n(nx), x, s\right] \\ &= n\int_0^\infty \exp[-sx]\mathcal{S}_n(nx)\mathrm{d}x \\ &= n\int_0^\infty \exp\left[-\frac{s}{n}y\right]\mathcal{S}_n(y)\frac{\mathrm{d}y}{n} \\ &= n\frac{\tilde{p}_1^n(\frac{s}{n})}{n} \\ &= \tilde{p}_1^n\left(\frac{s}{n}\right)\end{aligned}$$

Near the origin we use the results of section 3.3.2 to write $\tilde{p}_1(s) \approx 1 - \langle t\rangle s$, which only requires that the mean and normalisation of the probability distribution exist. Therefore in the limit $n \to \infty$ can write

$$\begin{aligned}\lim_{n\to\infty} \tilde{p}_1^n\left(\frac{s}{n}\right) &\approx \lim_{n\to\infty}\left(1 - \langle t\rangle\frac{s}{n}\right)^n \\ \tilde{\mathcal{A}}_n(s) &\approx \lim_{n\to\infty}\exp[-\langle t\rangle s]\end{aligned}$$

The Laplace transform $\mathcal{L}\left[\delta[x - \langle t\rangle], x, s\right] = \exp[-s\langle t\rangle]$ therefore the inverse Laplace transform of $\tilde{\mathcal{A}}_n(s)$ is

$$\mathcal{A}_n(x) = \delta[x - \langle t\rangle]$$

This shows that even for distributions with infinite variance $p_1(t)$, the average of many samples tends to $\langle t\rangle$, or that the sum of n i.i.d random variables with a common distribution function $\phi(t)$ tends to $n\langle t\rangle$ as $n \to \infty$. It should be noted here that this also holds for finite n.

A particular non-Poissonian distribution which will be important to us is the Pareto distribution $p_1(t) = (\gamma - 1)t^{-\gamma}\Theta[t - 1]$ where $\Theta[t]$ is the Heaviside theta function ensuring that $t \geq 1$. The Laplace transform of $p_1(t)$ is $(\gamma - 1)E_\gamma(s)$ where

$\Re\{s\} > 0$ and the exponential integral function $E_\gamma(s) \equiv \int_1^\infty t^{-n} \exp[-st]\mathrm{d}t$ [4]. The distribution of the sum of n i.i.d. random variables with a common Pareto distribution function $\mathcal{S}_n(t)$ does not exist in a closed form [12]. The Laplace transform of $\mathcal{S}_n(t)$ does however, I have not been able to invert it analytically. In section 3.5.2 I demonstrate that it is possible to use numerical methods to invert the Laplace transform for a particular value of n, though first we must discuss numerical methods of inverting the Laplace transform.

3.5 Numerical inversion of a Laplace transform

Numerical methods for inverting Laplace transforms have been the subject of extensive work in computer science and mathematics, for a review of the existing work see [19], but it can also be very useful in physics. A specific example relevant to this thesis is the generation of non-uniform random variables from a particular distribution. One of the methods of generating non-uniform random numbers from a specific probability density function $p(t)$ is to use the inversion method [27]. To avoid confusion with Laplace transform inversion methods, I will refer to the inversion method to generate non-uniform random numbers as the inversion method for random numbers. For the case where the analytic form of the cumulative density function $P(t)$ is known, a uniform random number $u \in [0, 1]$ can be generated and the equation $u = P(t)$ solved for t. Ridout [69] points out that if the Laplace transform of either $p(t)$ or $P(t)$ is known, then the inversion method for random numbers can be used by numerically inverting the Laplace transform. Numerical Laplace transform inversion finds the numerical value of the pdf, $p(t)$, or the cdf, $P(t)$, for a particular value of t, as we discuss in more detail in this section. A route finder routine such as Newton-Raphson [66] can be used to find the value of t that solves the equation $P(t) = u$ to within the desired accuracy.

Numerical inversion of the Laplace transform can be done in a number of different ways [19], but the method that I use is the Fourier-series method [1], which I discuss here. The Bromwich contour integral can be rearranged to be purely along the real line. We make the change of variable $s = c + iv$, split the integral and make a change of dummy variable $v \to -v$. We also know

$\Re[\tilde{f}(c+iv)] = \Re[\tilde{f}(c-iv)]$ and $\Im[\tilde{f}(c+iv)] = -\Im[\tilde{f}(c-iv)]$.

$$
\begin{aligned}
f(t) &= \frac{1}{2\pi i}\int_{c-i\infty}^{c+i\infty} \exp[st]\tilde{f}(s)\mathrm{d}s \\
&= \frac{1}{2\pi}\int_{v=-\infty}^{\infty} \exp[(c+iv)t]\tilde{f}(c+iv)\mathrm{d}v \\
&= \frac{1}{2\pi}\left(\int_{v=-\infty}^{0} \exp[(c+iv)t]\tilde{f}(c+iv)\mathrm{d}v + \int_{v=0}^{\infty} \exp[(c+iv)t]\tilde{f}(c+iv)\mathrm{d}v\right) \\
&= \frac{1}{2\pi}\left(-\int_{v=\infty}^{0} \exp[(c-iv)t]\tilde{f}(c-iv)\mathrm{d}v + \int_{v=0}^{\infty} \exp[(c+iv)t]\tilde{f}(c+iv)\mathrm{d}v\right) \\
&= \frac{\exp[ct]}{2\pi}\int_{v=0}^{\infty} (\cos[vt] - i\sin[vt])(\Re[\tilde{f}(c-iv)] + i\Im[\tilde{f}(c-iv)])\mathrm{d}v \\
&+ \frac{\exp[ct]}{2\pi}\int_{v=0}^{\infty} (\cos[vt] + i\sin[vt])(\Re[\tilde{f}(c+iv)] + i\Im[\tilde{f}(c+iv)])\mathrm{d}v \\
&= \frac{\exp[ct]}{2\pi}\int_{v=0}^{\infty} (\cos[vt] - i\sin[vt])(\Re[\tilde{f}(c+iv)] - i\Im[\tilde{f}(c+iv)])\mathrm{d}v \\
&+ \frac{\exp[ct]}{2\pi}\int_{v=0}^{\infty} (\cos[vt] + i\sin[vt])(\Re[\tilde{f}(c+iv)] + i\Im[\tilde{f}(c+iv)])\mathrm{d}v \\
&= \frac{\exp[ct]}{\pi}\int_{v=0}^{\infty} \cos[vt]\Re[\tilde{f}(c+iv)] - \sin[vt]\Im[\tilde{f}(c+iv)]\mathrm{d}v
\end{aligned}
$$

Because the Laplace transform is blind to $t < 0$, we are at liberty to set $f(t < 0) = 0$, and functions that do not have $f(t < 0) = 0$ will still result in the same Laplace transform.

$$
\begin{aligned}
0 &= \frac{\exp[ct]}{\pi}\int_{v=0}^{\infty} \cos[vt]\Re[\tilde{f}(c+iv)] - \sin[vt]\Im[\tilde{f}(c+iv)]\mathrm{d}v \\
0 &= \cos[vt]\Re[\tilde{f}(c+iv)] - \sin[vt]\Im[\tilde{f}(c+iv)]
\end{aligned}
$$

This means we can simplify down to the form of the inverse Laplace transform that will be useful

$$
f(t) = \frac{2\exp[ct]}{\pi}\int_{v=0}^{\infty} \cos[vt]\Re[\tilde{f}(c+iv)]\mathrm{d}v \tag{3.13}
$$

To numerically integrate this we can use the trapezium rule where h is the step-size.

$$
\begin{aligned}
f(t) \approx f_h(t) &= h\left(\frac{f(0)+f(h)}{2}\right) + h\left(\frac{f(h)+f(2h)}{2}\right) + ... \\
&= \frac{h}{2}f(0) + h\sum_{k=1}^{\infty} f(kh)
\end{aligned}
$$

Practically we cannot sum infinitely many terms, so we use a truncated sum, explained below. For the inversion equation 3.13, we get the following. We also write down a truncated version.

$$f_h(t) \approx \frac{h \exp[ct]}{\pi} \left(\Re[\tilde{f}(c)] + 2 \sum_{k=1}^{\infty} \cos[kht] \Re[\tilde{f}(c + ikht)] \right) \tag{3.14}$$

$$f_{h,K}(t) \approx \frac{h \exp[ct]}{\pi} \left(\Re[\tilde{f}(c)] + 2 \sum_{k=1}^{K} \cos[kht] \Re[\tilde{f}(c + ikht)] \right) \tag{3.15}$$

There are two sources of error in these sums. Firstly there is the discretisation error from the conversion of an integral into a sum, e_d, and there is the truncation error due to the fact that we cannot compute infinitely many terms e_t. The discretisation error for the trapezium rule is of order $h^3 f''$ [66]. Davis and Rabinowitz [23] note that numerical integration by the trapezoidal rule for periodic functions gives results which are significantly more accurate than this error estimate would indicate. Abate and Whitt [1] claim that this is because the errors tend to cancel for oscillating integrands. Dubner and Abate [29] derive the discretisation error by using a Fourier series. The name in the literature for inversion by this kind of sum is therefore the Fourier-series method.

$$e_d = \sum_{k=1}^{\infty} \exp\left[-\frac{2ck\pi}{h}\right] \left(f\left(\frac{2k\pi}{h} + t\right) + \exp[2ct] f\left(\frac{2k\pi}{h} - t\right) \right)$$

For a probability density function, $f(t)$ must decay as $t \to \infty$ and must be integrable. Dubner and Abate [29] note that the error for a pdf is then of order $e_{d,\text{pdf}}$ for $h \leq \frac{\pi}{2t}$, if there is some constant C such that $f(t) \leq C$ for all t. .

$$e_{d,\text{pdf}} \sim C \exp[-\frac{c\pi}{h}] \tag{3.16}$$

This is a significantly smaller error than $h^3 f''$ as claimed.

If the Fourier transform $\tilde{f}(s)$ is not oscillatory, then the truncation error can be computed by Poisson's summation formula [23]. Dubner and Abate [29] note that there are classical results for truncation error of a Fourier series, but computing them requires knowledge of $f(t)$. In my implementation of this sum (section 3.5.1), K is not chosen in advance. The sum is stopped when the oscillations have converged to within the desired numerical accuracy ϵ. If $\tilde{f}(s)$ is not oscillatory, then the sum will oscillate due to $\cos[kht]$. This implies that the sum can be stopped when the most recent maxima, $s_{\max}$, and minima $s_{\min}$ of the sum satisfy

$s_{\max} - s_{\min} = \epsilon$. For oscillatory $\tilde{f}(s)$ there are two sources of oscillation, the slowest one determining the most recent maxima and minima. The example in section 3.5.1 computes fragments of the sum on parallel cores, which means that we can no longer identify local maxima and minima. I use the less robust method of finding the sum of a large number of recent terms $s_N = 2\frac{h\exp[ct]}{\pi}\sum_{k=r-N}^{r}\cos[kht]\Re[\tilde{f}(c+ikh)]$ where r is the most recent term added, and terminating the sum when $s_N < \epsilon$.

Appropriate choices of K, h, c can be found by trial and error, though K can be set dynamically as described above. In this thesis we use numerical Laplace transform inversion on probability distributions. The knowledge of $e_{d,\text{pdf}}$ and the condition $h \leq \frac{\pi}{2t}$ allows us to set limits and relations to h, c; for instance we can set $\frac{c}{h} = 1000$ to control the discretisation error. We can then systematically reduce h from an upper limit of $h \leq \frac{\pi}{2t}$ until the values of the sums have converged to within the desired accuracy, see section 3.5.2 and appendix D for examples.

There is another interesting version of the Fourier inversion sum ([1], equation 3.6).

$$F_{h,K}(t) \approx \frac{ht}{\pi} + \frac{2}{\pi}\sum_{k=1}^{K}\frac{\sin[kht]}{k}\Re[\tilde{f}(-ikh)] \tag{3.17}$$

This is very useful for the inversion method for random numbers, as the Laplace transform of the pdf is put in, and the cdf at those values is returned. This allows it to be used directly in a numerical root finder algorithm as described above. Equation 3.14 is more useful for us in two ways. Firstly, the Laplace transform only has to be well defined for $s \geq 0$. Secondly, later in this thesis we will want $\mathcal{L}^{-1}[\tilde{p}(W|s), s, t]$ and use $\int_0^W p(W'|t)\mathrm{d}W'$ in the inversion method for random numbers, however if we were to use a Laplace inversion method which gives us the cdf from the the Laplace transform of the pdf, the inverse Laplace sum returns $\int_0^t p(W|t')\mathrm{d}t'$.

3.5.1 Routine for numerical inversion

We will now examine the method I used for numerical Laplace transform inversion based on the work of the previous sections. The methods as presented in the literature require a multi-precision computing environment to numerically invert Laplace transforms, moreover one which can handle special functions in complex variables. Abate and Whitt [2] note that "special measures" are required to deal

with round-off error in limited precision environments, and through experience, I have found that this is true. I therefore present my numerical Laplace inverter ($\mathcal{L}^{-1}[\tilde{f}(s), s, t]$ for a particular value of t) in Mathematica. It uses parallel cores to compute fragments of the sum in equation 3.14. A programming language must be used that allows for high precision computing, and can evalutate the necessary functions with complex arguments. C++ requires special measures to allow for arbitrary precision evalutation, and currently does not have a reliable way of computing the exponential integral function with complex arguments, which is why I chose Mathematica.

deltak is the number of terms to compute at each step. The value of the complete sum at the end of each step is stored in *storesum*. Since we are adding *deltak* terms each step, we have to use the less robust method of checking when the maximum and the minimum of the last number of steps have converged to the desired accuracy, as discussed in section 3.5. $Bshift = c$ from equation 3.14 which is the $\Re\{s\}$ of the vertical part of the Bromwich contour, to the right of all singularities. The desired accuracy is *epsilon*.

The example below has $\frac{c}{h} = 1000$ to control the discretisation error, as discussed in section 3.5. I chose to set the example number of terms to store to be $storenumber = 250$, as this covers a large number of oscillations of the example function.

```
(*Required libraries for parallel evaluation of sums using ParallelSum*)
Needs["SubKernels`LocalKernels`"]
Needs["SubKernels`RemoteKernels`"]

(*Adjustable input parameters for the summation*)
(*Number of parallel cores to launch*)
cores = 10
(*Number of terms to compute for each step of ParallelSum*)
deltak = 250
(*Prefactor for h found by trial and error*)
hprefactor = 0.001
(*Prefactor for c to minimise discretisation error for a pdf*)
cprefactor = 1000.0
(*Desired accuracy*)
epsilon = 1.0*10^-5
(*Number of recent terms for storage to check convergence to within epsilon*)
storenumber = 250

(*Example parameters for the particular example Laplace transform*)
g = 2.5`20
t = 10.2`20
n = 6

(*Create slaves for ParallelSum*)
LaunchKernels[cores]
```

```
(*stepsize h and Bromwich contour shift Bshift ( = c) computed*)
h = hprefactor/t
Bshift = cprefactor h

(*Particular function to be inverted, denoted LTFn[s_, parameters]*)
(*Complex variable s*)

(*Example function with parameters n, g*)
LTFn[s_, n_, g_] := ((-1 + g) ExpIntegralE[g, s/n^(1/(g - 1))])^n

(*Initial private variables*)
(*switch == 1 -> while loop continues, switch == 0 -> exits while loop*)
switch = 1
(*Initial sum index*)
kmin = 1
(*sum index at end of first step*)
kmax = deltak
(*The position to replace next in storesum is storesum[storecounter] *)
storecounter = 1

(*Initialisation of storage for storenumber recent terms*)
Array[storesum, storenumber]
For[i = 1, i <= storenumber, i++, storesum[i] = i]

(*First term k = 0*)
sum = N[Re[LTFn[Bshift, n, g]], 20]

(*Each term in the sum for k > 0 is given by*)
Term[k_,h_,T_,Bshift_,g_]:=2 Cos[k h T] N[Re[LTFn[Bshift + i k h, g]], 20]

While[switch == 1,
(*Compute deltak terms of the sum*)
partsum = ParallelSum[Term[k,h,T,Bshift,g], {k, kmin, kmax}];
(*Update full sum*)
sum = sum + partsum;
(*New values of k for next step*)
kmin = kmax + 1;
kmax = kmin + deltak;
(*Overwrite oldest sum stored in storesum*)
storesum[storecounter] = sum; storecounter++;
If[storecounter > storenumber, storecounter = 1, 0];
(*If Maximum - Minimum < target accuracy break out of while loop*)
If[Max[Array[storesum, deltak]] - Min[Array[storesum, deltak]] < epsilon,
switch = 0, switch = 1]]

(*Result.*)
pdf=N[h Exp[Bshift t] sum/Pi,20]

(*Free slaves for ParallelSum*)
CloseKernels[]
```

3.5.2 Sum of power law distributed random numbers

To demonstrate the usefulness of numerical Laplace transform inversion we can investigate the sum of N independent identically distributed random variables drawn from the power law distribution of the form $p_1(t) = (\gamma - 1)t^{-\gamma}\Theta[t-1]$. It is a non-trivial function $\mathcal{S}_{\gamma,N}(T)$ where $T = \sum_{i=1}^{N} t_i$ and does not exist in a closed form [12]. We can consider the renormalised variable

$$X = \frac{\sum_{i=1}^{N}(t_i - \langle t \rangle)}{N^{\frac{1}{\gamma-1}}} = \frac{T}{N^{\frac{1}{\gamma-1}}} - \langle t \rangle N^{\frac{\gamma-2}{\gamma-1}} \tag{3.18}$$

where $\langle t \rangle$ is the mean of $p_1(t)$. The distribution of X, $W_N(X)$ has a stable distribution in the limit of $N \to \infty$

$$\lim_{N\to\infty} W_N(X) = \frac{1}{(\gamma-1)\pi} \int_{t=0}^{\infty} \exp[-at] \cos\left[t^{\frac{1}{\gamma-1}} X + bt\right] t^{\frac{2-\gamma}{\gamma-1}} \mathrm{d}t \tag{3.19}$$

where $a = -(\gamma-1)\Gamma[1-\gamma]\cos\left[\frac{(\gamma-1)\pi}{2}\right]$ and $b = (\gamma-1)\Gamma[1-\gamma]\sin\left[\frac{(\gamma-1)\pi}{2}\right]$ [71] for $2 < \gamma < 3$. It should be pointed out here that X is allowed to be negative, and has a minimum value $W_{\min} = N^{\frac{\gamma-2}{\gamma-1}}(1 - \langle t \rangle)$ as the smallest allowed value of each pick t_i is one. We know from section 3.4.3 the distribution of the partially normalised variable $V = \frac{T}{N^{\frac{1}{\gamma-1}}}$, $P_{\gamma,N}(V)$ can be related to $\mathcal{S}_{\gamma,N}(T)$ by

$$P_{\gamma,N}(V) = N^{\frac{1}{\gamma-1}} \mathcal{S}_{\gamma,N}(N^{\frac{1}{\gamma-1}} V) \tag{3.20}$$

We also know that its Laplace transform $\tilde{P}_{\gamma,N}(s)$ can be related to $\tilde{\mathcal{S}}_{\gamma,N}(s)$ by

$$\tilde{P}_{\gamma,N}(s) = \tilde{\mathcal{S}}_{\gamma,N}\left(\frac{s}{N^{\frac{1}{\gamma-1}}}\right) \tag{3.21}$$

We can find $P_{\gamma,N}(V)$ for finite N, make the axis shift to X and verify the stable distribution limit. We should note that the smallest allowed value of V is $V_{\min} = N^{\frac{\gamma-2}{\gamma-1}}$. We proceed by taking the Laplace transform $\tilde{P}_{\gamma,N}(s)$ and inverting it. The Laplace transform $\mathcal{S}_{\gamma,N}(T)$ is

$$\begin{aligned} \mathcal{S}_{\gamma,N}(T) &= \left(\mathcal{L}[p_1(t), t, s]\right)^N \\ &= \left((\gamma-1)E_\gamma(s)\right)^N \qquad \text{for } \Re\{s\} > 0 \end{aligned}$$

where $E_\gamma(s)$ is the exponential integral function defined by

$$E_\gamma(s) = \int_1^\infty \frac{\exp[-st]}{t^\gamma} \mathrm{d}t$$

This means the Laplace transform we wish to invert is

$$\tilde{P}_{\gamma,N}(s) = \left((\gamma-1)E_\gamma\left(\frac{s}{N^{\frac{1}{\gamma-1}}}\right)\right)^N \quad \text{for } \Re\{s\} > 0 \tag{3.22}$$

$P_{\gamma,N}(V)$ is a probability distribution spread over the positive real line, and therefore has a global maximum and can never be negative. This means we can use the error estimate in equation 3.16. We see that the error is controlled by the ratio $\frac{c}{h}$ and for convenience I set $\frac{c}{h} = 1000$ in the simulations. As in the example of numerical Laplace transform inversion in appendix D we have to systematically reduce $h < \frac{1}{V}$ to ensure the sum converges properly. We find that setting $h = \frac{1}{1000V}$ is sufficient in the region $[V_{\min} + 0.001, 100.0]$ (data not shown). Here I compute a range of $V = \{V_1, V_2, ...\}$, and therefore I used the result of the previous sum when setting the desired target accuracy, epsilon, $\text{epilon}_k = 0.001 P_{\gamma,N}(V_{k-1})$, with an initial epsilon of 1×10^{-6}. This does not provide the actual error on the sum, it merely ensures that the sum has converged, so we approximate the error in the following way. Allow the sum to dynamically set its cuttoff value K, and then continue summing to an upper limit which is a multiple of K, $8K$ for instance. Any convergence to the true value past the chosen K can then be seen, and the error estimated as the modulus of the difference between the sum at K and $8K$.

The distributions $P_{\gamma,N}(V)$ for $N = \{6, 25, 100, 250, 1000\}$ were found, and the shift $V \to X$ was taken to give the distributions $W_N(X)$, which can be plotted against the asymptotic limit $W(X)$. The time taken to complete each point depended on N, x but ranged from 1×10^1 to 1×10^3 seconds. The log log plot (figure 3.3a) shows that the distributions have the same power law tail behaviour as the asymptotic limit even for small N. The linear plot around the origin (figure 3.3b) shows that $W_N(X)$ does indeed tend to $W(X)$ as N is increased. We note here that it would probably be faster, more accurate and less complicated to directly simulate this by adding the correct number of random variables together, and we will come to a similar conclusion when we use numerical Laplace transform inversion again in chapter 5. As a test, I computed the error on the sum for $N = 250$, in the manner described above, and the error bars are smaller than the size of the points.

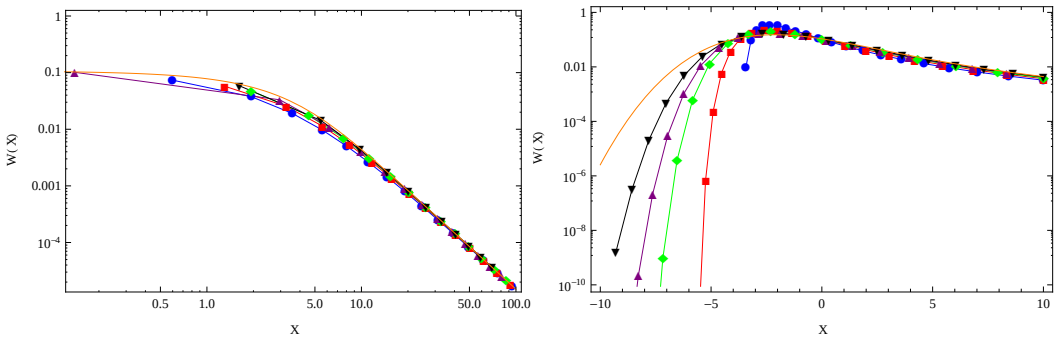

(a) (b)

Figure 3.3 *$W_N(X)$ for $\gamma = 2.5$, ($N = 6$: Blue circles), ($N = 25$: Red squares), ($N = 100$: Green diamonds), ($N = 250$: Purple upwards pointing triangles), ($N = 1000$: Black downwards pointing triangles), (Stable distribution $W(X)$: Orange line). Figure 3.3a is a log log plot showing that the tail of the distributions $W_N(X)$ tends quickly to the tail of the asymptotic distribution $W(X)$ even for small N. Figure 3.3b is a log linear plot showing where the discrepancy between the distributions $W_N(X)$ and $W(X)$ lies, that it persists even for large N, but $W_N(X)$ is clearly tending to $W(X)$ as N increases.*

3.6 Chapter summary

In this chapter we have reviewed some of the mathematical framework which addresses stochastic processes in continuous time. The renewal and semi-Markov processes do not require Poissonian time distributions, and are therefore suited to discussing non-Markovian processes. The renewal process will be useful in chapter 5, however we saw that solving semi-Markov processes analytically can become very complicated. It is for this reason that in the next chapter, when we investigate the non-Markovian ASEP further, we will use numerical methods. We also saw that one of the most frequently occurring questions when investigating renewal or semi-Markov processes is the sum of a number of random variables, which we investigated using convolution theorem. To do this we needed to explore Laplace transforms and complex contour integration, and showed that analytic Laplace transform inversion is useful, but can become prohibitively difficult. We then investigated numerical Laplace transform inversion and used it to investigate the sum of i.i.d random variables drawn from a power law distribution with finite mean and infinite variance. As with renewal processes, numerical inversion of Laplace transforms to solve problems involving the sum of random variables will also appear again in chapter 5.

Chapter 4

A non-Markovian TASEP

In previous chapters we discussed the importance of driven diffusive systems in non-equilibrium statistical physics, in particular the TASEP on a ring as a paradigmatic example. The Markovian TASEP, and some of the many results from the literature, were presented in chapter 2. We noted that a Poissonian waiting time distribution makes the TASEP Markovian as no other distribution has the required memoryless property. We then saw the example of a non-Markovian TASEP where the non-Poissonian waiting time distribution was a gamma function. The fact that there was no outstanding qualitative difference between this and the basic Markovian TASEP, in particular no new condensation phenomena, leads us in this chapter to consider an entirely different class of waiting time distributions, those with power law tails. We will briefly discuss the semi-Markov process and the renewal process in the context of solving the non-Markovian TASEP analytically. We will then investigate the non-Markovian TASEP numerically, observe an interesting condensation effect and attempt to predict how this affects the system in the thermodynamic limit.

4.1 The non-Markovian TASEP

In this section we define the model that we will use to investigate non-Markovian effects in the Totally Asymmetric Simple Exclusion Process (TASEP). It mirrors the definition used in section 2.8 and Gorissen and Vanderzande [42] for the Gamma distributed non-Markovian ASEP.

The non-Markovian TASEP is a one dimensional lattice of L sites which

contain $N < L$ particles which have the mutual exclusion property, an illustration of which is given in figure 4.1. Particles may only move to an adjacent site and we also restrict them to move in one direction only, which by convention we take to be to the particle's right. The lattice has periodic boundary conditions, ensuring that when a particle moves off the final site it appears on the initial site, which can be thought of as the TASEP on a ring. The process is in continuous time which we implement using the waiting time algorithm described in chapter 2 and reiterated here. Initially each particle is assigned a time to its first attempted move which is a random variable drawn from the waiting time distribution $p_1(t)$. Once that time has elapsed that particle moves if that transition is allowed, or remains stationary if it is blocked. The particle is then assigned a new time which is the sum of its current time and another random variable drawn from the waiting time distribution $p_1(t)$. We can see that the time of the n^{th} attempted move of a particular particle is the sum of n independent random variables drawn from the common probability distribution $p_1(t)$, the distribution of this is $\mathcal{S}_n(t)$ as discussed in chapter 3. We call this time the "particle clock time" as it can be thought of as an alarm clock for that particle; when it rings, the particle makes an attempt to move.

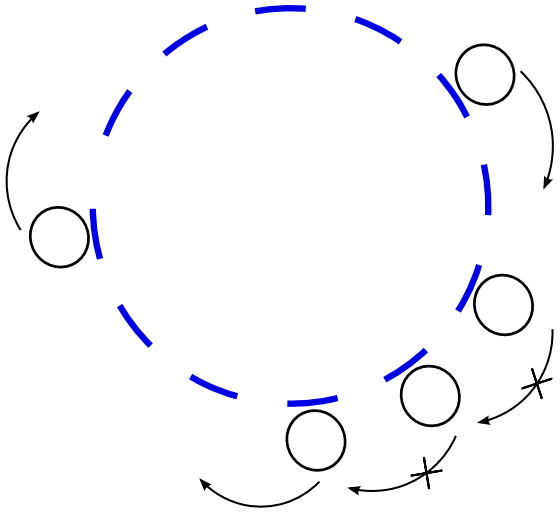

Figure 4.1 *A cartoon of the TASEP with periodic boundary conditions. Particles: circles, allowed moves: arrows, prohibited moves: arrows with crosses through them. A duplicate of figure 1.2*

If the waiting time distribution is non-Poissonian, the TASEP on a ring is non-Markovian (see section 2.7). In this thesis we will investigate the effect of having a waiting time distribution with a power law tail. When I refer to the non-Markovian TASEP without specifying the waiting time distribution, the default waiting time is Pareto distributed $p_1(t) = (\gamma - 1)t^{-\gamma}\Theta[t-1]$ where $\Theta[x]$ is the

Heaviside theta function ensuring that $t \geq 1$.

4.2 Non-Markovian TASEP as a renewal or semi-Markov process

In this section we attempt to apply the renewal and semi-Markov processes from chapter 3 to the analytic solution of the non-Markovian TASEP. In the case where the non-Markovian TASEP has a single particle, this is both an example of a semi-Markov process and a renewal processes coupled to a counter recording the particle's location.

In the case where $N = 1$, the non-Markovian TASEP is a renewal process. The probability that the particle will have moved exactly n spaces by time t is given by $\int_{t'=0}^{t} \mathcal{S}_n(t')\mathrm{d}t'$, where $S_n(t)$ is the distribution of the sum of n independent identically distributed (i.i.d) random variables drawn from a common distribution, here $p_1(t)$, as discussed in chapter 3. For $N > 1$ the time of the n^{th} attempted move of a particle will be a random variable distributed according to $\mathcal{S}_n(t)$, but this may not correspond to its location as now particles may interact and block each-other. The non-Markovian TASEP corresponds to N concurrent renewal processes which are coupled to N position counters. As renewal theory deals with a single renewal process, and has no way of taking into account the interaction of the position counters, it will not let us construct a full analytic solution of the non-Markovian TASEP.

The non-Markovian TASEP with n particles can be written in the language of semi-Markov processes by considering the state of the system to be the location of the particle. The Markov transition matrix for the semi-Markov process with a single particle is

$$p_{ij} = \begin{cases} 1 \text{ for } j = i + 1, i \neq L \\ 1 \text{ for } j = L, i = 1 \\ 0 \text{ otherwise} \end{cases}$$

where the sites are labelled i, j. The waiting time matrix is

$$w_{ij}(t) = \begin{cases} p_1(t) \text{ for } p_{ij} = 1 \\ \infty \text{ otherwise} \end{cases}$$

We see that for an infinite lattice the matrices become infinitely large, and may be impossible to handle analytically. We see however that multiple particles complicates matters further by having N copies of the single particle process whose positions interact. This semi-Markov process would need some way of including the mutual exclusion interaction. This would require knowledge of where the upstream particle is and what time it has drawn, whereas all we have are the probabilities that a particle is in a particular site at a particular time, with a particular waiting time. If mean field theory was valid here, we could ignore the correlations between particles and express the interaction as a probability, as we did computing the steady state flux in chapter 2. This means that we cannot solve the non-Markovian TASEP analytically using this semi-Markov process framework alone. I have not attempted to solve the ZRP using this method, but multiple particles would require multiple interacting versions of the single particle process, as above. We will consider the relationship between the non-Markovian ZRP and the non-Markovian TASEP further in chapter 7.

Instead of the states of the semi-Markov process corresponding to sites, they could correspond to the configurations of the lattice $\mathcal{C}$. $\mathcal{C}$ is a list of the occupation numbers of the sites τ_i, $\mathcal{C} = \{\tau_1, \tau_2, ..., \tau_L\}$, where τ_i is zero if site i is unoccupied and one if it is occupied. The waiting times between sites would not be random variables drawn from $p_1(t)$, but the difference between the smallest particle clock time at the current move, and the smallest particle clock time at the next move. We could use the probability that a recurrent event occurs at time t, $U(t) = \sum_{i=0}^{\infty} \mathcal{S}_i(t)$. We can write $U_i(t)$ is the probability that particle i makes an attempt at time t, and therefore write $U_N(t) = \sum_{i=0}^{N} U_i(t)$ to get the probability that any particle makes an attempt at time t. The probability distribution governing transitions between states is then the probability that particle i has an event at time t given that the previous event was particle j attempting to move at time t', $U_{ij}(t, t')$, though this is not a distribution I know how to write down. Even if it could be found, and this re-interpretation of the semi-Markov process does not assist us as it suffers from the same limitations as the single particle problem; for large lattices the matrices become hard to use.

4.3 Simulating the non-Markovian TASEP

We have seen in the previous section the difficulty in solving the semi-Markovian TASEP analytically, and so we proceed numerically. I wrote a program to

simulate the non-Markovian TASEP in C++ using the waiting time algorithm and drawing power law distributed random variables using the inversion for random numbers [27]. For the case where the analytic form of the cumulative density function $P(t)$ is known, as it is for the Pareto distribution, a uniform random number $u \in [0, 1]$ can be generated and the equation $u = P(t)$ solved for t. We generate random numbers using the Mersenne-Twister algorithm.

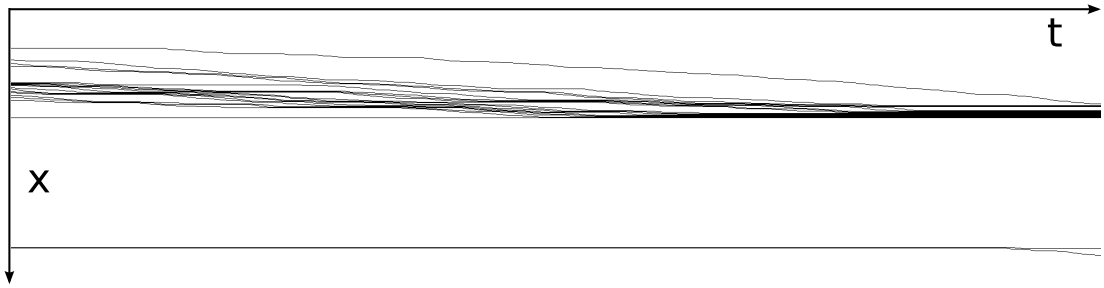

Figure 4.2 *Illustration of particles on the lattice in the process of forming a condensate*

Plotting the radial distribution functions (figure 4.3), as discussed in section 2.2, we immediately notice the characteristic property of the semi-Markovian TASEP; the appearance of condensation. We do not observe numerically a sharp crossover for finite L between condensation and a more free flowing state like the Markovian steady state as we increase γ though we will argue below that for the power law decay parameter $\gamma > 3$, we do not see condensation effects. For $2.3 < \gamma < 3$ we do see condensation. For $\gamma < 2.3$ we cannot access the non-Markovian TASEP for reasonable L due to the speed at which the simulations run. As we discussed in chapter 2 condensations effects do not occur in the TASEP on a ring unless a form of disorder is introduced. This non-Markovian TASEP has indistinguishable particles and sites, but condensation effects are present.

For condensation to occur we need particles to stop for long enough for particles behind them to catch up, which implies that the first particle must have picked a time which, on average, must be much larger than the mean. For $\gamma > 3$ the waiting time distribution has finite mean and variance and central limit theorem applies, which implies that large deviations from the mean are exponentially suppressed. This leads us to the hypothesis that the requirement for condensation is a waiting time distribution with infinite variance i.e. $\gamma < 3$.

As a measure of comparison between this model and the Markovian TASEP on a ring, we look at the "fundamental diagram", figure 4.4. The fundamental diagram is the relationship between the flux of particles around the ring J and

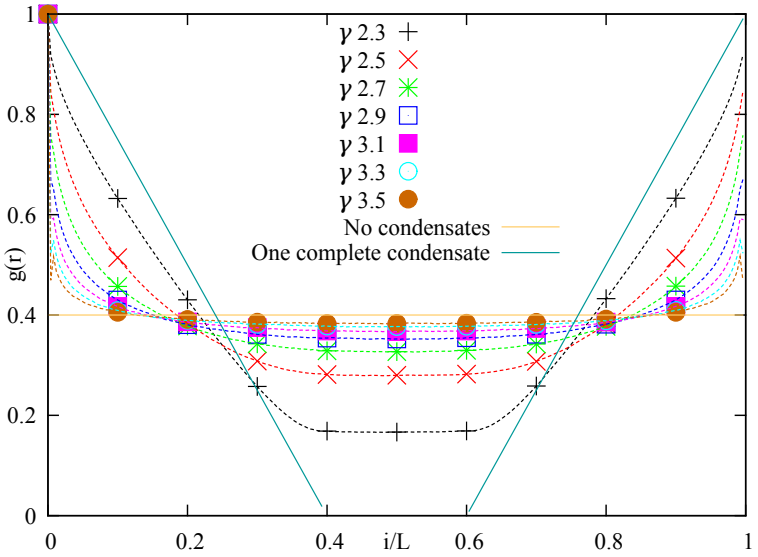

Figure 4.3 *Radial distribution function for $\rho = 0.4$, $L = 250$. The dashed lines and associated points represent the simulation data, the solid lines are the computed $g(r)$ from section 2.2 to show the expected radial distribution function in the no condensation and one complete condensate conditions. Error bars not shown as they are smaller than the size of the points.*

the density. We measure J in the simulations by choosing a site, the first site for instance, and incrementing a counter by one every time a particle leaves that site. Dividing the counter by the clock time of the last particle to attempt to move at the end of the simulation gives J. In chapter 2 we derived the relationship between flux and density for the Markovian TASEP on a ring $J = p\rho(1-\rho)$ where p is the probability that a particle makes a transition in unit time. Since p isn't constant in the non-Markovian TASEP, we approximate it by $p \approx \bar{w}^{-1} \equiv \langle t \rangle^{-1}$ where $\langle t \rangle$ is the mean of $p_1(t)$. Figure 4.4 is a plot of $J\bar{w}$ and for a Markovian TASEP on a ring we expect to see a symmetric function $\rho(1-\rho)$ irrespective of γ. $\rho(1-\rho)$ is the product of the steady state densities of particles and holes, the symmetry about $\rho = 0.5$ being indicative of particle-hole symmetry.

We see that as we decrease γ particle hole symmetry is increasingly broken, and we also notice that even taking into account $\langle t \rangle$, as we decrease γ we decrease the flux. In figure 4.5 we can see that as we increase L we also decrease the flux. I claim that it becomes a power law eventually, and I discuss this in more depth in section 6.9.

A condensate is stationary on the lattice, due to being blocked by an immobile particle. The presence of condensates will therefore decrease the flux. The

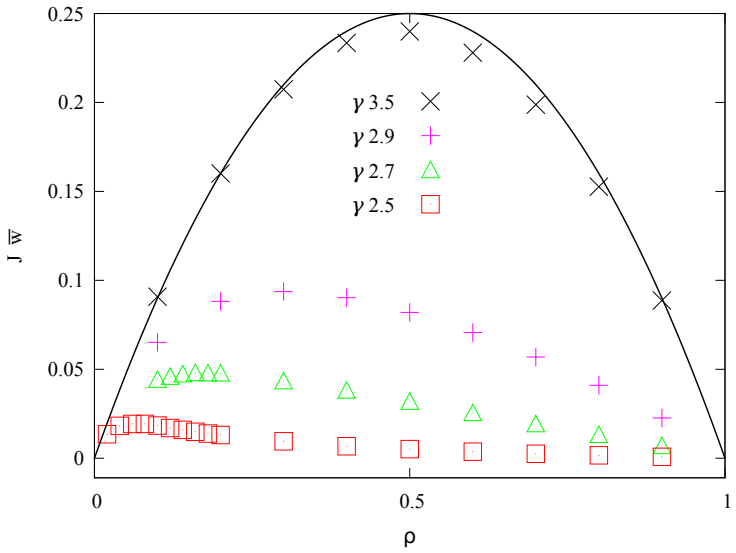

Figure 4.4 *Fundamental diagram (flux density plot) for semi-Markovian TASEP on a ring $L = 500$. Markovian steady state result $J\bar{w} = \rho(1-\rho)$ shown for comparison: black line.*

decrease of the flux with increasing L and/or decreasing γ is indicative of an increasing fraction of time spent in the condensed state.

4.4 Full spatial condensation in the non-Markovian TASEP

The characteristic property of the simulations of the non-Markovian TASEP we have discussed previously in this chapter is the presence of condensation without the presence of disorder. Moreover we find that the condensates we see are not finite fractions of the total number of particles co-existing with a "background fluid" of particles as in the ZRP, but these are condensates which contain all the particles on the lattice; which we call spatially complete condensates. They are caused by a particular particle picking a time large enough to allow all other particles on the lattice to catch up. For convenience we call spatially complete condensates *full condensates* and the particle at the front of a full condensate the *pack-leader*. The full condensate starts to exist when all particles on the lattice become blocked by the pack-leader. I detect them in simulations by checking, once a particle has moved, how far away the next upstream particle is. If that particle is $L-N$ places away, then all the particles on the lattice are in consecutive spaces, and a full spatial condensate exists. The condensate ends when the time

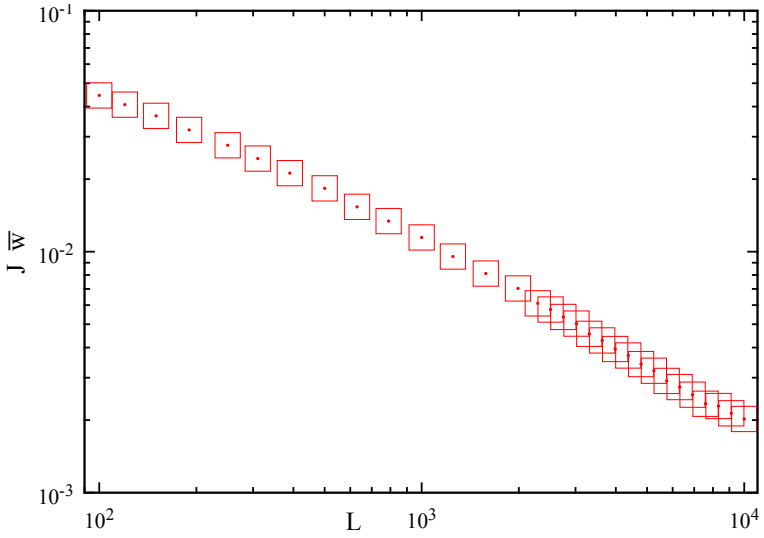

Figure 4.5 *Decreasing flux with increasing L for $\gamma = 2.5$, $\rho = 0.1$*

chosen by the pack-leader elapses and it moves off.

We wish to investigate the properties of full condensates as they may prove to be the key to understanding the thermodynamic limit of the non-Markovian TASEP. If we know the timescale associated with the lifetime of a full condensate, and the timescale corresponding to the time between full condensates, then we can predict the fraction of time we are in the stationary jam (also known as the *solid phase*) as opposed to the more free-flowing state where particles are not fully condensed (the *fluid phase*). The fraction of time that a full condensate has been present for at the end of a simulation is given the symbol f, and we look at the behaviour of f against γ and lattice size L in figure 4.6.

Figure 4.6 is inconclusive about what number the fraction of time spent in the condensate, f, tends towards. This data is compatible with all $f \to 1$ and $f \to c(\gamma, \rho)$ where $c(\gamma, \rho)$ is some finite fraction $0 < f < 1$ which is in principle dependent on γ, ρ.

The two lifetimes associated with a full condensate are; the lifetime of the solid phase, l_s and the lifetime of the fluid phase l_f. Over the range of L accessible from the simulations, the averages $\bar{l}_s$ and $\bar{l}_f$ are straight lines on a log-log plot, i.e. they have a power law dependence on L. Fitting a power law of the form aL^b to $\bar{l}_s$ and $\bar{l}_f$, we can find the exponents b. In figure 4.7 we see b plotted against γ for fixed $\rho = 0.1$.

Figure 4.7 shows us that the exponent of L corresponding to the mean fluid lifetime is always larger than for the mean inter-condensate lifetime. Expressing

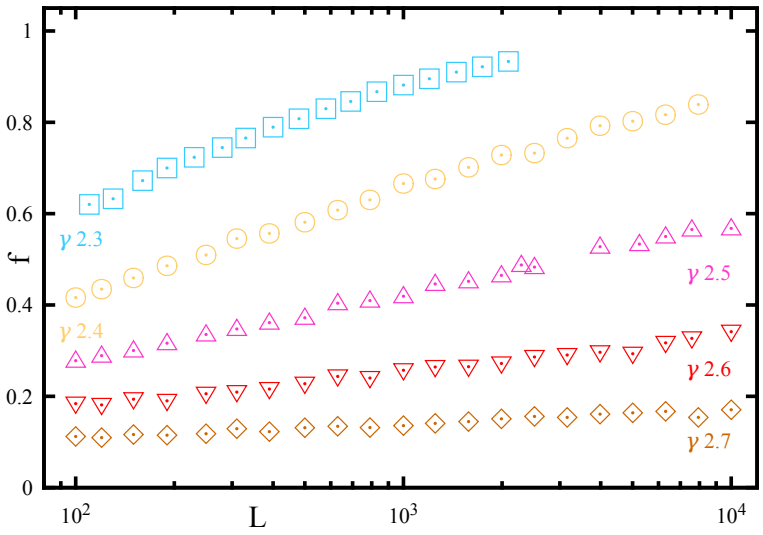

Figure 4.6 *Fraction of time spent in the full condensate for* $\rho = 0.1$

this separation of timescales mathematically we can see that using these we can predict that the fraction of time spent in the full condensate, f, tends to one in the thermodynamic limit.

$$\begin{aligned} \bar{l}_s &\sim L^\alpha \\ \bar{l}_f &\sim L^\beta \\ f &\sim \frac{L^\alpha}{L^\alpha + L^\beta} \\ &\to 1 \end{aligned}$$

Since $\alpha > \beta$. If $f \to 1$ then the full condensate is nearly always present in the thermodynamic limit, so the condensate is complete in space and time.

4.5 Predicting the presence of the full condensate

In the previous section we saw that in the non-Markovian TASEP there existed spatially complete condensates, and we concluded from the simulations that these full condensates existed for a fraction of time that approaches one in the thermodynamic limit. We will now attempt to see if this accords with a mathematical understanding of the system.

The condensation of the system from the fluid to the solid phase once a pack-leader has been chosen is illustrated in figure 4.8. As can be seen in the figure, the

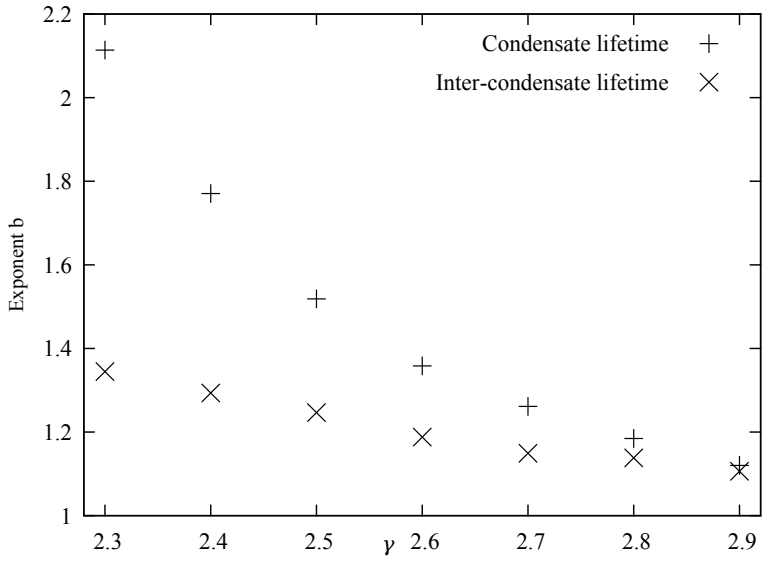

Figure 4.7 *Exponent b of the fitting of $\bar{l}_s$ and $\bar{l}_f$ to aL^b as a function of γ for $\rho = 0.1$*

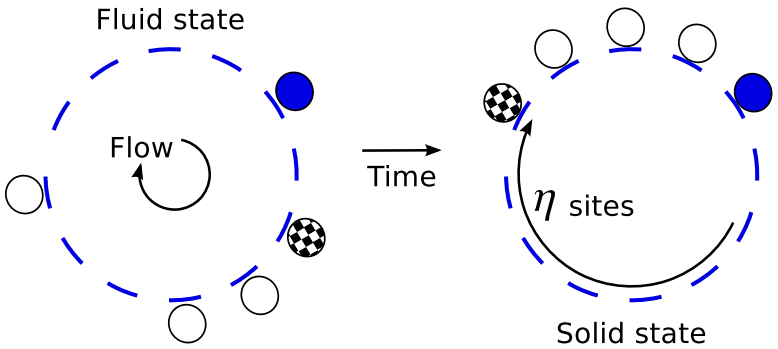

Figure 4.8 *A cartoon of the formation of a spatially complete condensate once the pack-leader (filled circle) is chosen. The last particle in the full condensate (circle filled with chessboard pattern) must travel η spaces to reach its resting place.*

time picked by the pack leader must be greater than the time required to get the last particle in the full condensate to its final location. If the last particle must move η sites to come to its resting place at the back of the condensate, the time picked by the pack leader must be greater than the sum of the η waiting times picked by the last particle, i.e. the sum of η samples from $p_1(t)$, $T_\eta = \sum_{i=1}^{\eta} t_i$. Technically the first move made by the last particle will be a fraction of a waiting time since at the time the pack-leader stops, the final particle has used some of its chosen waiting time, but as η becomes large we ignore this contribution.

We start with the naive picture inspired by extreme event theory. A pack leader time must be anomalously large, and therefore a rare event. We hypothesise that

a fluid phase exists which is (mostly) free flowing and can be well described by the steady state of the Markovian TASEP. Out of this a full condensate forms when the pack leader is chosen, which is a rare event. Once the pack leader moves off from the front of the condensate, the system reverts to the fluid phase.

We define the condensate ratio, R_c as measure of the existence of condensates in the system.

$$R_c = \frac{\langle T_\eta \rangle}{\tau} \tag{4.1}$$

Here $\langle T_\eta \rangle$ is the mean time for which a pack leader must be stationary to form a full condensate, and τ is the characteristic time we must wait to pick a time $\langle T_\eta \rangle$. In section 3.4.3 we saw that the weak law of large numbers implies that for $\gamma > 2$ the sum of η i.i.d random variables drawn from $p_1(t) = (\gamma - 1)t^{-\gamma}\Theta[t-1]$ is strongly peaked around $\eta\langle t \rangle$, where $\langle t \rangle$ is the mean of $p_1(t)$. Using a similar idea we can show that for $1 < \gamma < 2$, $T_\eta = \sum_{i=1}^{\eta} t_i \sim O(\eta^{\frac{1}{\gamma-1}})$.

The distribution of the sum of η i.i.d random variables drawn from $p_1(t)$ is $\mathcal{S}_\eta$. We know that $\mathcal{L}\left[\mathcal{S}_\eta(y), y, s\right] = \tilde{p}_1^{\eta}(s)$. We can use the change of variable $V = \frac{T}{\eta^{\frac{1}{\gamma-1}}}$ and the Laplace transform of the distribution of V, $P_{\gamma,\eta}(V)$, as we did in section 3.5.2 to express $\tilde{P}_{\gamma,\eta}(s)$ in terms of $\tilde{p}_1(s)$.

$$\tilde{P}_{\gamma,\eta}(s) = \tilde{\mathcal{S}}_{\gamma,\eta}\left(\frac{s}{\eta^{\frac{1}{\gamma-1}}}\right) \tag{4.2}$$

$$= \left(\tilde{p}_1\left(\frac{s}{\eta^{\frac{1}{\gamma-1}}}\right)\right)^{\eta} \tag{4.3}$$

Near the origin we use the results of section 3.3.2 to write $\tilde{p}_1(s) \approx 1 + (\gamma - 1)\Gamma[1-\gamma]s^{\gamma-1}$, which only requires that the normalisation of the probability distribution exists. Therefore in the limit $n \to \infty$ can write

$$\begin{aligned}
\lim_{\eta\to\infty} \tilde{P}_{\gamma,\eta}(s) &= \lim_{\eta\to\infty}\left(\tilde{p}_1\left(\frac{s}{\eta^{\frac{1}{\gamma-1}}}\right)\right)^{\eta} \\
&= \lim_{\eta\to\infty}\left(1 + \frac{(\gamma-1)\Gamma[1-\gamma]s^{\gamma-1}}{\eta}\right)^{\eta} \\
&\approx \lim_{\eta\to\infty} \exp[(\gamma-1)\Gamma[1-\gamma]s^{\gamma-1}]
\end{aligned}$$

This shows that the distribution $P_{\gamma,\eta}(V)$ becomes independent of η. Using conservation of probability (see section 3.4.3) we can write $\mathcal{S}_\eta(T) = \eta^{\frac{1}{\gamma-1}} P_{\gamma,\eta}(V)$,

which implies that the η dependence of the sum must be of order $\eta^{\frac{1}{\gamma-1}}$ as $P_{\gamma,\eta}(V)$ becomes independent of η as η becomes large. The intuition from extreme value theory is the sum of η samples from a distribution with no mean is dominated by the largest individual sample. The largest value of η picks from a Pareto distribution (i.e. $p_1(t)$) has an η dependency of $\eta^{\frac{1}{\gamma-1}}$ [40], so this intuition holds here.

To see how $\langle T_\eta \rangle$ behaves we want to see how the number of picks required to move the last particle to the back of the condensate, η, scales with L. We have found a way of taking into account the collisions and blockages between particles as they collapse down to the full condensate. Suppose a particle has picked a time large enough to make it a pack leader on site x. We can label the remaining particles $1, 2, \ldots, n-1$ as we encounter them going backwards around the ring. If a full condensate forms, particle i will come to rest at site $x-i$ before the pack leader moves off. We can compute the expected distance between each particle by making the assumption that the fluid phase is adequately described by the all configurations equally likely steady state of the Markovian TASEP. A lattice of L sites with a constant probability ρ of containing a particle can be considered to be L trials where the probability of success (having a particle fill that site) is ρ. The locations of the particles will be Poisson distributed, and therefore the expected spacing between successes is $\rho^{-1} = \frac{L}{N}$. Particle 1 cannot collide with anything before it comes to rest, hence it will travel $\eta_1 = 1/\rho$ on average. Particle 2 can collide with 1 in two ways. In the mean field approximation, the probability that a move is blocked, and the pick is wasted is ρ. This will generate an extra $\rho\eta_2$ steps. Particle 2 may also become blocked due to particle 1 picking an uncommonly large time, so becoming a temporary blockage. The number of extra steps generated will be proportional to the size of the largest pick made by particle 1. In total $\eta_2 = \frac{2}{\rho} + \rho\eta_2 + a\left(\eta_1^{\frac{1}{\gamma-1}}\right)$, where a is some constant of proportionality. The same logic will apply for $\eta_i = \frac{i}{\rho} + \rho\eta_i + a\left(\eta_{i-1}^{\frac{1}{\gamma-1}}\right)$ for $1 < i < n-1$. Iterating this and keeping only the terms to the power of $\frac{1}{\gamma-1}$ or larger we find that the scaling of $\eta_{n-1} = \eta \sim L + \mathrm{O}(L^{\frac{1}{\gamma-1}})$.

The probability that we draw a time larger than $\langle T_\eta \rangle$ from $p_1(t)$ is $\langle T_\eta \rangle^{1-\gamma}$. The expected number of picks until we draw such a time is then $\langle T_\eta \rangle^{\gamma-1}$. Then the expected time until any one of the n movers picks such a time will then be

$\tau = \frac{\langle t \rangle \langle T_\eta \rangle^{\gamma-1}}{\rho L}$.

$$\begin{aligned} R_c &= \frac{\langle T_\eta \rangle}{\tau} \sim L \langle T_\eta \rangle^{2-\gamma} \\ &\sim \begin{cases} L \left(\eta \langle t \rangle\right)^{2-\gamma} & \text{for } \gamma > 2 \\ L \left(\eta^{\frac{1}{\gamma-1}}\right)^{2-\gamma} & \text{for } 1 < \gamma < 2 \end{cases} \\ &\sim \begin{cases} L^{3-\gamma} & \text{for } \gamma > 2 \\ L^{\frac{2-\gamma}{\gamma-1}} & \text{for } 1 < \gamma < 2 \end{cases} \end{aligned} \tag{4.4}$$

As the exponent of L in R_c is positive for $1 < \gamma < 3$ we always expect condensates in the thermodynamic limit. This mirrors what we see in simulations.

4.6 Moving beyond the naive model

In this section we see that although the model used in the last section is sufficient to account for the observed presence of condensates in the parameter region $\gamma < 3$ of the non-Markovian TASEP, it fails in a number of areas. We will see why it fails, and what we would have to know in order to predict the behaviour of the system in the thermodynamic limit.

4.6.1 Expected values

The lifetime of the fluid phase l_f will be dominated by whichever of the two following timescales increases most strongly with L; the time required to pick a pack leader time (τ), or the time required to collapse particles down into a full condensate (the catch-up time C). In the previous section we assumed that the fluid phase could be well modelled by the steady state of the Markovian TASEP, i.e. that all configurations were equally likely. We used this to construct the recursive argument that led to the result that $\eta \sim L$, where η is the number of attempted moves required for the last particle of a full condensate to travel to its resting place. The sum of η picks from $p_1(t)$ in the region $2 < \gamma < 3$ is given by the weak law of large numbers (see section 3.4.3) to give the catch-up time $C = T_\eta \sim \eta \langle t \rangle \sim L$. We had $\tau = \frac{\langle t \rangle \langle T_\eta \rangle^{\gamma-1}}{\rho L} \sim L^{\gamma-2}$. In the region $1 < \gamma - 1 < 2$, so C will be the dominant contribution in $l_f \sim L$. The pack leader will pick a time drawn from the underlying Pareto distribution $p_1(t)$ conditioned on being larger

than C, $p_1(t|t \geq C) = \mathcal{N} t^{-\gamma} \Theta[t - C]$, where $\mathcal{N}$ is the normalisation constant.

$$\begin{aligned} p_1(t|t \geq C) &= \mathcal{N} t^{-\gamma} \Theta[t - C] \\ \int_{t'=0}^{\infty} p_1(t'|t' \geq C) \mathrm{d}t' &= \mathcal{N} \int_{t'=C}^{\infty} t'^{-\gamma} \mathrm{d}t' \\ (\gamma - 1) C^{\gamma - 1} &= \mathcal{N} \end{aligned}$$

The mean of $p_1(t|t \geq C)$ is

$$\begin{aligned} \int_{t'=0}^{\infty} t' p_1(t'|t' \geq C) \mathrm{d}t' &= (\gamma - 1) C^{\gamma - 1} \int_{t'=C}^{\infty} t'^{1-\gamma} \mathrm{d}t' \\ &= (\gamma - 1) C^{\gamma - 1} \frac{C^{2-\gamma}}{\gamma - 2} \\ &= \frac{\gamma - 1}{\gamma - 2} C \\ &= \langle t \rangle C \end{aligned}$$

where $\langle t \rangle$ is the mean of $p_1(t)$. The mean pack leader time will therefore be proportional to C. The lifetime of the condensate will then be the time picked by the pack leader minus the time required to get the final particle to catch up. Since both times are proportional to L, the lifetime of the condensate will also be proportional to L. We can see in figure 4.7 that this is a severe under-estimate of the solid lifetime.

The fraction of time spent in the condensate could then be written as

$$f \sim \frac{l_s}{l_s + l_f}$$

which implies that the fraction of time spent in the condensate tends to a finite fraction, in principle dependent on γ or ρ. This is contrary to the separation of timescales that we encountered in figure 4.7.

4.6.2 Distributions

It is possible that simply by looking at the mean of the distributions, we are not getting the full picture, and so we attempt to gain some more understanding by looking at the distributions directly. The statistics that may be relevant to the prediction of the fraction of time spent in the condensate are the pack-leader lifetime, the condensate lifetime and the inter-condensate lifetime. If there is

a simple argument which allows us to explain these distributions, we expect it to be an extreme value argument. The relevant extreme value distribution for an underlying distribution with a power-law tail is the Fréchet distribution [40]. We also expect that if the distributions have power-law tails, then the decay parameter of said tails will equal the underlying decay parameter γ, since both the distribution of the sum, and the distribution of the largest of a number of i.i.d random variables from a Pareto distribution have the decay parameter γ. In this section we investigate these two expectations.

In this thesis we assume that a set of numbers that are the product of simulations (the condensate lifetimes for instance) can be thought of as random variables drawn from some underlying distribution. We plot the distributions by turning them into a empirical cumulative distribution function, or sum-polygon (see appendix E). We could construct a histogram normalised by the number of datapoints which would be an empirical approximation to the probability distribution, however the number of datapoints per bin in the tail vanishes, and so the histogram can be a poor approximation to the tail of a probability distribution. I have found that the tails of distributions are better represented graphically with the empirical c.d.f.

Consider the largest of a number of η random variables drawn from $p_1(t) = (\gamma - 1)t^{-\alpha}$, T. The cumulative probability distribution $P(V)$ where $V = \frac{T}{\eta^{\frac{1}{\alpha-1}}}$ is the Fréchet distribution, [40]

$$P\left(V\right) = \exp[-V^{-\alpha+1}] \tag{4.5}$$

We can fit the Fréchet distribution to the data by using α and η as fitting parameters. If the Fréchet distribution is a good fit to the data we expect $\alpha \approx \gamma$, as that corresponds to the sum of Pareto distributed random variables with the correct decay parameter. α, η are found by minimising the sum of squares of the residuals between the data and the fit, where the residuals are given by $\log[\text{Data}(x)] - \log[\text{Fit}(x)]$.

In figure 4.9 we see that all the lifetimes have long tails, so we can rule out exponential decays. We see that the Fréchet distribution fits best at the lower end of the distribution and appears to overestimate tail end, i.e. underestimate the decay parameter. We also notice that the inter-condensate time distribution appears to have a kink which we have not been able to explain. We see visually that the Fréchet distribution seems to fit well to pack-leader lifetime and poorly

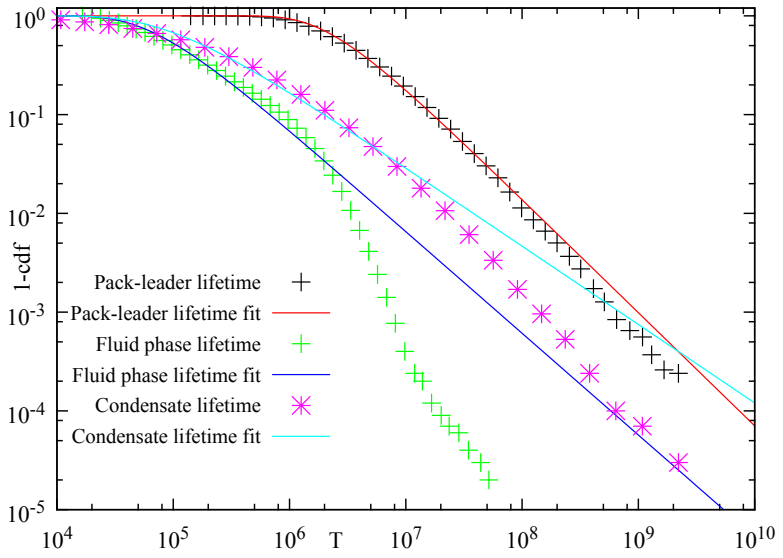

Figure 4.9 *The distributions of the condensate and fluid lifetimes and the distribution of times picked by the pack-leader for* $\gamma = 2.4$, $\rho = 0.1$, $L = 6300$ *with fitted Fréchet distributions, for* 100000 *full spatial condensates.*

for the others. To measure the goodness of fit of the Fréchet distributions to the data we can use the single sample Kolmogorov-Smirnov statistic, as discussed in appendix E. The critical KS value for a data set with n values is $\frac{1.22}{\sqrt{n}}$ [77]. A KS test statistic below the critical KS value means that the data is compatible with being drawn from the fit with significance level $p = 0.05$. We use $\gamma = 2.4, \rho = 0.1, L\epsilon(100, 7940)$ to test the Fréchet distribution for a range of L, and we saw that the Fréchet distribution is indeed a consistently poor fit to the condensate lifetime and inter-condensate lifetime distributions, and the goodness of fit of the Fréchet distribution to the pack leader time becomes increasingly poor with increasing L, see figure 4.10a. In figure 4.10b we see that the fitted decay parameter α under-predicts γ more strongly for increasing L.

We have seen that a simple minded extreme value argument will not allow us to explain the distributions seen numerically. We now address the second expectation, that the decay parameter of the observed distributions will equal γ since both the distribution of the sum, and the distribution of the largest of a number of i.i.d random variables from a Pareto distribution share the same decay parameter as the Pareto distribution itself γ. We can use the techniques laid out in [18] and discussed in appendix E.2 to compute the most likely decay parameter α and the value at which the distribution best fits a power law, x_m. The best fit was obtained at the very tail of the distributions tested, and the tail

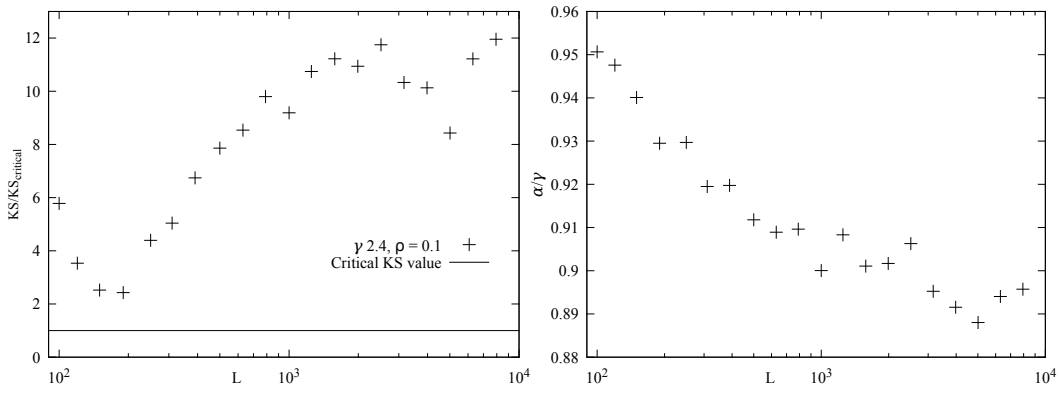

(a) *Increasing poorness of fit of the Fréchet distribution*

(b) *Decay parameter of the tail*

Figure 4.10 *Fitting the Fréchet distribution to the pack leader time distribution for* $\gamma = 2.4,\ \rho = 0.1$

was always consistent with being drawn from a power law distribution with a significance of $p < 0.05$. In figure 4.11 we can see that the computed α oscillated strongly, which we believe to be due to the small number of data points which form the tail of the distributions. α for the pack-leader time and the condensate lifetime oscillates around γ, and the fitted form for the inter-condensate time is consistent with α tending towards γ for increasing L. The form of the decay to γ was chosen as it appeared to be a good fit. The fitting was performed in gnuplot and the errors are the asymptotic standard errors it obtains from the final variance-covariance matrix. This is at least re-assuring that the tail of the distribution appears to have the predicted decay parameter γ, although this does not assist us with computing the mean of the distributions due to the non-universal behaviour of the distributions away from the tail. We will see in chapter 6 examples of distributions which have a tail of γ and a mean which grows with a non-universal power of L.

4.6.3 Interacting condensates

The naive model we postulated requires that a condensate forms, dissolves into the fluid state, and reforms again. If there are some number of particles which have not moved between consecutive condensates, then the pack leader of the second condensate was chosen during the lifetime of the preceding one, and the condensates cannot be said to be independent. In figure 4.12 we see that the fraction of condensates which interact increases with increasing L, the effect being stronger at lower γ. From this we expect all condensates to interact in the

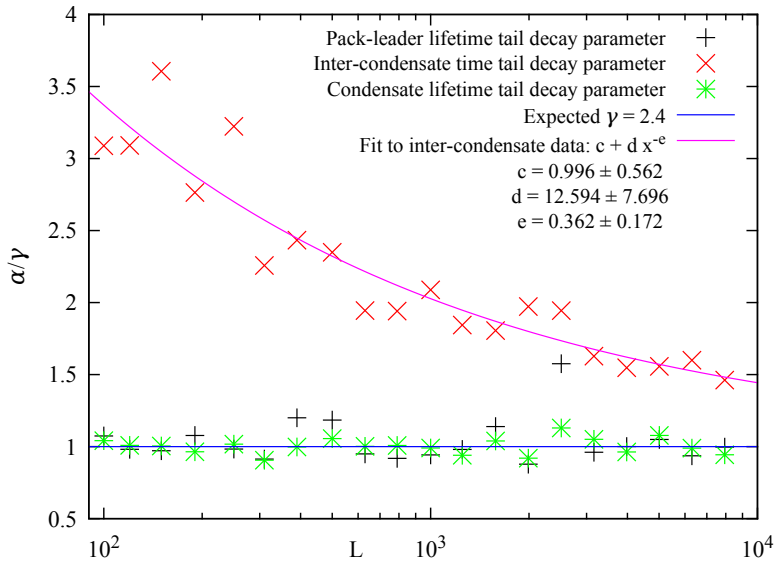

Figure 4.11 *Decay parameter of the tail v.s. expected γ and L for $\gamma = 2.4$, $\rho = 0.1$*

thermodynamic limit, and so we need a new mathematical model which includes the effects of pack leaders being chosen within the preceding condensate.

To probe the interaction of condensates numerically we require very high L and/or values of γ closer to 2, as we saw in figure 4.12. The speed of the continuous time Monte Carlo simulations with the waiting time algorithm becomes prohibitively slow at high L and/or low γ, i.e. when the effects of interacting condensation becomes stronger. From figure 4.7 we saw that the characteristic timescales of the condensate grow super-linearly with L, and that this effect is stronger at γ close to 2. This implies that for large L and/or small γ particles are more likely to be blocked by larger times. Since particles which are blocked continue to make attempted moves by drawing attempt times from the waiting time distribution, the proportion of random variables which results in a successful move shrinks. The generation of random numbers can be computationally costly, and if we can avoid generating random numbers which result in failed moves, then we should. Specifically I use the Mersenne-Twister method for efficient generation of random numbers, which turns out to be the limiting step in terms of the performance of my simulations. A algorithm in which prohibited events does not occur is known as "rejection free". In chapter 5 we create such a rejection free algorithm by using the blocked waiting time distribution $p(W;T)$.

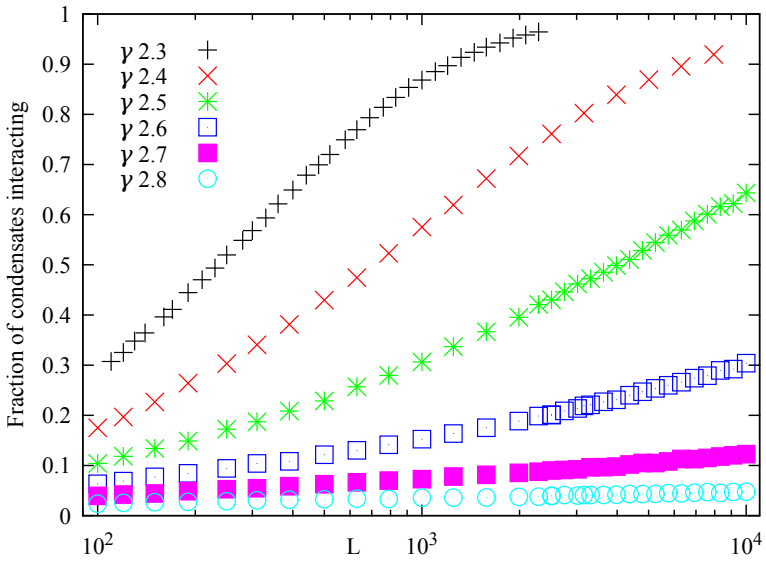

Figure 4.12 *Fraction of condensates interacting for* $\rho = 0.1$

4.7 Chapter summary

In this chapter we investigated a non-Markovian TASEP with a power law distributed waiting time. We discussed using either the renewal process or the semi-Markov process to solve the non-Markovian TASEP analytically, and came to the conclusion that neither of these methods would assist us unless there is only a single particle on the lattice. We investigated the non-Markovian TASEP numerically and our choice of the waiting time distribution reveals a condensation effect whereby every particle on the lattice is blocked by a single particle. We call this spatially complete condensate a full condensate. This condensate is different to the examples from the literature discussed in chapter 2 as it requires no disorder in the particles or sites, and unlike the non-Markovian ZRP it contains all particles, rather than a finite fraction of them. There appears to be a separation of timescales between the lifetime of a full condensate and the time between full condensates, which leads us to the conclusion that the full condensate exists for a fraction of time approaching one in the thermodynamic limit, thus the condensate can be said to be complete in space and time. We attempt to provide a simple mathematical explanation of the observed behaviour using the idea that a time large enough to create a full condensate must be a rare event, and therefore once the pack leader moves off, the entire condensate will return to the fluid state. This fails in a number of areas, not least predicting that the thermodynamic limit will have a finite fraction of time spent in the full condensate. We discover

that we need the blocked waiting time distribution $p(W;T)$, where T is the time a particle is blocked for and W is the time after T has elapsed that the particle makes its first successful move attempt. The blocked waiting time distribution is a way of integrating out the unsuccessful attempts to move, and therefore can be used to create a rejection free simulation algorithm. We find that, in the thermodynamic limit, pack-leaders of consecutive condensates are chosen in the previous condensate, and therefore $p(W;T)$ is necessary to make any further progress on the mathematics too.

Chapter 5

A rejection-free algorithm for simulating blocked stochastic systems

In the previous chapter we investigated the non-Markovian TASEP and found that a question arose in two different contexts: given a particle makes a transition to a site at time zero, and the site in front is occupied until time T, what is the probability that the particle makes its first successful move at time $T + W$, $p(W;T)$? The distribution $p(W;T)$ we refer to as the blocked waiting time distribution. In this chapter we find the Laplace transform of the blocked waiting time distribution $p(W;s)$. Using the methods we discussed in chapter 3 we can find a general approximation for $p(W;T)$ for large T, $p_A(W;T)$, directly from $p(W;s)$. Numerical Laplace transform inversion on $p(W;s)$ for a range of T shows us that $p_A(W;T)$ is a good fit to $p(W;T)$ even for relatively small T. This allows us to create an accelerated simulation algorithm for the non-Markovian TASEP which is rejection-free. We test the accelerated algorithm against the standard Monte Carlo method and show for T larger than some T_c the two simulation methods give results which are statistically compatible with the expectation that they are samples drawn from the same underlying distribution, i.e. that the two simulation methods produce equivalent results.

5.1 The blocked waiting time distribution

In simulations of the TASEP, a particle can become blocked until time T. We wish to solve the following renewal problem (see chapter 3); given that there is a renewal process where the inter-event time is given by the waiting time distribution $p_1(t)$, what is the probability that the first event that occurs after T happens at time $T + W$? Cast in terms of moving particles in the TASEP this is: given a particle makes a transition to a site at time zero, and the site in front is occupied until time T, what is the probability that the particle makes its first successful move at time $T+W$, $p(W;T)$? This is an interesting problem in itself, but as we saw in the previous chapter, a solution to it is necessary to make any more progress with the non-Markovian TASEP.

Let t_i be the i^{th} pick from $p_1(t)$. The particle makes a number of failed attempts to move, n, such that $\sum_{j=1}^{n} t_j < T$ and $\sum_{j=1}^{n+1} t_j > T$. The probability that the last pick of some sequence of arbitrary length occurs at time t is $\omega(t)$, which is related to the last event of a sequence of n events occurring at time t, $\mathcal{S}_n(t)$ (discussed at length in section 3.4) with the number of events n integrated out. Using this, the probability that the first successful attempt happens at $T + W$ given that $W > 0$ and the last of some sequence of picks before it happens at time $t < T$ is given by $\omega(t)p_1(T+W-t)$. It is irrelevant when the last preceding event happens as long $t < T$, so we integrate this out to get the distribution of the first successful $p(W;T)$.

$$p(W;T) = \int_{t'=0}^{T} \omega(t')p_1(T + W - t')\mathrm{d}t'$$

We can see that this is a convolution if we define $\lambda[a;b] \equiv p_1(a + b)$. The convolution is blind to W, so we can Laplace transform on T safely. We use the notation $\mathcal{L}[p(t),t,s] = p(s)$. We note that $\lambda[s;0] \equiv \mathcal{L}[p_1(t),t,s]$

$$p(W;T) = \int_{t'=0}^{T} \omega(t')\lambda[T - t';W]\mathrm{d}t' \tag{5.1}$$

$$p(W;s) = \omega(s)\lambda[s;W] \tag{5.2}$$

$\omega(s)$ can be written down with a renewal argument (see chapter 3, page 467 of [36]). Consider a series of consecutive picks from p_1, with the first pick defining $t = 0$. The probability that the last pick of some sequence occurs at t is $\omega(t)$, which can be written in terms of another sequence finishing sooner. The delta

function comes from the pick at $t = 0$, which can be thought of as the last pick of some preceding behaviour.

$$\omega(t) = \int_{t'=0}^{t} \omega(t')p_1(t-t')\mathrm{d}t' + \delta(t) \tag{5.3}$$

$$\begin{aligned}\omega(s) &= \omega(s)p_1(s) + 1 \\ &= \frac{1}{1-p_1(s)}\end{aligned} \tag{5.4}$$

So the Laplace transform of the blocked waiting time distribution $p(W;s)$ is given by

$$p(W;s) = \frac{\lambda[s;W]}{1-\lambda[s;0]} \tag{5.5}$$

5.1.1 Poissonian blocked waiting time distribution

In this section we check the result for the Poisson distribution. Since the Poisson distribution has the memoryless property, the probability that an event occurs at $T+W$ given that it did not occur in T is the probability that the event occurs at time W, see chapter 2, i.e. $p(W;T) = p(W) = \lambda\exp[-\lambda W]$. We can show that the blocked waiting time distribution has this property.

$$\begin{aligned}\tilde{p_1}(s) &= \frac{\lambda}{\lambda+s} \\ \lambda[s;W] &= \frac{\lambda\exp[-\lambda W]}{\lambda+s} \\ p(W;s) &= \frac{\lambda[s;W]}{1-\lambda[s;0]} \\ &= \frac{\lambda\exp[-\lambda W]}{s}\end{aligned}$$

The inverse Laplace transform $\mathcal{L}^{-1}[s^{-1},s,t] = 1$ so the Poissonian blocked waiting time distribution is

$$p(W;T) = \lambda\exp[-\lambda W] \tag{5.6}$$

as required.

5.1.2 Power law waiting time distribution

We wish to find the blocked waiting time distribution for the power law waiting time distribution $p_1(t) = (\gamma - 1)t^{-\gamma}\Theta[t-1]$ that we used in the non-Markovian TASEP. Power laws occur in various subjects including in queueing problems, where Laplace transform analysis of heavy tailed distributions is well established [78].

$$
\begin{aligned}
p_1(t) &= (\gamma-1)t^{-\gamma}\Theta[t-1] \\
\tilde{p_1}(s) &= (\gamma-1)E_\gamma(s) \\
\lambda[W;s] &= \begin{cases} \exp[sW](\gamma-1)E_\gamma(s) & \text{for } 0 \le W < 1 \\ \exp[sW](\gamma-1)W^{1-\gamma}E_\gamma(sW) & \text{for } W > 1 \end{cases}
\end{aligned}
$$

where $E_\gamma(s)$ is the exponential integral function defined $E_\gamma(s) \equiv \int_1^\infty \exp[-st]t^{-\gamma}\mathrm{d}t$ [4]. For $W > 1$

$$
p(W;s) \;=\; \frac{\exp[sW](\gamma-1)W^{1-\gamma}E_\gamma(sW)}{1-(\gamma-1)E_\gamma(s)}
$$

Rather than attempt the full analytic inversion, in this chapter we will show that the large blocking time, T, approximation is sufficient for our needs.

5.2 Asymptotics of the blocked waiting time distribution

We saw in the previous chapter that as L increases in the non-Markovian TASEP, the time picked by the pack-leader increases. This implies that in the thermodynamic limit, particles which are blocked by the pack-leader will be blocked for very large times, so we would like to find $p(W;T)$ in the limit of large T. Using the results of chapter 3 we can find an asymptotic form for the blocked waiting time distribution by looking at the rightmost singularity of $p(W;s)$.

The singularities of $p(W;s)$ occur at the singularities of $\lambda[s;W]$, the branch cuts of either $\lambda[s;W]$ or $\lambda[s;0]$, and when $\lambda[s;0] = 1$. Since $p(W;T)$ must be a normalisable probability distribution, there can be no singularities with $\Re\{s\} > 0$. We see that for any normalised probability distribution $\int_{-\infty}^{\infty} p_1 \mathrm{d}t = \lim_{s\to 0}\lambda[s;0] = 1$ there will always be a singularity at the origin. This means that

for any properly normalised waiting time distribution $p_1(t)$, if we can expand $p(W;s)$ about $s = 0$, as we did in section 3.3.2, and then invert the Laplace transform term by term, we can find an approximation to $p(W;T)$ as $T \to \infty$, $p_A(W;T)$.

It should be quickly noted here that we cannot use the limit rule for division to write

$$\lim_{s\to 0} p(W;s) = \frac{\lim_{s\to 0}\lambda[s;W]}{\lim_{s\to 0}(1-\lambda[s;0])}$$

as this requires that both limits $\lim_{s\to 0}\lambda[s;W]$ and $\lim_{s\to 0}\lambda[s;0]$ exist and $\lim_{s\to 0}\lambda[s;0] \neq 1$, which is not satisfied.

5.2.1 Power law waiting time distribution

For the particular case of the Pareto distributed waiting time distribution $p_1(t) = (\gamma-1)t^{-\gamma}\Theta[t-1]$ discussed above, both the numerator and the denominator have branch cuts running from $-\infty \to 0$ so we must approach $s = 0$ from $\Re\{s\} > 0$. The dominant term in the $s \to 0$ expansion is the term with the most negative power of s. We proceed by expanding out the denominator in terms of s as $s \to 0$. The series expansion of $E_\gamma(s)$ up-to order 2 (using results 6.5.3, 6.5.4, 6.5.9 and 6.5.29 from [4] or the result of section 3.3.2) is

$$E_\gamma(s) \approx s^{\gamma-1}\Gamma[1-\gamma] + \frac{1}{\gamma-1} - \frac{s}{\gamma-2} + \frac{s^2}{2(\gamma-3)}$$

The denominator is

$$1-(\gamma-1)E_\gamma(s) \approx s^{\gamma-1}\Gamma[2-\gamma] + \frac{(\gamma-1)s}{\gamma-2} - \frac{(\gamma-1)s^2}{2(\gamma-3)}$$

For $2 < \gamma < 3$ the lowest power of s is -1. We pull that term out as a common factor.

$$(1-(\gamma-1)E_\gamma(s))^{-1} \approx \frac{(\gamma-2)}{(\gamma-1)s}\left(1 + \frac{(\gamma-2)s^{\gamma-2}\Gamma[2-\gamma]}{\gamma-1} - \frac{(\gamma-2)s}{2(\gamma-3)}\right)^{-1}$$

Sufficiently close to 0 for $\gamma > 2$, $|x| < 1$ where $x = \frac{(\gamma-2)s^{\gamma-2}\Gamma[2-\gamma]}{\gamma-1} - \frac{(\gamma-2)s}{2(\gamma-3)}$ which means we can use the Maclaurin series of $(1+x)^{-1}$ to expand the denominator

of $p(W;s)$ out.

$$(1-(\gamma-1)E_\gamma(s))^{-1} \approx \frac{(\gamma-2)}{(\gamma-1)s}\left(1-x+x^2+...\right)$$

The contribution from the denominator of $p(W;s)$ with the most negative power of s is $\frac{(\gamma-2)}{(\gamma-1)s}$. Note that this expansion breaks down as $\gamma \to 2$. For $W > 1$

$$p(W;s) \overset{s\to 0}{\approx} \frac{\exp[sW](\gamma-2)W^{1-\gamma}E_\gamma(sW)}{s} \tag{5.7}$$

which can be inverted, using the recursion relation $nE_{n+1}(z) = \exp[-z] - zE_n(z)$ [4] to get

$$p(W;s) \overset{s\to 0}{\approx} \frac{(\gamma-2)W^{1-\gamma}}{s(\gamma-1)} - \frac{(\gamma-2)\exp[sW]W^{2-\gamma}E_{\gamma-1}(sW)}{(\gamma-1)}$$

We know the following two Laplace transforms.

$$\mathcal{L}[1,T,s] = s^{-1}$$
$$\mathcal{L}[p_1(T+W),T,s] = \lambda[W;s] = \exp[sW](\gamma-1)W^{1-\gamma}E_\gamma(sW) \text{ for } W > 1$$
$$\mathcal{L}^{-1}[\exp[sW]W^{1-\gamma}E_\gamma(sW),s,T] = (T+W)^{-\gamma} \text{ for } W > 1$$

Hence we can inverse the Laplace transform $p(W;s)$.

$$p(W;T) \overset{T\to\infty}{\approx} \langle t\rangle^{-1}\left(W^{1-\gamma} - (T+W)^{1-\gamma}\right) \text{ for } W > 1 \tag{5.8}$$

where $\langle t\rangle$ is the mean of $p_1(t)$, $\langle t\rangle = \frac{\gamma-1}{\gamma-2}$. We return to the discussion of this result and its normalisation in the following section.

5.2.2 Asymptotic hypothesis

In the previous section we found the asymptotic form for blocked waiting time corresponding to the Pareto distributed waiting time. In order achieve this we found an approximation for the asymptotic form for the denominator of the Laplace transform, i.e. $\omega(s)$, by expanding it about its rightmost singularity at $s = 0$. We will use that technique again here to find a more general form for the asymptotics of the blocked waiting time distribution.

We saw (equation 5.1) that the blocked waiting time distribution could be

written

$$p(W;T) = \int_{t'=0}^{T} \omega(t')\lambda[T-t';W]\mathrm{d}t' \tag{5.9}$$

and in 5.3 that the Laplace transform of $\omega(t)$ could be written in terms of the Laplace transform of the waiting time distribution $p_1(s)$.

$$\omega(s) = \frac{1}{1-p_1(s)}$$

We can use the results of section 3.3.2 to write

$$p_1(s) \overset{s\to 0}{\approx} 1 - s\langle t\rangle$$

if the mean, $\langle t\rangle$, exists. This implies that

$$\omega(s) \overset{s\to 0}{\approx} \frac{1}{s\langle t\rangle}$$
$$\omega(t) \overset{t\to \infty}{\approx} \langle t\rangle^{-1}$$

The probability that the last event of some sequence of events occurs in the time interval $t, t+\mathrm{d}t$ is $\omega(t)\mathrm{d}t$. This implies that we could think of $\omega(t)$ as the rate of occurrence of events in a recurrent sequence. Once the transients have died away, we would indeed expect the rate of occurrence of events to be the inverse of the mean time between events.

We expect that the asymptotic form for $\omega(t)$ is a valid approximation for large but finite t after the transients in it have died away. Further we expect that for sufficiently large T, the integral in equation 5.9 is dominated by the contribution where $\omega(t)$ can be approximated by $\langle t\rangle^{-1}$. We use the change of variable $u = T + W - t'$ and the definition of the survival function from chapter 3, $S_1(t) \equiv \int_t^\infty p_1(t)\mathrm{d}t = 1 - \int_0^t p_1(t)\mathrm{d}t$.

$$\begin{aligned} p(W;T) &\approx \langle t\rangle^{-1} \int_{t'=0}^{T} p_1(T+W-t')\mathrm{d}t' \\ &\approx \langle t\rangle^{-1} \int_{W}^{T+W} p_1(u)\mathrm{d}u \\ &\approx \langle t\rangle^{-1} \left(S_1(W) - S_1(T+W)\right) \end{aligned}$$

We wish to have T as a parameter, and use this as a blocked waiting time probability distribution for W, so it needs to be normalised. The integral of

the survival function is

$$\begin{aligned}\int_{W=0}^{\infty} S_1(W)\mathrm{d}W &= \int_{W=0}^{\infty}\int_{t=W}^{\infty} p_1(t)\mathrm{d}t\mathrm{d}W \\ &= \int_{t=0}^{\infty}\int_{W=0}^{t} p_1(t)\mathrm{d}W\mathrm{d}t \\ &= \int_{t=0}^{\infty} t p_1(t)\mathrm{d}t \\ &= \langle t\rangle\end{aligned}$$

We can define $z(T) \equiv \int_{W=0}^{\infty} S_1(W+T)\mathrm{d}W \equiv \int_{W=0}^{\infty}\int_{t=W+T}^{\infty} p_1(t)\mathrm{d}t\mathrm{d}W$ to find that the integral of $\langle t\rangle^{-1}\left(S_1(W) - S_1(T+W)\right)$

$$\begin{aligned}\int_{W=0}^{\infty} \langle t\rangle^{-1}\left(S_1(W) - S_1(T+W)\right)\mathrm{d}W &= \langle t\rangle^{-1}\left(\langle t\rangle - z(T)\right) \\ &= 1 - \langle t\rangle^{-1} z(T)\end{aligned}$$

Applying this as a normalisation factor allows us to write our hypothesis for the large blocking time, T, behaviour of the blocked waiting time distribution, $p_A(W;T)$.

$$p_A(W;T) = \frac{S_1(W) - S_1(T+W)}{\langle t\rangle - z(T)} \tag{5.10}$$

We will now check this works for the two examples we have investigated, the Poissonian waiting time distribution and the Paretian waiting time distribution. For $p_1(t) = \lambda\exp[-\lambda t]$, $S_1(W) = \exp[-\lambda W]$, $z(T) = \lambda^{-1}\exp[-\lambda T]$ so

$$\begin{aligned}p(W;T) &= \frac{\exp[-\lambda W] - \exp[-\lambda(W+T)]}{\lambda^{-1}\left(1 - \exp[-\lambda T]\right)} \\ &= \lambda\exp[-\lambda W]\end{aligned}$$

as required.

For $p_1(t) = (\gamma - 1)t^{-\gamma}\Theta[t-1]$, $z(T) = \frac{T^{2-\gamma}}{\gamma - 2}$ so

$$S_1(W) = \begin{cases} \exp[-\lambda W] & \text{for } W > 1 \\ 1 & \text{for } 0 < W < 1 \end{cases}$$

$$p_A(W;T) = \begin{cases} \frac{W^{1-\gamma} - (T+W)^{1-\gamma}}{\langle t \rangle - \frac{T^{2-\gamma}}{\gamma-2}} & \text{for } W > 1 \\ \frac{1-(T+W)^{1-\gamma}}{\langle t \rangle - \frac{T^{2-\gamma}}{\gamma-2}} & \text{for } 0 < W < 1 \end{cases}$$

which is indeed compatible with the result from the previous section, and is superior because it is also normalised. Plotting this in figure 5.1, we notice that there are two distinct power law regions, when $W \ll T$ $p_A(W;T) \sim W^{1-\gamma}$ and for $W \gg T$ $p_A(W;T) \sim W^{-\gamma}$. This is a decrease in the decay rate of the p.d.f for small W, which we intuitively understand as something like the measurement paradox (see section 3.1): given that the times between attempted moves occurs as a renewal process, then a time chosen at random is more likely to fall in a large inter-event waiting time than a small one, which leads to a reinforcement of the distribution for $W \ll T$. We expect the tail of the distribution to have the decay parameter γ as large W will be dominated by a single large pick before T, the distribution of which has a power law tail with decay parameter γ.

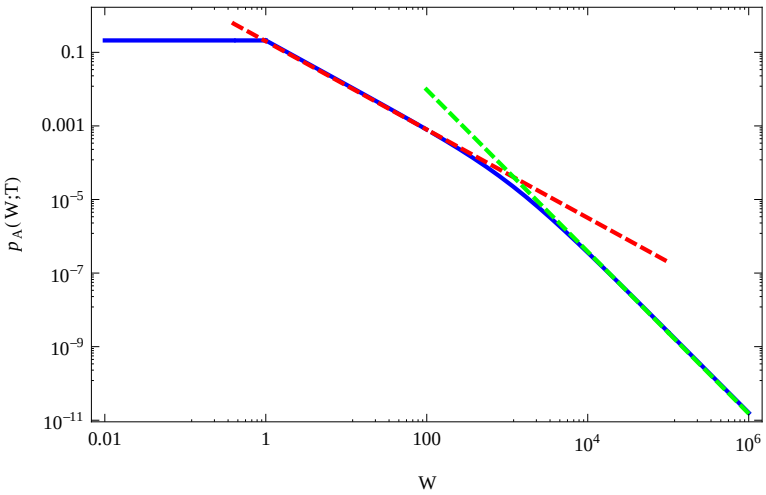

Figure 5.1 $p_A(W;T)$, $T = 1000.0$, $\gamma = 2.2$. *Note that though* $p_A(W;T)$ *appears flat for* $W < 1$ *it is slowly varying. Red dashed line: power law* $\sim W^{-1.2}$, *Green dashed line: power law* $\sim W^{-2.2}$

In the remainder of this chapter we will ascertain how good an approximation $p_A(W;T)$ is to $p(W;T)$ and for what value of T it becomes valid. In section 5.4 we will compare $p_A(W;T)$ with $p(W;T)$ obtained by numerical Laplace

transform inversion from $p(W;s)$. In section 5.5 we compare $p_A(W;T)$ with $p(W;T)$ obtained directly by sampling $p_1(t)$ until the sum of random times exceed T. In section 5.6 we present an accelerated simulation method for the non-Markovian TASEP using $p_A(W;T)$, which in section 5.7 we show is equivalent to the simulation method used in chapter 4 for a blocking time T larger than some crossover blocking time T_c.

5.3 Integrals of $p_A(W;T)$

In this section we compute some of the integrals of $p_A(W;T)$ required for the remainder of this thesis.

It is immediately obvious that the survival function $S_A(x;T)$ for $x \geq 1$ can be written

$$\begin{aligned} S_A(x;T) &\equiv \int_{W=x}^{\infty} p_A(W;T)\mathrm{d}W \\ &= \frac{x^{2-\gamma} - (x+T)^{2-\gamma}}{\gamma - 1 - T^{2-\gamma}} \end{aligned} \tag{5.11}$$

The survival function $S_A(x;T)$ for $0 < x < 1$, $T > 1$ can be written

$$\begin{aligned} S_A(x;T) &\equiv \int_{W=x}^{\infty} p_A(W;T)\mathrm{d}W \\ &= \int_{W=x}^{1} p_A(W;T)\mathrm{d}W + S_A(1;T) \\ &= \int_{W=x}^{1} \frac{1-(T+W)^{1-\gamma}}{\langle t\rangle - \frac{T^{2-\gamma}}{\gamma-2}}\mathrm{d}W + \frac{1-(1+T)^{2-\gamma}}{\gamma-1-T^{2-\gamma}} \\ &= \frac{(\gamma-2)(1-x) + (1+T)^{2-\gamma} - (x+T)^{2-\gamma} + 1 - (1+T)^{2-\gamma}}{\gamma-1-T^{2-\gamma}} \\ &= \frac{(\gamma-2)(1-x) - (x+T)^{2-\gamma} + 1}{\gamma-1-T^{2-\gamma}} \end{aligned} \tag{5.12}$$

5.3.1 Expected waiting time conditioned on $W > x \geq 1$

The blocked waiting time distribution conditioned on $W > x \geq 1$ can be written

$$p_A(W|W > x; T) = \frac{p_A(W; T)\Theta[W - x]}{S_A(x; T)} \tag{5.13}$$

$$= \frac{W^{1-\gamma} + (T + W)^{1-\gamma}}{\frac{\gamma - 1 - T^{2-\gamma}}{\gamma - 2}} \Theta[W - x] \frac{\gamma - 1 - T^{2-\gamma}}{x^{2-\gamma} - (x + T)^{2-\gamma}}$$

$$= \frac{W^{1-\gamma} + (T + W)^{1-\gamma}}{x^{2-\gamma} - (x + T)^{2-\gamma}} (\gamma - 2)\Theta[W - x] \tag{5.14}$$

The expected W for $W > x \geq 1$ and a given T, $\langle W|W > x; T\rangle$, is slightly more complicated as the integral of each individual term diverges but the sum is convergent. We replace the upper limit with Ω, take $\Omega \to \infty$ and make the change of variable $u = T + W$. We can safely set $\Omega = \infty$ for $\int_{u=T+1}^{\Omega+T} u^{1-\gamma} \mathrm{d}u$ as this integral converges regardless of Ω, and since $T << \Omega$, $\int_{u=\Omega}^{\Omega+T} u^{2-\gamma} \mathrm{d}u \to 0$.

$$\langle W|W > x; T\rangle = \int_{W=0}^{\infty} W p_A(W|W > x; T) \mathrm{d}W$$

$$= (\gamma - 2) \frac{\lim_{\Omega\to\infty} \int_x^{\Omega} W^{2-\gamma} - W(T + W)^{1-\gamma} \mathrm{d}W}{x^{2-\gamma} - (x + T)^{2-\gamma}}$$

$$\lim_{\Omega\to\infty} \int_x^{\Omega} W^{2-\gamma} - W(T + W)^{1-\gamma} \mathrm{d}W$$

$$= \lim_{\Omega\to\infty} \left(\int_x^{\Omega} W^{2-\gamma} \mathrm{d}W - \int_{u=T+x}^{\Omega+T} (u - T) u^{1-\gamma} \mathrm{d}u \right)$$

$$= \lim_{\Omega\to\infty} \left(\int_x^{\Omega} W^{2-\gamma} \mathrm{d}W - \int_{u=T+x}^{\Omega} u^{2-\gamma} \mathrm{d}u - \int_{u=\Omega}^{\Omega+T} u^{2-\gamma} \mathrm{d}u + T \int_{u=T+x}^{\Omega+T} u^{1-\gamma} \mathrm{d}u \right)$$

$$= \int_x^{T+x} W^{2-\gamma} \mathrm{d}W + T \int_{u=T+x}^{\infty} u^{1-\gamma} \mathrm{d}u$$

$$= \frac{(T + x)^{3-\gamma} - x^{3-\gamma}}{3 - \gamma} + \frac{T(T + x)^{2-\gamma}}{\gamma - 2} \tag{5.15}$$

Therefore

$$\langle W|W > x; T\rangle = \frac{\frac{\gamma-2}{3-\gamma} \left((T + x)^{3-\gamma} - x^{3-\gamma} \right) + T(T + x)^{2-\gamma}}{x^{2-\gamma} - (x + T)^{2-\gamma}} \tag{5.16}$$

5.3.2 Expected waiting time

For the expected value of W for a given T, $\bar{W}$, we can use the above result.

$$\begin{aligned}
\bar{W} &= \int_0^\infty W p_A(W;T)\mathrm{d}W \\
\frac{(\gamma-1)-T^{2-\gamma}}{(\gamma-2)}\bar{W} &= \int_0^1 W - W(T+W)^{1-\gamma}\mathrm{d}W + \int_1^\infty W^{2-\gamma} - W(T+W)^{1-\gamma}\mathrm{d}W \\
\frac{(\gamma-1)-T^{2-\gamma}}{(\gamma-2)}\bar{W} &= I_1(W,T) + I_2(W,T)
\end{aligned}$$

where

$$\begin{aligned}
I_1(W,T) &= \int_0^1 W - W(T+W)^{1-\gamma}\mathrm{d}W \\
&= \frac{1}{2} + \frac{(1+T)^{2-\gamma}(-2+\gamma+T) - T^{3-\gamma}}{(-3+\gamma)(-2+\gamma)} \\
&\approx \frac{1}{2}
\end{aligned}$$

We have already computed $I_2(W;T)$, equation 5.15

$$I_2(W;T) = \frac{(T+1)^{3-\gamma}-1}{3-\gamma} + \frac{T(T+1)^{2-\gamma}}{\gamma-2}$$

So the mean time blocked for a given waiting time T for large T is

$$\bar{W} \approx \frac{T^{3-\gamma}}{(3-\gamma)(\gamma-1)} - \frac{\gamma-2}{2(3-\gamma)} \tag{5.17}$$

We note that this grows with T though with a sub-linear power for $\gamma > 2$.

5.4 Numerical inversion of the blocked waiting time distribution

We have an asymptotic form for the blocked waiting time distribution, $p(W;T)$, in the large blocking time limit. Using the techniques described in chapter 3 we can invert the Laplace transform of $p(W;s)$ numerically to compare it against the asymptotic limit. This will allow us to see how quickly and accurately we can perform the inversion, and how large T has to be in order that $p_A(W;T)$ is a good fit to $p(W;T)$. Note that although we are interested in finding the distribution of W for a particular T, the Laplace transform took $T \to s$, so we invert the

Laplace transform by taking $s \to T$ where W is a parameter.

For an underlying waiting time distribution $p_1(t) = (\gamma - 1)t^{-\gamma}\Theta[t-1]$,

$$p(W;s) = \begin{cases} \frac{\exp[sW](\gamma-1)E_\gamma(s)}{1-(\gamma-1)E_\gamma(s)} & \text{for } 0 < W < 1 \\ \frac{\exp[sW](\gamma-1)W^{1-\gamma}E_\gamma(sW)}{1-(\gamma-1)E_\gamma(s)} & \text{for } W > 1 \end{cases}$$

and the asymptotic form as T becomes large is $p_A(W;T)$ for $W > 1$.

$$p_A(W;T) = \frac{W^{1-\gamma} - (T+W)^{1-\gamma}}{\langle t \rangle - \frac{T^{2-\gamma}}{\gamma-2}}$$

We reiterate the inversion sum, equation 3.14, here.

$$f_{h,K}(t) \approx \frac{h\exp[ct]}{\pi}\left(\Re[\tilde{f}(c)] + 2\sum_{k=1}^{K}\cos[kht]\Re[\tilde{f}(c+ikh)]\right)$$

We have to choose appropriate values for parameters of the inversion sum; position of the Bromwich contour line along the real axis, c, the step-size of the sum, h, and the number of terms to include in the sum, K. K can be chosen dynamically by stopping the sum once it has converged to within accuracy as described in section 3.5, this controls the truncation error. Since we are inverting the Laplace transform of a probability distribution, the discretisation error of the sum is proportional to $\exp[-\frac{c}{h}]$. Since we require $h < \frac{\pi}{2T}$ we set $h = \frac{1}{T}$ and $c = \frac{a}{T}$, so the discretisation error is controlled by $\exp[-a]$. We now need to find a numerically by systematically increasing it, until the sum has converged to the desired accuracy, see figure 5.2 as an example. For the range of W, T, γ that we will use, a value of $a = 10$ was found to be sufficient.

In figure 5.3 is plotted the ratio of the numerical Laplace inversion for $p(W;T)$ to the asymptotic form $p_A(W;T)$ for a range of W, T. It can be seen that the asymptotic form fits the distribution well even for relatively small T, the fit becoming better with increasing T. In figure 5.4 we show the fractional error $\Delta_f = \frac{|p(W;T)-p_A(W;T)|}{p_A(W;T)}$ and the time required to invert the Laplace transform for $\epsilon = 0.001$ and $\gamma = 2.2$. These graphs also show that the asymptotic form of the blocked waiting time distribution $p_A(W;T)$ is a good approximation to $p(W;T)$ even for small T, and the approximation improves with increasing T. The time required to perform the inversion was of order tens of seconds. We have not been able to invert the Laplace transform for values of W higher than those shown due to a numerical error of unknown origin; one possible explanation being that

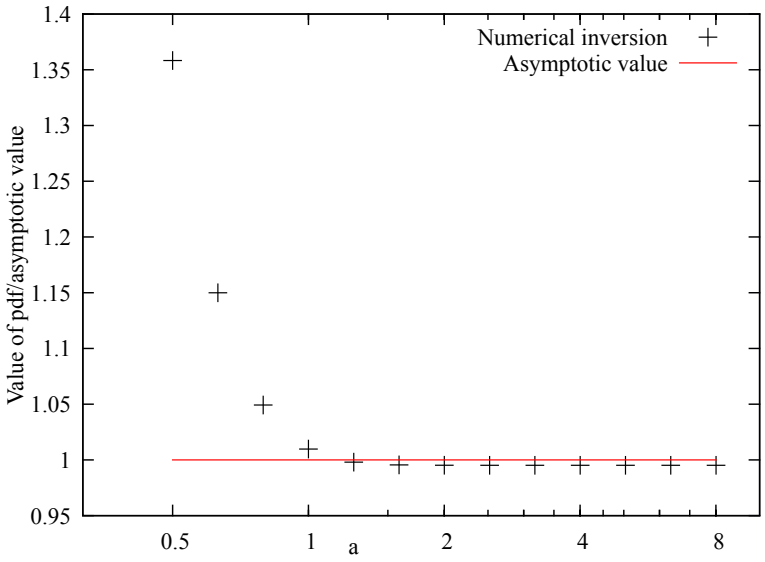

Figure 5.2 *Increasing a for $W = 10$, $T = 1000.0$, $\gamma = 2.2$*

when the cdf of $p(W;T)$ gets close to zero, Mathematica cannot evaluate $p(W;s)$ sufficiently accurately. In figures 5.3 and 5.4 there are two independent sources of error, numerical errors in the inversion of $p(W;T)$ and discrepancies between $p(W;T)$ and $p_A(W;T)$. Since we know there is an issue with the numerical inversion of the Laplace transform at high W this is a possible cause for the apparent deterioration of the fit of $p_A(W;T)$ to $p(W;T)$ at high W.

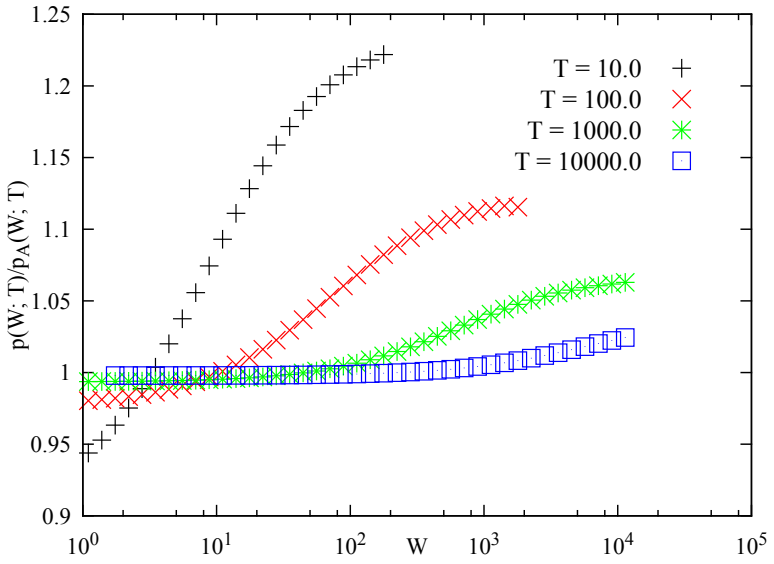

Figure 5.3 *Plotting the ratio of the attained numerical value for $p(W;T)$ to the expected asymptotic form $p_A(W;T)$ for large T*

The fact that the asymptotic form and the numerical Laplace transform inversion are never separated by an order of magnitude allows us to optimise the

numerical inversion by choosing what ratio $a = \frac{c}{h}$ is needed for the appropriate accuracy. This should result in the appropriate compromise between speed and accuracy.

$$\epsilon p_A(W;T) \sim \exp[-a]$$
$$a = -\log[\epsilon p_A(W;T)] \tag{5.18}$$

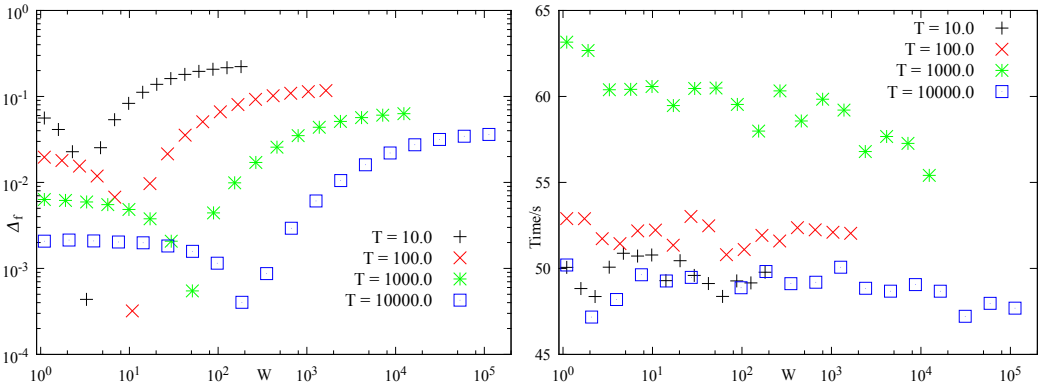

(a) *Fractional error* $\Delta_f = |p(W;T) - p_A(W;T)|/p_A(W;T)$

(b) *Time taken to invert Laplace transform*

Figure 5.4 *Inverse Laplace transform for* $\gamma = 2.2$ *with dynamic a (equation 5.18)*

5.5 Comparison of numerically obtained $p(W;T)$ to $p_A(W;T)$

In this section we numerically sample $p(W;T)$ N times for particular values of T to build up an empirical distribution $p_N(W;T)$. We then compare it with $p_A(W;T)$ by eye and by use of the one sample Kolmogorov-Smirnov test, as described in appendix E.

We obtain the empirical distribution $p_N(W;T)$ for a particular T by sampling W in the following way N times: choose a set of random numbers drawn from the common probability distribution $p_1(t)$, $\{t_1, ..., t_n\}$ such that $\sum_{i=1}^{n-1} t_i < T$ and $W = \sum_{i=1}^{n} t_n > T$. In this section $N = 1 \times 10^6$. This allows us to build up the empirical c.d.f as described in appendix E. We plot one minus the empirical c.d.f, denoted $S_N(W;T)$, because I have found it to be a more reliable method of displaying large tails of distributions than the empirical p.d.f. One minus the c.d.f of $p_A(W;T)$ is the survival function, $S_A(W;T)$ (equations 5.11 and 5.12).

5.5.1 Comparison by eye

Visually $S_A(W;T)$ is a very good fit to $S_N(W;T)$ even for very small T, as illustrated in figure 5.5. There is the usual scatter at the tail end, which we take into account in the next section by using a Kolmogorov-Smirnov test.

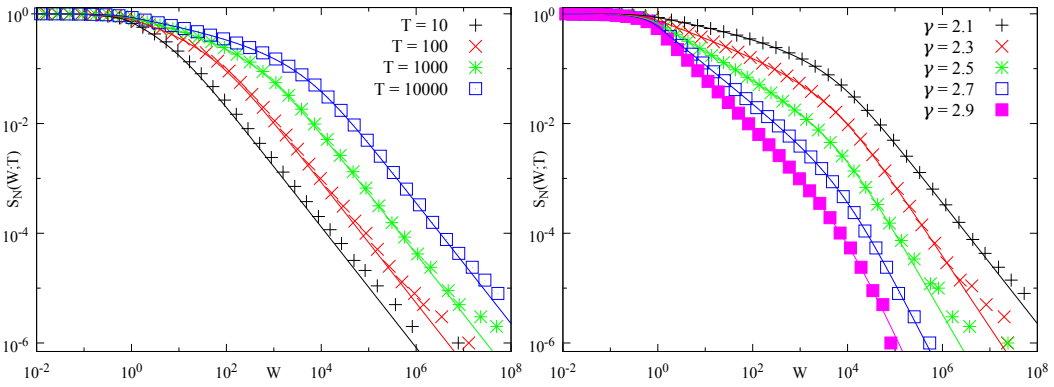

(a) $\gamma = 2.1$ *range of* T **(b)** $T = 10000$ *range of* γ

Figure 5.5 $S_N(W;T)$ *with the associated* $S_A(W;T)$, $N = 1 \times 10^6$

5.5.2 Comparison by the one sample Kolmogorov-Smirnov test

The one sample Kolmogorov-Smirnov test, as described in appendix E, is a method of testing whether an empirical probability distribution is statistically compatible with the hypothesis that it is a random sample drawn from the proposed probability distribution. If the KS value is smaller than the critical KS value shown, we accept the hypothesis that the dataset is compatible with $p_A(W;T)$ at the significance level $p = 0.05$.

Figure 5.6 shows that for $\gamma \geq 2.5$ and $T \gtrsim 1000$, $p_N(W;T)$ is compatible with $p_A(W;T)$. It also shows that the fit improves with increasing γ and T. One possible explanation for this is to use the fact that the function $p_A(W;T)$ becomes a good approximation to $p(W;T)$ once the transients in $\omega(t)$ have settled down. For high γ more events can fit in a time T than for lower γ as the mean of $p_1(t)$ increases as γ decreases, so we expect the transients of $\omega(t)$ to die away faster for higher γ.

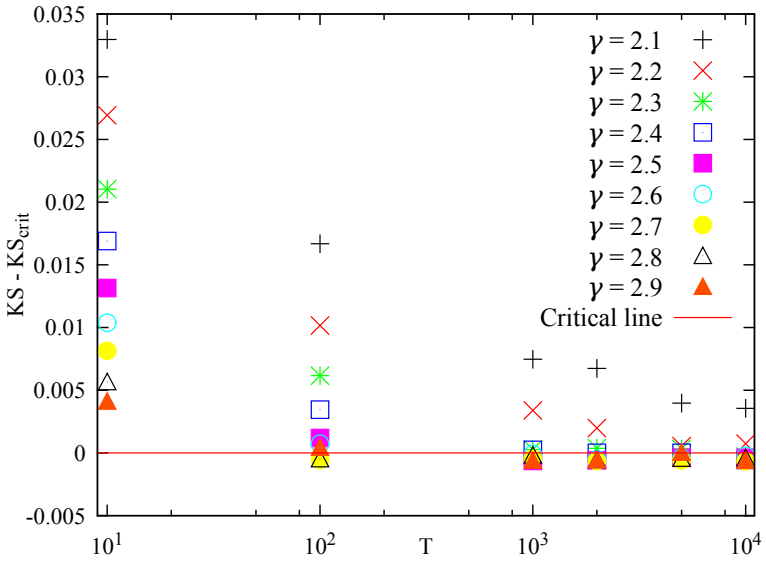

Figure 5.6 *Comparison of $S_N(W;T)$ obtained numerically with $S_A(W;T)$ for a range of γ and T, $N = 1 \times 10^6$.*

5.6 Rejection-free simulation method

In this section we improve the basic continuous time Monte Carlo method for simulating the non-Markovian TASEP, which we will refer to hereafter as the "brute force method". As discussed in chapter 4 there are problems with the brute force method when looking at lattices of large size L and small γ. We found that as L increases, the mean time picked by a pack leader increases. This implies that particles which become blocked make increasingly large numbers of attempted and failed moves, which is wasteful as pseudo random numbers can be computer intensive to generate. In my optimised codes, I found the Mersenne-Twister random number generator to be the limiting step. We can make the simulation "rejection-free" if particles know what time they will be blocked for, as they can then use $p(W;T)$ to choose a time W after T has expired that they will move. This is in effect integrating out the failed moves and we expect that it will make the simulations significantly faster.

Consider the case where at time zero, an unblocked particle draws a large time W_1 from $p_1(t)$ such that a number of particles eventually become blocked by it. We can index them sequentially, the first particle in the condensate is labelled 1, the particle behind it 2 and so on. Say particle 2 comes to rest behind particle 1 at time C_2, the time it is blocked for is $T_2 = W_1 - C_2$. It can then draw a time W_2 from $p(W;T_2)$. This particle will then move at $W_2 + T_2 = W_2 + W_1 - C_2$. Since a

particle can only become blocked by moving to the space immediately behind an upstream particle and particles can only move in one direction, a particle which is unblocked will remain so for at least that move. This implies that a particle can always know how long it will be blocked for, $p(W;T)$ can always be used and the simulation of the non-Markovian TASEP can be made rejection-free.

We call the continuous time Monte Carlo method with the waiting time distribution $p(W;T)$ the "accelerated method". It is identical to the brute force method detailed in section 4.1 except that the time to the next attempted move is now not a random variable t drawn from the waiting time distribution $p_1(t)$, but a random variable $T+W$ drawn from the distribution $p(W;T)$, where T is the time for which the particle in question is blocked i.e. the time for which the target site is occupied.

To draw times at random from $p(W;T)$ directly using the inversion method for random numbers (see section 3.5) we would need the analytic form of $p(W;T)$ which, for the Pareto waiting time distribution, we do not have. As discussed in section 3.5, we could use numerical techniques to solve $\int_0^W p(v;T)\mathrm{d}v = u$, where u is a uniformly chosen random variable $u \in (0,1)$, to draw random numbers from $p(W;T)$. Since we would only need numerical values of $p(W;T)$ we could use numerical Laplace transform inversion to find these without having the analytic form of $p(W;T)$. For this to be an improvement over the brute force algorithm the numerical Laplace transform inversion would need to be both quick and accurate. We showed in section 5.4 that the time taken to invert the Laplace transform is of the order of tens of seconds, and there may be issues with the numerical routine at the extremes of W. This is not sufficiently fast for small T to be a worthy replacement for simply drawing the required number of random numbers. We did however find that the asymptotic form $p_A(W;T)$ is a good fit to $p(W;T)$ even for relatively small T. In section 5.5 we saw that for $\gamma \geq 2.5$, the $p(W;T)$ obtained numerically is compatible with $p_A(W;T)$ for $T \gtrsim 1000$, and that it required higher T for lower γ. Since the expected pack-leader waiting time increases with decreasing γ so we expect the blocking times experienced by particles at low γ will be sufficient to allow $p(W;T)$ to be well approximated by $p_A(W;T)$.

To implement the accelerated method we will use the asymptotic form for $p(W;T)$ for large T, $p_A(W;T)$, in the inversion method for random numbers. For small blocking times, $T < T_c$, multiple picks of $p_1(t)$ can be used such that $\sum_{i=1}^{n-1} p_1(t) < T$ but $\sum_{i=1}^{n} p_1(t) > T$, and for large blocking times $T > T_c$, we use $p_A(W;T)$ directly. In the next section we will discuss how to determine a

value for the the crossover, T_c, between these two regimes so that the brute force method and the accelerated method are statistically equivalent. We note that the brute force method is equivalent to the accelerated method with $T_c = \infty$.

5.7 Calibrating the accelerated method

In this section we use both the brute force and accelerated algorithms for the simulation of the non-Markovian TASEP, and compare the following distributions by eye and by using the two sample Kolmogorov-Smirnov test (see appendix E): inter-condensate time, pack-leader lifetime and condensate lifetime. We suppose that if the distribution of a particular statistic from one simulation method is statistically compatible with the distribution of that statistic from the other method, then the simulation methods can be said to be equivalent for that statistic. We discuss what makes two distributions statistically compatible below. If the simulation methods are equivalent for all the distributions we test, we suppose that the two simulation methods are themselves equivalent. We can use this requirement that the brute force and accelerated methods should be compatible to set a value for the crossover blocking time T_c in the accelerated method.

5.7.1 Comparison by eye

We start by comparing the distributions of the inter-condensate time, pack-leader lifetime and condensate lifetime by eye. We run the accelerated simulations with a range of crossover blocking times T_c. We discussed how the different distributions were defined, and their shapes in section 4.6.2 so here we are interested only in any systematic differences between them for different T_c. Since the brute force method is equivalent to the accelerated method with $T_c = \infty$, this is how we refer to it in this section. We find that no obvious systematic differences between any of the T_c when looking at the distributions by eye, and so in figure 5.7 we plot a single example.

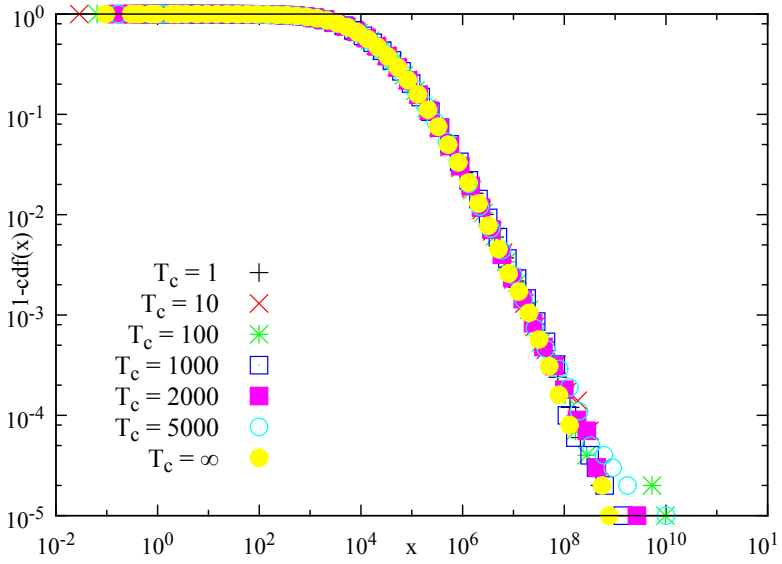

Figure 5.7 *Condensate lifetime distribution for* $L = 830$, $\rho = 0.1$, $\gamma = 2.3$, $T_c = (1, 10, 100, 1000, 2000, 5000, \infty)$

5.7.2 Comparison by the two sample Kolmogorov-Smirnov test

The two sample Kolmogorov-Smirnov test, as described in appendix E, is a method of testing whether two empirical probability distributions are statistically compatible with the hypothesis that they are drawn from the same underlying probability distribution. Here we test the same statistics that we looked at by eye, but more rigorously. The standard deviation shown was computed by using the bootstrap technique described in appendix E with $N = 500$.

In figures 5.8a, 5.8b and 5.8c we show examples of the computed two sample KS statistics for the inter-condensate lifetime, pack-leader lifetime and condensate lifetime respectively, all for $\gamma = 2.3$. If the KS value is smaller than the critical KS value shown, then the datasets are compatible with being drawn from the same underlying probability distribution with $p = 0.05$. We see that the inter-condensate lifetime and condensate lifetimes for $T_c \geq 10$ are compatible with $T_c = \infty$, though the error bars are quite large. The pack-leader lifetime seems to have the largest scatter, though discarding the obvious outlier at $T_c = 1000$ I claim that the KS values presented are consistent with $\mathrm{KS} - \mathrm{KS}_{\mathrm{crit}} \lesssim 0$ for $T_c \geq 10$.

Since the presented examples for $\gamma = 2.3$ are representative of the complete range of $\gamma = (2.3, 2.4, 2.5, 2.6, 2.7, 2.8, 2.9)$ tested, we can take a weighted average

of $\mathrm{KS} - \mathrm{KS}_{\mathrm{crit}}$ over γ in order to ascertain a value of T_c which works for any γ. Figures 5.8d, 5.8e,5.8f show the mean of the KS statistics weighted by the inverse of the variance versus T_c. It can be seen that on average the KS statistic indicates that the distributions $T_c \geq 10$ are compatible with $T_c = \infty$. The pack leader lifetime seems to be the most sensitive to T_c and since there is no significant difference between the speeds of the accelerated simulations and $T_c = 2000$ has the smallest weighted average KS statistic, I choose $T_c = 2000$ for the remainder of the thesis. The increase in simulation speed afforded by the accelerated method was dependent on γ, with smaller γ experiencing a larger increase in speed. This acceleration, which for $\gamma = 2.3$ was over a factor of ten, allows us to perform simulations for $\gamma < 2.3$, which we discuss in the following chapter.

5.8 Chapter summary

In this chapter we discussed the blocked waiting time distribution $p(W;T)$, which is the probability that if a particle is blocked for time T it will make its first successful move at time $T + W$. We computed an approximation for $p(W;T)$ as $T \to \infty$, $p_A(W;T)$, for the Poissonian and Paretian distributed waiting times directly from $p(W;s)$. Using our knowledge of Laplace transforms from chapter 3 we found a general form of $p_A(W;T)$, which was compatible to the forms found for the Poissonian and Paretian blocked waiting times. Numerical Laplace transform inversion was significantly slower than simply choosing a set of random numbers such that $\sum_{i=1}^{n-1} p_1(t) < T$ and $\sum_{i=1}^{n} p_1(t) > T$, however it did reveal that $p_A(W;T)$ is a good approximation to $p(W;T)$ even for relatively small T. The distributions of the inter-condensate time, pack-leader lifetime and condensate lifetime from the two simulation methods were compared by eye, and by the two sample Kolmogorov Smirnov test to find the crossover blocking time $T_c = 2000$ for which the brute force and accelerated simulations return statistically equivalent results.

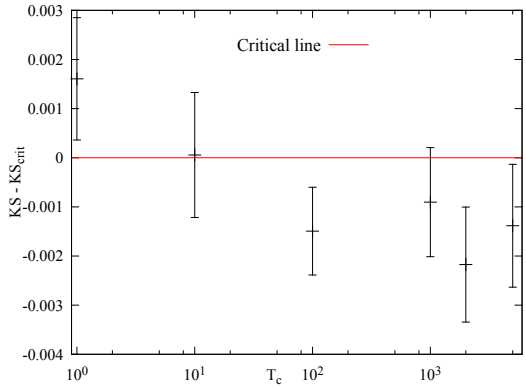

(a) *KS - KS critical for the inter-condensate lifetime* $\gamma = 2.3$

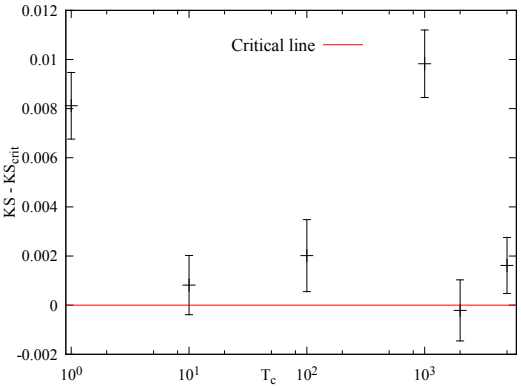

(b) *KS - KS critical for the pack-leader lifetime* $\gamma = 2.3$

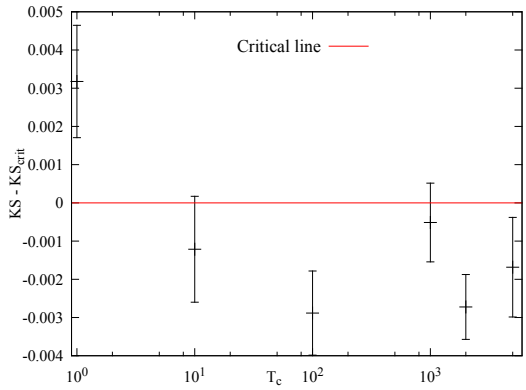

(c) *KS - KS critical for the condensate lifetime* $\gamma = 2.3$

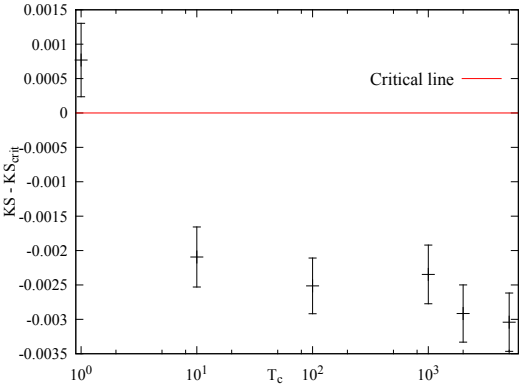

(d) *Weighted mean of KS - KS critical for the inter-condensate lifetime for* $\gamma = (2.3, 2.4, 2.5, 2.6, 2.7, 2.8, 2.9)$

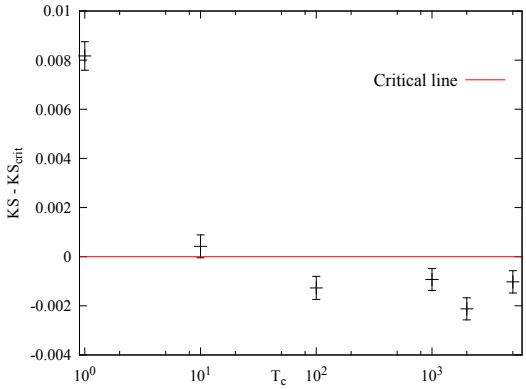

(e) *Weighted mean of KS - KS critical for the pack-leader lifetime for* $\gamma = (2.3, 2.4, 2.5, 2.6, 2.7, 2.8, 2.9)$

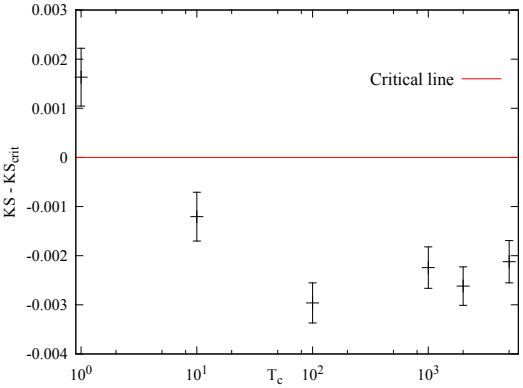

(f) *Weighted mean of KS - KS critical for the condensate lifetime for* $\gamma = (2.3, 2.4, 2.5, 2.6, 2.7, 2.8, 2.9)$

Figure 5.8 *Comparison of* $T_c = (1, 10, 100, 1000, 2000, 5000)$ *with* $T_c = \infty$ *for* $L = 830$, $\rho = 0.1$. *If the data point is below the critical line at* $KS - KS_{crit} = 0$ *the data is statistically compatible.*

Chapter 6

Results from the rejection-free algorithm for the non-Markovian TASEP

In the previous chapter we investigated the blocked waiting time distribution $p(W;T)$ and its large T approximation $p_A(W;T)$, and used them to construct a rejection free accelerated algorithm for the simulation of the non-Markovian TASEP. We checked that the two methods produced results that were statistically compatible, and in this chapter we use the accelerated simulations to look again at the non-Markovian TASEP. It was argued in chapter 4 that there was a separation of timescales between the lifetime of the full condensate and the time between full condensates, which would cause the fraction of time spent in the condensate, f, to tend to one in the thermodynamic limit. We investigate f for a range of γ, L to further demonstrate the compatibility of the two simulation methods, and show that $\gamma < 2.4$ allows us to see f tending to one as required. We concluded in chapter 4 that there was an increasing chance of two consecutive condensates interacting, i.e. for a number of particles to remain stationary between full condensates. To understand the thermodynamic limit we need to understand how the mean blocking time T and the mean waiting time W behave after a number of consecutive condensates, and we will investigate this analytically using $p_A(W;T)$ and simulations with $\gamma < 2.4$.

6.1 Fraction of time spent in the condensed state

In section 4.4 we looked at the fraction of time spent in the spatially complete condensate, f (a traffic jam containing every particle on the lattice). We argued due to the observed separation of timescales between the condensate lifetime and the fluid lifetime (figure 4.7) that f should tend to one in the thermodynamic limit, however f directly from the brute force simulations (figure 4.6) was also consistent with tending to a finite fraction. In principle we would like to have had access to higher L and smaller γ, since the brute force simulations could not handle $\gamma < 2.3$. We used the accelerated simulations described in the previous chapter to fill figure 4.6 with new data. In figure 6.1 we can see that the accelerated simulations (filled points and $\gamma = 2.1, 2.2$) match the values of f from the brute force simulations, and we can also clearly see $\gamma = 2.1, 2.2, 2.3$ tending to one. From this data we cannot rule out the possibility that the fraction of time spent condensed tends to a constant, $f_\infty(\gamma)$ where $f_\infty(\gamma) \to 1$ as $\gamma \to 2$, however we will argue in this chapter that $f_\infty(\gamma) \to 1$ for $\gamma < 3$.

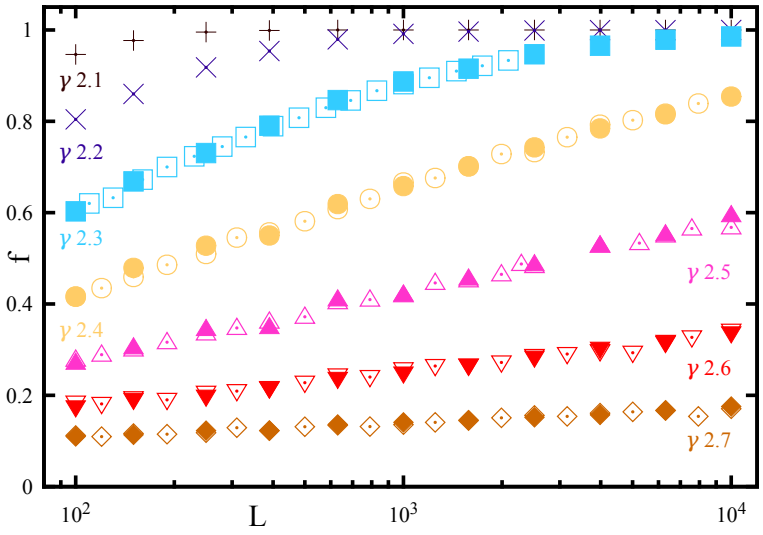

Figure 6.1 *Fraction of time spent in the full condensate f for $\rho = 0.1$. Brute force simulations are open points $\gamma \geq 2.3$, and accelerated simulations are filled points $\gamma \geq 2.3$ and all data $\gamma < 2.3$*

6.2 Probability of complete condensate dissolution

We showed in figure 4.12 that the fraction of condensates which formed from remnants of the preceding condensate increases with L. The initial condensate

had, by definition, a pack-leader which picked a time large enough to allow all other particles on the lattice to catch up with it. Therefore we assume the time that particles are blocked for is sufficiently large to replace $p(W;T)$ with $p_A(W;T)$. Using this assumption we can compute the probability that a condensate will dissolve completely to the fluid i.e. once the pack-leader particle moves off, all particles must move at least once.

To assist with the following discussion we label the particles as we move backwards (upstream) through the condensate. The pack-leader is particle 1, the next particle upstream is 2, and so on, making the last particle in the condensate particle N. Consider the case where i particles move off from the front of the condensate once the pack-leader has moved. To form a new condensate from the remnants of the old one, the next particle $N-i$ must choose a time large enough for the i particles downstream of it to return to the back of the condensate. The time required to move the i^{th} particle to the back of the condensate C_i is the time required for it to travel $L-N$ places. As we argued in section 4.5 $C_i \sim L$ and any dependence on i is sub-dominant, so we drop the index, C.

We can therefore see that in order not to form a condensate out of the remnants of the previous condensate, we require all particles to have chosen a time $W < C$. The probability that all $N-1$ particles choose $W < C$ is H^*.

$$\begin{aligned} H^* &= \prod_{i=2}^{N} \left(1 - \int_{W_i=C}^{\infty} p_A(W_i;T_i)\mathrm{d}W_i\right) \\ &\approx \exp\left(-\sum_{i=2}^{N} \int_{W_i=C}^{\infty} p_A(W_i;T_i)\mathrm{d}W_i\right) \end{aligned}$$

since $\int_{W_i=C}^{\infty} p_A(W_i;T_i)\mathrm{d}W_i < 1$.

$$\int_{W=C}^{\infty} p_A(W;T)\mathrm{d}W = \frac{C^{2-\gamma} - (C+T)^{2-\gamma}}{\gamma - 1 - T^{2-\gamma}}$$

for $\gamma > 2$, see equation 5.11. We wish to see how $\int_{W=C}^{\infty} p_A(W;T)\mathrm{d}W$ depends on C and therefore L. We will see below that the blocking time T increases as we go deeper into the full condensate, so $C \leq T < \infty$. At the minimum blocking time $T_{\min} = C$

$$\begin{aligned} \frac{C^{2-\gamma} - (C+T_{\min})^{2-\gamma}}{\gamma - 1 - T_{\min}^{2-\gamma}} &= \frac{C^{2-\gamma}(1-2^{2-\gamma})}{\gamma - 1 - C^{2-\gamma}} \\ &\sim C^{2-\gamma} \end{aligned}$$

as T approaches ∞

$$\frac{C^{2-\gamma} - (C+T)^{2-\gamma}}{\gamma - 1 - T^{2-\gamma}} \rightarrow \frac{C^{2-\gamma}}{\gamma - 1} \sim C^{2-\gamma}$$

so we suppose

$$\int_{W_i=C}^{\infty} p_A(W_i; T_i) \mathrm{d}W \sim C^{2-\gamma}$$

regardless of T_i. This implies that we can write

$$\begin{aligned} H^* &\approx \exp\left(-\sum_{i=2}^{N} \int_{W_i=C}^{\infty} p_A(W_i; T_i) \mathrm{d}W_i \right) \\ &\sim \exp\left(-\sum_{i=2}^{N} C^{2-\gamma} \right) \\ &\sim \exp[-(\rho L - 2) C^{2-\gamma}] \\ &\sim \exp[-L^{3-\gamma}] \end{aligned}$$

Therefore the probability that a condensate will fully break apart in the thermodynamic limit tends to zero for $\gamma < 3$, and one for $\gamma > 3$. In the thermodynamic limit this full block will never dissolve, and this leads to consecutive condensates being formed.

Figure 4.7 showed that $C \sim L$ was indeed an underestimate, but as not so far off as to invalidate this as an acceptable assumption. If $C \sim L^{\beta(\gamma)}$, $\beta(\gamma) \geq 1$ as suggested by figure 4.7, this alters H^* to give

$$\begin{aligned} H^* &\sim \exp[-(\rho L - 2) C^{2-\gamma}] \\ &\sim \exp[-L^{(2-\gamma)\beta(\gamma)+1}] \end{aligned}$$

which predicts that the crossover occurs when $\beta(\gamma) = \frac{1}{\gamma - 2}$, which may occur at a different point to $\gamma = 3$. We will examine $\beta(\gamma)$ from simulations below.

From H^* we can compute the probability that consecutive condensates interact $1 - H^* \sim 1 - \exp[-L^{3-\gamma}]$. We fit the following function to the fraction of condensates interacting σ: $1 - A\exp[-BL^{\nu}]$ in figure 6.2. We see that this is an appropriate fitting form. $\gamma = 2.8$ and $\gamma = 2.9$ are not shown as they increase imperceptibly on the used scale, however the increasing σ for $\gamma = 2.9$

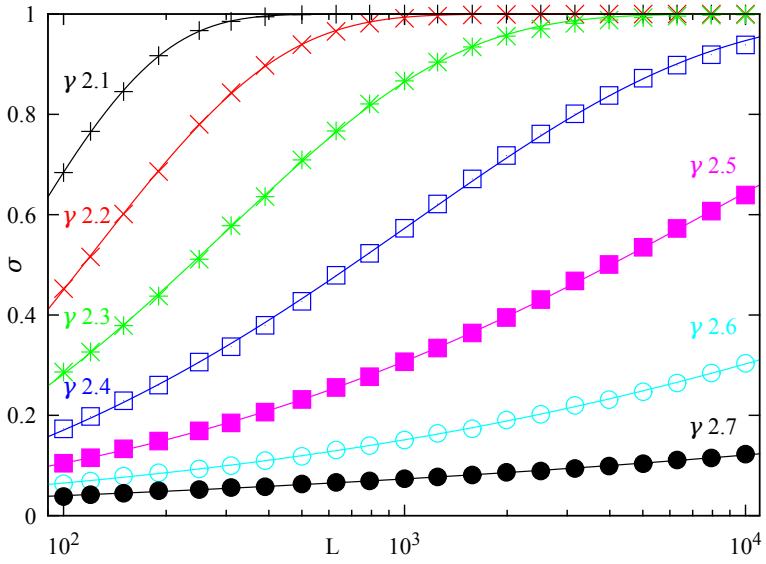

Figure 6.2 *Fraction of condensates interacting, σ, v.s. L for a range of γ*

is reassuring that the crossover between the fully condensed regime and the less condensed region occurs at $\gamma > 2.9$. The fitting parameter ν is shown for a range of γ in figure 6.3a. As claimed ν is always positive even for $\gamma = 2.9$. Since $(2-\gamma)\beta(\gamma)+1 = \nu$, we can re-arrange figure 6.3a to plot $\beta(\gamma)$, figure 6.3b. We see that there could be issues with $\gamma = 2.1, 2.9$ being too close to transition points, as evidenced by their substantially larger standard errors, but that it seems as if the critical value of $\beta_c = \frac{1}{\gamma-2}$ occurs in the region $\gamma > 2.9$. A critical $\gamma = 3.0$ is consistent with our data and I have not been able to conclusively pin down exactly where the crossover is, if it is indeed a discontinuous transition.

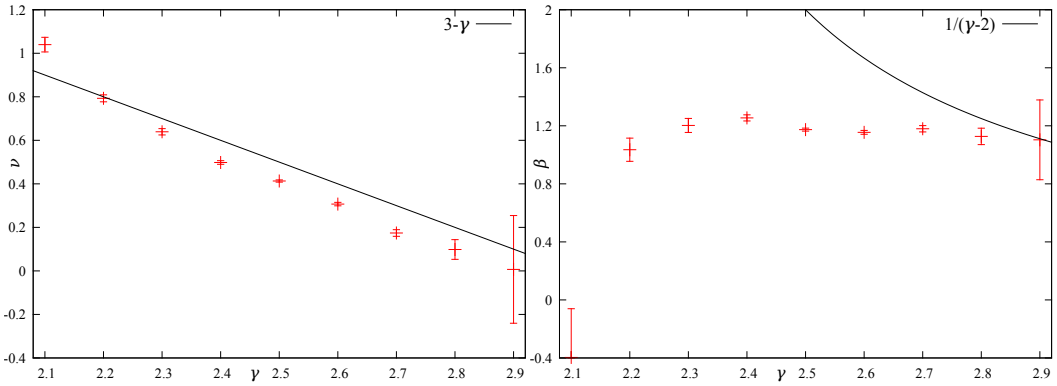

(a) *Fitting parameter ν* **(b)** *Exponent of the catchup time, $\beta(\gamma)$*

Figure 6.3 *Fraction of condensates interacting σ.*

6.3 Blocking time in consecutive condensates

Previously we have argued for the existence of condensates being formed from the remains of a preceding condensate. An interesting question to ask is; on average, how does the waiting time W chosen by a particle and its blocking time T depend on its position in the condensate. In figure 6.4 we show a cartoon of condensates interacting. We also label the particles in the condensate as we did previously with the following extension, the initial pack-leader is particle 1, this number increases as we go back through the condensate, particle N is the last particle of the initial condensate, particle $N+1$ is the initial pack-leader once it has moved around the system and joined the back of the new condensate, etc. We found that the condensate itself moves backwards around the system as particles move from the front to the back by traversing the lattice.

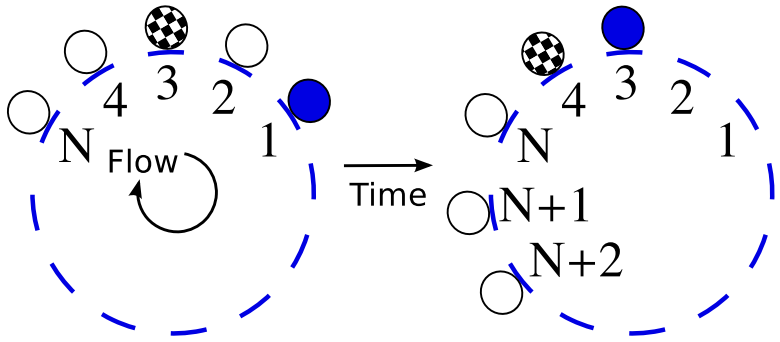

Figure 6.4 *A cartoon of consecutive condensates, the current pack-leader is the filled circle, the next pack-leader is the circle filled with chessboard pattern. Also illustrated is the numbering of particles in consecutive condensates.*

We can find the mean of W_i, T_i by splitting the data from the simulations up into runs of consecutive condensates. In figure 6.5 we see that the average of T_i, $\bar{T}_i$ and the average of W_i, $\bar{W}_i$, initially increases with i, and then saturates to a constant value. In the previous section where we computed the probability that a condensate completely dissolves H^* we assumed that $T > C$. By definition the time picked by the first pack-leader is larger than C, and now we see that on average T increases with i, so this assumption is valid. We also see that the saturation level increases with L.

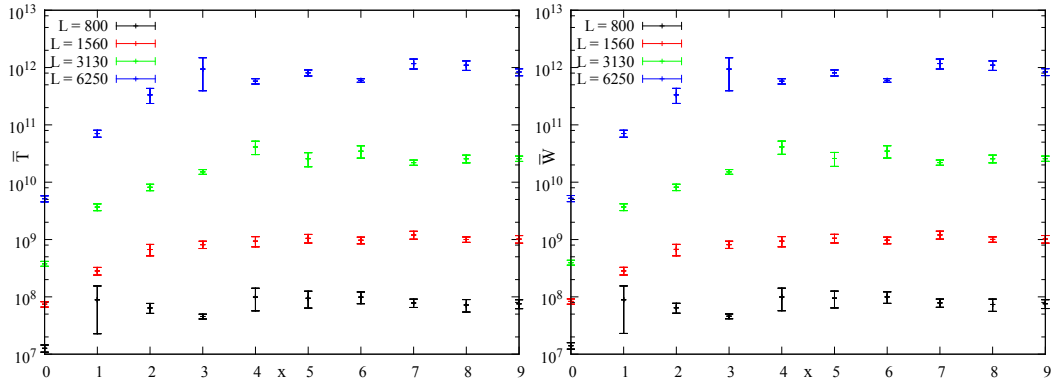

(a) *Saturation of* $\bar{T}_i$ **(b)** *Saturation of* $\bar{W}_i$

Figure 6.5 *Saturation of* $\bar{T}_i$ *and* $\bar{W}_i$ *with* $x = \frac{i}{N}$, $\rho = 0.1$, $\gamma = 2.2$

6.4 Saturation of W, T in consecutive condensates

Previously we saw that in the thermodynamic limit we expect condensates never to fully break up, and therefore condensates form from the remains of the preceding condensate. We see from simulations that initially T, W increase as we move back through the condensate and then saturate to a particular value. In this section we attempt to understand mathematically this increase and then eventual saturation, with the aim of predicting how the saturation level scales with L.

6.4.1 Mathematical understanding of the saturation

We start off with some definitions. The arrival time of particle i at its resting site in the condensate is A_i. The departure time of particle i from its resting site in the condensate is D_i. The time that particle i is blocked once it comes to rest is T_i. The time after unblocking that particle i waits before it moves off is W_i, which is drawn from the blocked waiting time distribution $p(W_i; T_i)$. N is the number of particles in the system. We use the extended particle labelling so that $N+1$ is the first particle when it has rejoined the back of the condensate. We also have W_0, which is the time picked by the first particle, i.e. the first pack-leader. $\Delta T_i = T_i - T_{i-1}$ is the change in the blocking time at particle i from its previous value.

To set the system up, we take the arrival time of the first particle to define $t = 0$, and that it is large enough to cause all the remaining particles to catch

up, so it becomes the first pack leader. We then need the following assumptions; We assume the remaining particles catch up very quickly to the first pack leader, $A_i = 0$ for $1 \leq i \leq N$, and that we can use the catch-up time $C = L(1-\rho)\langle t \rangle$ as the mean time taken for a particle to traverse the mostly empty lattice.

We can now define the following recursion relations.

$$D_i = D_{i-1} + W_i = \sum_{j=1}^{i} W_j \tag{6.1}$$

$$T_i = D_{i-1} - A_i \tag{6.2}$$

$$A_{N+i} = D_i + C \tag{6.3}$$

$$T_i = \begin{cases} \sum_{j=1}^{i-1} W_j & \text{for } i \leq N \\ D_{N+i-1} - D_i - C = \sum_{j=i+1}^{N+i-1} W_j - C & \text{for } i > N \end{cases} \tag{6.4}$$

We make a change of variable to make the notation continuous $x = \frac{i-1}{N}$ and push the extra factor of N into the definition of W such that $W_{i-1} \equiv W_{Nx} \equiv W(x)$. This gives

$$\Delta T(x) = \begin{cases} W(x) & \text{if } x < 1 \\ W(x) - W(x-1) & \text{if } x > 1 \end{cases}$$

We assume that the random variable W is well represented by the mean (equation 5.17), and then take $N \to \infty$ such that x becomes continuous

$$\begin{aligned} W(x) = \bar{W}(x) &\approx \frac{1}{(3-\gamma)(\gamma-1)} T(x)^{3-\gamma} \\ T'(x) &= \begin{cases} \frac{1}{(3-\gamma)(\gamma-1)} T(x)^{3-\gamma} & \text{if } x < 1 \\ \frac{1}{(3-\gamma)(\gamma-1)} \left(T(x)^{3-\gamma} - T(x-1)\right) & \text{if } x > 1 \end{cases} \\ T(0) &= W(0) \end{aligned} \tag{6.5}$$

We solve for $T(x)$ in the region $x < 1$ and find

$$T(x) = \left(\frac{(\gamma-2)x}{(3-\gamma)(\gamma-1)} + W(0) \right)^{\frac{1}{\gamma-2}}$$

For $x > 1$, a power law ansatz x^ν is a solution of equation 6.5 under the condition that $\nu = 0$, which suggests a constant solution. The exponential decay to a saturation $T(x) = T_\infty + ae^{-bx}$ is a solution to equation 6.5 under the condition

that $\frac{d}{e^d-1} = \frac{T_\infty^{-(\gamma-2)}}{(\gamma-1)}$. A second condition can be attained by matching the forms of $T(x)$ at $x = 1$ from above and below to get $-abe^{-b}(3-\gamma)(\gamma-1) = (T_\infty + ae^{-b})^{3-\gamma} - W(0)^{\frac{3-\gamma}{\gamma-2}}$.

6.4.2 Predicting the saturation level of T, W

Given that we have shown that W_i and T_i converge to a steady state where they become independent of i, we can look at the mean values of W and T, $\bar{W}$ and $\bar{T}$, using equation 5.17.

$$T_{N+i} = \sum_{j=i+1}^{N+i-1} W_j - C \tag{6.6}$$

We take the average $\bar{T} = \langle \sum_{j=i+1}^{N+i-1} W_j - C \rangle$ and use the mean-field type approximation $f(\bar{T}) = f(\bar{T})$ allowing us to write the following, where $\bar{W}$ is the expected W drawn from the distribution $p(W;\bar{T})$,

$$\begin{aligned}
\bar{T} &= (N-1)\bar{W} - C \\
\bar{W} &\approx \frac{\bar{T}^{3-\gamma}}{(3-\gamma)(\gamma-1)} - \frac{\gamma-2}{2(3-\gamma)} \\
\bar{T} &\approx \rho L \left(\frac{\bar{T}^{3-\gamma}}{(3-\gamma)(\gamma-1)} - \frac{\gamma-2}{2(3-\gamma)} \right) - L(1-\rho)\langle t \rangle
\end{aligned}$$

Plotting $y = \bar{T}$ alongside $y = a\bar{T}^{3-\gamma} - b$ we see there are two roots, for which in general we cannot get an analytic form. We can simplify this by keeping only the dominant term to get

$$\begin{aligned}
\bar{T} &\approx \frac{\rho L \bar{T}^{3-\gamma}}{(3-\gamma)(\gamma-1)} \\
&\approx \left(\frac{\rho L}{(3-\gamma)(\gamma-1)} \right)^{\frac{1}{\gamma-2}}
\end{aligned} \tag{6.7}$$

Since W and T are related, the level of the saturation for W is

$$\begin{aligned}
\bar{W} &\sim \bar{T}^{3-\gamma} \\
&\sim L^{\frac{3-\gamma}{\gamma-2}}
\end{aligned}$$

6.5 Comparison of predicted saturation level with simulations

In this section we look at how well the prediction of the saturation of the average blocking time, T, for consecutive condensates fits the data from simulations, and how that data is acquired.

For particular values of γ, L, ρ we run a simulation until we find a consecutive condensate which extends backwards for $10\rho L$ particles, i.e. until $x = 10$. We store the W and T for each particle in the condensate along with that particles position in the condensate. We repeat this for 10000 such consecutive condensates. Due to the fact that there is a finite probability of complete condensate dissolution we have been unable to sample such extended condensates for $\gamma > 2.3$ at the sizes of L that are accessible. To take the average T a large number of repeats is needed due to the large fluctuations in any particular condensate.

I have not been able to fit the ansatz $T(x) = T_\infty - T_D(x)$, where $T_D(x)$ is some decaying function, to the saturation directly. The forms of $T_D(x)$ that were tried are $T_D(x) = a\exp[-bx]$, $T_D(x) = ax^{-b}$ and $T_D(x) = a\exp[-bx^c]$. I have also tried an exponential increase to an upper limit $T(x) = \exp[ax]\left(1 + \frac{e^{ax}}{\mathrm{Tinf}}\right)^{-1}$, so in order to get the level of the saturation I have to assume that the final value $T(10)$ is a sufficiently good approximation to T_∞. In figure 6.6 is plotted $\frac{T(10)}{\bar{T}}$ where $\bar{T}$ is the predicted saturation level (equation 6.7). It can be seen that the prediction is typically orders of magnitude larger than the saturation level observed, however the fact that $\frac{T(10)}{\bar{T}}$ appears to be roughly constant indicates that we may have identified the correct scaling with L albeit with an incorrect prefactor.

6.6 Relaxing the mean-field type assumption for the saturation of T

In the previous section we concluded that predicted saturation level of the blocking time T (equation 6.7) was correct up-to a prefactor. In this section we see if relaxing the assumptions required to derive equation 6.7 fix the prefactor.

To derive the saturation level for T (equation 6.7) we started with the relation $T_{N+i} = \sum_{j=i+1}^{N+i-1} W_j - C$ (equation 6.5), where C is the catchup time and W_j is

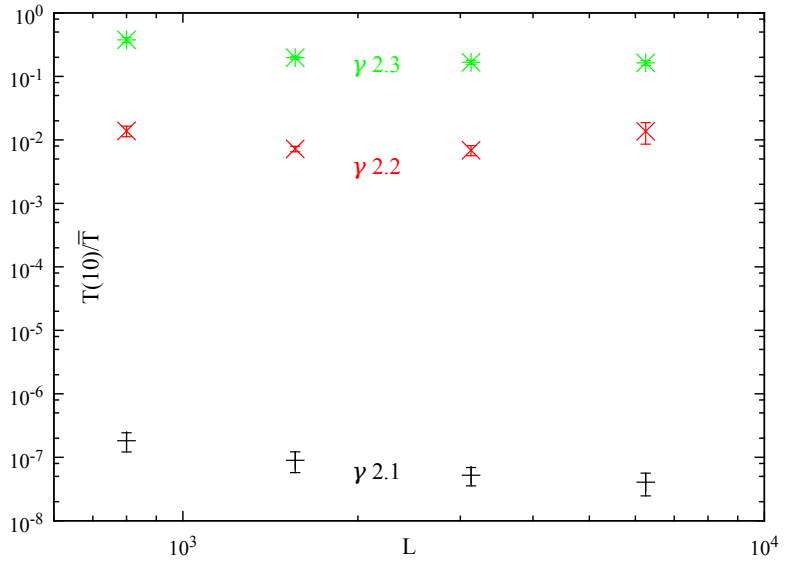

Figure 6.6 *The ratio of the blocking time at $x = 10$, $T(10)$, to the predicted saturation level $\bar{T}$ for $\gamma = (2.1, 2.2, 2.3)$, $L = (800, 1560, 3130, 6250)$, $\rho = 0.1$*

a random variable drawn from $p_A(W; T_i)$. To solve it we assumed that we could use the mean-field like assumption and so replace the actual values of T_i with $\bar{T}$. This led to $\langle \sum_{j=i+1}^{N+i-1} W_j \rangle = (N-1)\bar{W}$ where $\bar{W}$ is the expected W drawn from the distribution $p(W; \bar{T})$. This ignores the fact that each W_i is drawn from a distribution with a different T_i. Equation 6.5 says that as T scales back through the condensate, T_{N+i} is a random variable which is the sum of the $N-1$ random variables W_j. Each W_j is a random variable drawn from the distribution $p_A(W; T_i)$.

We start with a bief discussion of stable distributions (see Feller [36]). We use the notation $\stackrel{d}{=}$ to denote that two random variables, X, Y have the same distribution, and that $Y \stackrel{d}{=} mX + c$ means that the distributions of X, Y differ only by location and scale parameters. If random variables X are i.i.d random variables with distribution R, and $S_n = \sum_{i=1}^{n} X_i$, then, $S_n \stackrel{d}{=} m_n X + c_n$. A simple example are two random variables both drawn from the normal distribution, which is an example of a stable distribution, having a sum which is also normally distributed. In this section, I will use the words "stable distribution" but what I mean is the more relaxed condition that average of a sum of random variables, $A_n = S_n n^{-1}$, tends to a particular distribution as $n \to \infty$, in a similar manner to the rescaled distributions of the sum that we investigated in chapter 3.

We make the following two claims in order to make progress here:

Claim 1 If T_i was constant, W_j would be i.i.d random variables and we would expect T_{N+i} to be a random variable drawn from a stable distribution $p_s(T)$, if N was large enough.

Claim 2 If T_i are random variables drawn from the stable distribution $p_s(T)$, using $T_{N+i} = \sum_{j=i+1}^{N+i-1} W_j - C$ and $p_A(W;T_i)$, this provides a condition on the resulting distribution of T_{N+i}. A flowchart of this is shown in figure 6.7. We suppose that the sum of a sufficiently large number of random variables T_{N+i}, which are related to the sum of W_i (which are independent random variables with a common analytic distribution but with a shape parameter being a random variable drawn from a stable distribution $p_s(T)$), has a stable distribution $p_{s2}(T)$. I have not been able to show this analytically, but we investigate it numerically in the following section. We note that the variance of $p_A(W;T)$ is infinite so we cannot use central limit theorem.

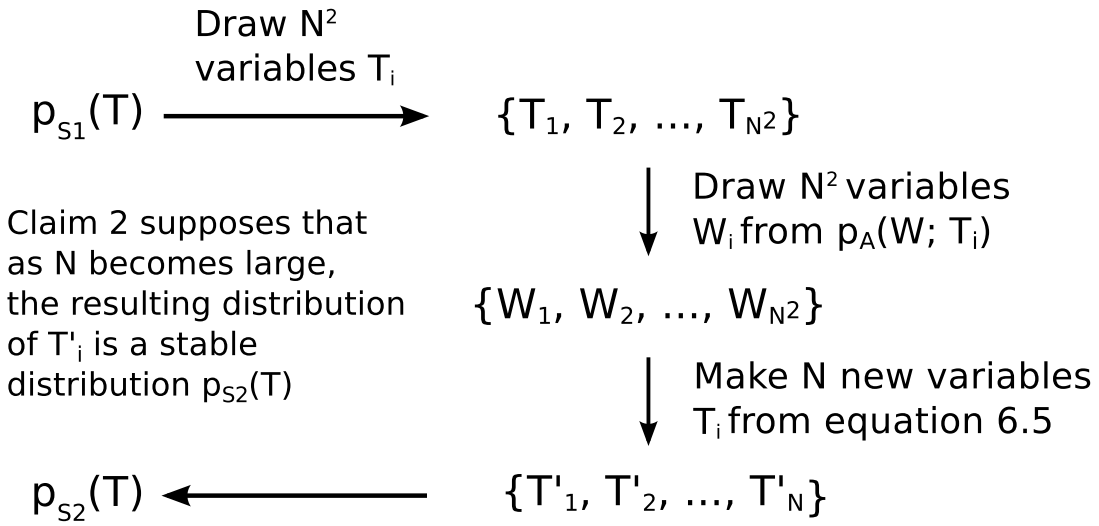

Figure 6.7 *A flowchart illustrating Claim 2*

Suppose that T_i are random variables drawn from the stable distribution $p_{s,1}(T)$. This implies that W_i are random variables drawn from related distributions, and we expect that the sum of $N-1$ such variables will have a stable distribution $p_{s,2}(T)$, if N is sufficiently large. $p_{s,1}(T)$ and $p_{s,2}(T)$ have expectations $\bar{T}_1$ and $\bar{T}_2$. If $\bar{T}_1 \neq \bar{T}_2$, $\bar{T}$ has not saturated to a finite value. Since we see the saturation of T in the simulations, we expect that the stable distributions continue to change as we move back through the condensate until they converge to a final stable distribution $p_s(T)$ with mean $\bar{T}$.

In this section we will sample $x = \frac{\sum_{j=i+1}^{N+i-1} W_j}{N}$ randomly, where W_j is a random variable drawn from $p_A(W;T_j)$ and T_j is a random variable drawn from $p_{\text{input}}(T)$

for a range of N. The empirical survival distribution (one minus the c.d.f) of x uses the notation $S_{N,T_{\text{initial}}}(x)$ to make plain what input data was used.

6.6.1 Stable distributions

In the previous section we made a pair of claims about stable distributions which we will test numerically here.

Firstly taking a fixed value of $T_f = 1 \times 10^{12}$ we compute the empirical survival distribution (one minus the c.d.f) $S_{N,T_f}(x)$ where x is the rescaled variable $x = \frac{\sum_{j=i+1}^{N+i-1} W_j}{N}$, W_j is a random variable drawn from $p(W;T_f)$, for a range of N. In figure 6.8a we can see that $S_{N,T_f}(x)$ tends to a particular distribution with increasing N, hence we consider claim one to be valid.

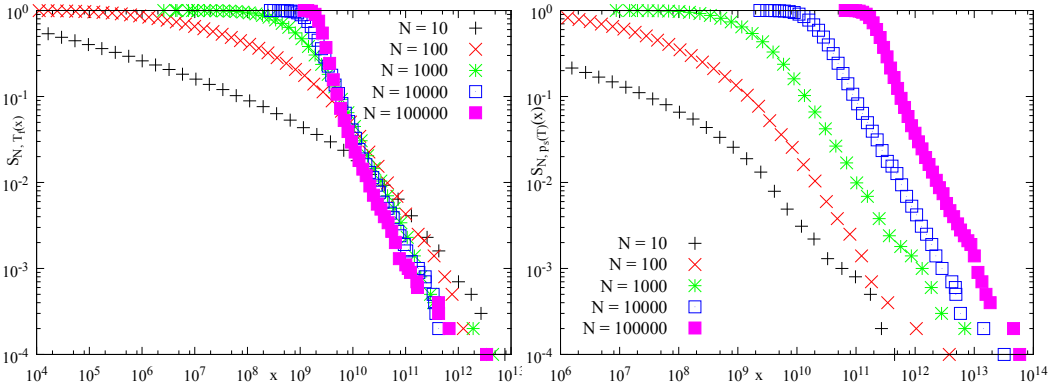

(a) *Empirical survival distribution* $S_{N,T_f}(x)$ *for* $N = (10, 100, 1000, 10000, 100000)$, $\gamma = 2.2$

(b) *Empirical survival distribution* $S_{N,p_s(T)}(x)$ *for* $N = (10, 100, 1000, 10000, 100000)$, $\gamma = 2.2$

Figure 6.8

Now we take the distribution of T, $p_s(T)$, gained from $S_{N=1\times10^5,T_f=1\times10^{12}}(x)$ which we believe to be stable, and compute the empirical survival distribution $S_{N,p_s(T)}(x)$ where x is the rescaled variable $x = \frac{\sum_{j=i+1}^{N+i-1} W_j}{N}$, W_j is a random variable drawn from $p_A(W;T_j)$ and T_j is a random variable drawn from $p_s(T)$ for a range of N. In figure 6.8b we can see that $S_{N,p_s(T)}(x)$ tends to a particular distribution with increasing N, hence we consider claim two to be valid.

6.6.2 Self-consistent sampling of T

In this section we see that if we take a stable distribution $p_{s,1}(T)$ to find a new distribution $p_{s,2}(T)$ as we did in the previous section, and repeat the process, using $p_{s,2}(T)$ to find $p_{s,3}(T)$ and so on, the distributions tend towards a fixed stable distribution $p_s(T)$. This can be streamlined, and made more like the situation seen in consecutive condensates by sampling T self-consistently.

We take the distribution of T, $p_{s,k-1}(T)$ which we believe to be stable, and compute the empirical survival distribution $S_{N,p_{s,k}(T)}(x)$ where x is the rescaled variable $x = \frac{\sum_{j=i+1}^{N+i-1} W_j}{N}$, W_j is a random variable drawn from $p_A(W;T_j)$ and T_j is a random variable drawn from $p_{s,k-1}(T)$ for a range of N and a number of k. We take $p_{s,1}(T)$ to be the distribution gained from $S_{N=1\times10^5,T_f=1\times10^{12}}(x)$ as we did in the previous section. In figure 6.9 we can see that $S_{N,p_{s,k}(T)}(x)$ tends to a particular distribution with increasing k, and we therefore believe that this method allows us to see the saturation of distribution of T with repeated sampling.

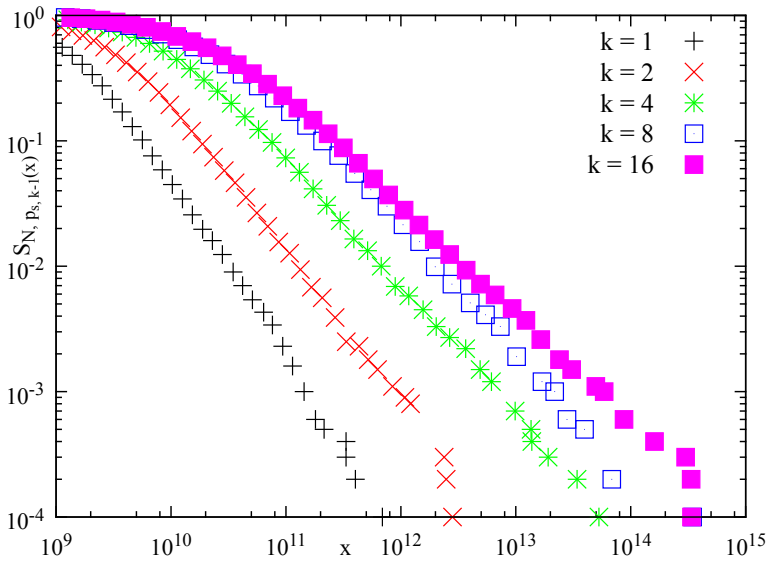

Figure 6.9 *Empirical survival distribution* $S_{N,p_{s,k}(T)}(x)$ *for* $N = 1995$, $\gamma = 2.2$, $k = [1, 12]$

The self-consistent sampling of T was done as follows; draw $N-1$ blocking times T_i at random from the set of σ T values, T_{store}, where $i = [1, N-1]$. Draw a waiting time W_i uniformly from the blocked waiting time distribution $p_A(W;T_i)$ for all i. Compute a new T value using equation 6.5: $T = \sum_{j=1}^{N-1} W_j - C$ (ensuring T is never negative by setting $T = 0$ if $\sum_{j=1}^{N-1} W_j - C < 0$) and replace the oldest T value in T_{store} with it. This can be done Z times, with the initial T_{store} being σ

copies of some value T_f. I found that this sampling method quickly forgets T_f so the resulting distributions are independent of T_f. I used $\sigma = 1 \times 10^4$, $Z = 1 \times 10^5$ and found that for sensible values of C, i.e. the order of magnitude found in the non-Markovian TASEP simulations, the distributions were also independent of C. This is because for large enough N, C is negligible compared with $\sum_{j=1}^{N-1} W_j$. The mean of the final T_{store} is T_{sc}

In figure 6.10 we can compare T_{sc} with the saturation of the mean blocking time T from the simulations. Figure 6.10a shows the ratio $\frac{\bar{T}}{T_{\text{sc}}}$ to show that the final value $T(10)$ appears to be well approximated by T_{sc}. Comparing figure 6.10b with figure 6.6 we can see that the T_{sc} is a significantly better approximation to the observed saturation level than the predicted blocking time $\bar{T}$ from equation 6.7. We also notice that $\frac{T(10)}{T_{\text{sc}}}$ seems relatively flat which is indicative of T_{sc} having the correct scaling form for L. The self-consistent sampling method has in effect fixed the prefactor in equation 6.7.

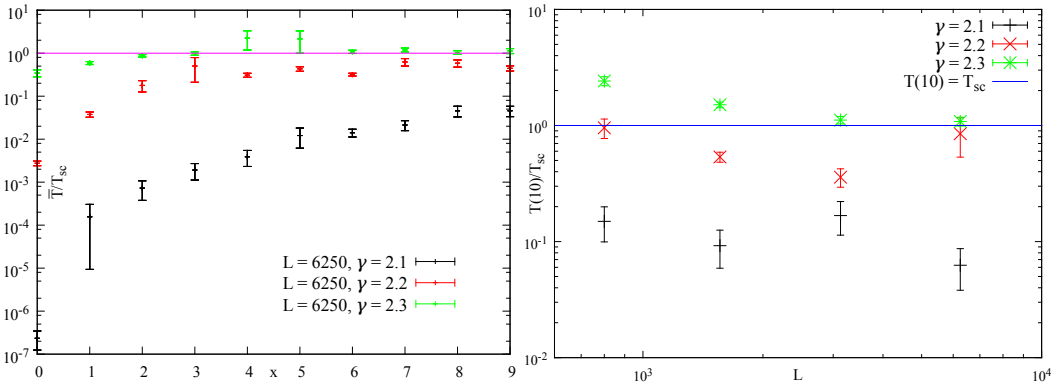

(a) $\bar{T}/T_{sc}$ *v.s. position in condensate* $x = i/N$ *for* $\rho = 0.1$, $L = 6250$, $\gamma = (2.1, 2.2, 2.3)$

(b) $T(10)/T_{sc}$ *for* $\gamma = (2.1, 2.2, 2.3)$, $L = (800, 1560, 3130, 6250)$, $\rho = 0.1$

Figure 6.10 *Comparison of self-consistent prediction* T_{sc} *with the saturation of* T

In figure 6.11 we compare the distribution of blocking times simulated using the self-consistent sampling T_{store} with the actual blocking time distribution, $p(T)$ from simulations at $x = 10$. We can see that the distributions are relatively closely matched though they appear to have slightly different tails and starting values. The discrepancy between the tails could be due to the value Z in the self-consistent sampling not being large enough to allow the sampling method to properly saturate to the final stable distribution. It is also possible that the distribution of blocking times obtained at $x = 10$ is not properly representative of the distribution of blocking times at $x = \infty$, but since we cannot sample

this directly, we cannot know. The discrepancy between the starting values and tails may also be due to method ignoring fluctuations in C. The fact that the distributions seem to consistently of the right order of magnitude despite these objections lends us confidence that this is a fair approximation method.

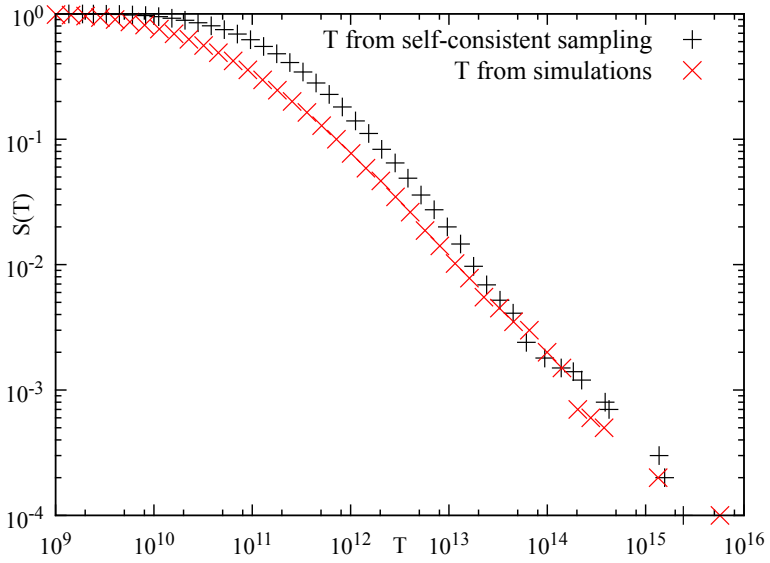

Figure 6.11 *Empirical survival distribution $S(T)$ for simulations with $L = 6250$, $\rho = 0.1$, $\gamma = 2.2$ and T_{store} for $N = 625$, $C = 0$, $\sigma = 1 \times 10^4$, $Z = 1 \times 10^5$*

6.7 Fraction of particles moved between consecutive condensates

In this section we predict the average fraction of particles which move between consecutive condensates and compare that result with simulations. The probability that a particular particle chooses a waiting time large enough to be a pack-leader $W > C$ given that it is blocked for a time T is (equation 5.11)

$$\begin{aligned} p(W > C; T) &= \int_C^\infty p_A(W; T) \mathrm{d}W \\ &= \frac{C^{2-\gamma} - (C+T)^{2-\gamma}}{\gamma - 1 - T^{2-\gamma}} \end{aligned}$$

We now use the mean-field like approximation that once the average T has saturated, we can replace the distribution of T with $\bar{T}$. This implies that each choice of W from $p(W; \bar{T})$ is independent, therefore if we consider the choice of

$W > C$ to be a success we have defined a Poisson process. The expected number of particles before the first success, m, is

$$\begin{aligned} m &= \left(p(W > C|\bar{T})\right)^{-1} \\ &= \frac{\gamma - 1 - \bar{T}^{2-\gamma}}{C^{2-\gamma} - (C + \bar{T})^{2-\gamma}} \\ &\approx \frac{\gamma - 1}{C^{2-\gamma}} \\ &\sim L^{\gamma-2} \end{aligned}$$

since $\bar{T} \gg C$. We see that this number increases with L, however the fraction of particles which move between condensates, $f_m \sim L^{\gamma-3}$, which tends to zero as $L \to \infty$. Unfortunately we have not been able to check this result against the simulations because of the difficulty in getting sufficient numbers of consecutive condensates for $\gamma > 2.3$ such that we see the saturation. Simulations for $\gamma = 2.3$ took weeks to finish, and I expect simulations of $\gamma = 2.4$ to take an order of magnitude more.

6.8 Mean pack-leader lifetime and the condensate lifetime

We have computed the saturation of the mean waiting time $\bar{W}$, whereas to compute the condensate lifetime we require the mean time picked by a pack-leader, $\bar{W}_{\mathrm{PL}}$. We have consistently assumed that a pack-leader must pick a waiting time larger than C, so first we need the expected W given that $W > C$ from equation 5.16.

$$\langle W|W > C; T\rangle = \frac{\frac{\gamma-2}{3-\gamma}\left((T + C)^{3-\gamma} - C^{3-\gamma}\right) + T(T + C)^{2-\gamma}}{C^{2-\gamma} - (C + T)^{2-\gamma}}$$

The mean pack-leader time at the saturation level is then $\langle W|W > C; \bar{T}\rangle$, and as $\bar{T} >> C$ we can keep the leading terms from the numerator and denominator

$$\begin{aligned}
\bar{W} &\approx \frac{\bar{T}^{3-\gamma}}{(3-\gamma)C^{2-\gamma}} \\
&\approx \frac{\left(\frac{\rho L}{(3-\gamma)(\gamma-1)}\right)^{\frac{3-\gamma}{\gamma-2}}}{(3-\gamma)\left(L(1-\rho)\langle t\rangle\right)^{2-\gamma}} \\
&= \frac{\rho^{\frac{3-\gamma}{\gamma-2}}}{(3-\gamma)\{(3-\gamma)(\gamma-1)\}^{\frac{3-\gamma}{\gamma-2}}\{(1-\rho)\langle t\rangle\}^{2-\gamma}} L^{\gamma-3+\frac{1}{\gamma-2}} \\
&\equiv \lambda L^{\Lambda}
\end{aligned}$$

The condensate lifetime is the waiting time of the pack-leader minus the catch-up time C. Since we have assumed that $C \sim L$, it is sub-dominant to $L^{\gamma-3+\frac{1}{\gamma-2}}$, the condensate lifetime $\bar{l}_s \sim L^{\gamma-3+\frac{1}{\gamma-2}}$.

In figure 6.12 we extend figure 4.7 using the data from the accelerated simulations. The two lifetimes associated with a full condensate are; the lifetime of the solid phase (the condensate), l_s and the lifetime of the fluid phase l_f. Over the range of L accessible from the simulations, the averages $\bar{l}_s$ and $\bar{l}_f$ are straight lines on a log-log plot, i.e. they have a power law dependence on L. Fitting a power law of the form aL^b to $\bar{l}_s$ and $\bar{l}_f$, we can find the exponents b. In figure 6.12 we see b plotted against γ for fixed $\rho = 0.1$ alongside the predicted exponents from $\bar{l}_f \sim L^1$ and $\bar{l}_s \sim L^{\gamma-3+\frac{1}{\gamma-2}}$. We see that $\bar{l}_f$ scales slightly faster than L, however we cannot rule out finite size effects in L, so we conclude that $\bar{l}_f \sim L^1$ is an acceptable approximation. $\bar{l}_s \sim L^{\gamma-3+\frac{1}{\gamma-2}}$ seems to overestimate b for small γ and underestimate b for large γ. A possible explanation of this discrepancy is the fact that $\bar{T}, \bar{W}$ used in our computation of $\bar{l}_s$ is only strictly valid when the condensate has fully saturated and never dissolves, which we cannot see in simulations with finite L.

6.9 Flux

In this section we discuss the flux of particles around the ring in the thermodynamic limit. Since the condensate is stationary, the current can only flow during the fluid phase. We showed that a vanishing fraction of the particles in the condensate moves between consecutive condensates. Putting these together we

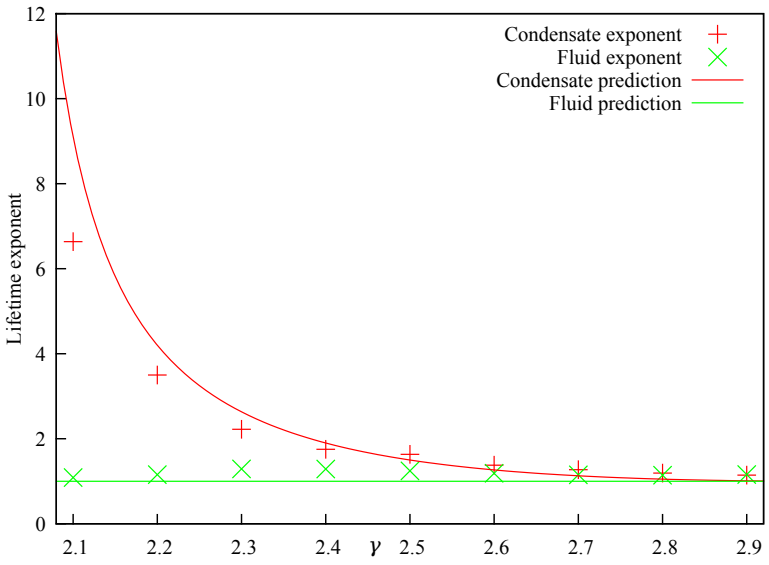

Figure 6.12 *Exponent b of the fitting of $\bar{l}_s$ and $\bar{l}_f$ to aL^b as a function of γ for $\rho = 0.1$*

get

$$\begin{aligned} J &= \frac{\text{Number of particles moved}}{\text{Time taken to move particles}} \\ &= \frac{m}{\bar{l}_f + \bar{l}_s} \\ &\sim \frac{L^{\gamma-2}}{L^{\gamma-3+\frac{1}{\gamma-2}}} \\ &\sim L^{1-\frac{1}{\gamma-2}} \end{aligned}$$

This vanishes as $L \to \infty$ as observed numerically. Unfortunately we have not been able to check this result against the simulations because of the difficulty in getting sufficient numbers of consecutive condensates for $\gamma > 2.3$ such that we see the saturation. For $\gamma \leq 2.3$ I ran simulations such that the length of the complete condensate was $5N$, and repeated this 1×10^5 times. Since the probability of complete condensate dissolution increases with fixed L and increasing γ, the probability that such an extended condensate occurs decreases, and the time required to run the simulations is strongly dependent on γ and L. Simulations for $\gamma = 2.3$ took weeks to finish, and I expect simulations of $\gamma = 2.4$ to take an order of magnitude more.

6.10 Chapter summary

In this chapter we use the accelerated algorithm described in the previous chapter to simulate the non-Markovian TASEP for higher L, but more significantly, for lower γ than was possible using the basic continuous time Monte Carlo algorithm described in chapters 2 and 4. It was argued in chapter 4 that there was a separation of timescales between the lifetime of the full condensate and the time between full condensates, which would cause the fraction of time spent in the condensate, f, to tend to one in the thermodynamic limit. Using the accelerated simulations for $\gamma < 2.4$ we can see directly that this is true, though we are still unable to simulate high enough L to see $f \to 1$ directly for $\gamma \geq 2.4$. We do however observe that that f increases for $\gamma \geq 2.4$.

We concluded in chapter 4 that there was an increasing chance of two consecutive condensates interacting, i.e. for a number of particles to remain stationary between full condensates. We showed that the probability that two consecutive condensates will interact tends to one as $L \to \infty$, and therefore to predict the behaviour of the system in the thermodynamic limit, we needed to understand how the mean blocking time T and waiting time W of a particle depends on its position in the consecutive condensate. We saw from simulations that after a sufficient number of particles into the condensate the mean T, W saturate to a finite value and that there is a vanishing fraction of particles which move between consecutive condensates. This leads us to the following picture of the thermodynamic limit: once a full condensate has formed on the system there will always be a macroscopic fraction of the number of particles on the system which are in a stationary condensate. A spatially complete condensate is always present except when a vanishing fraction of the condensate "chips" off from the front and makes a circuit of the lattice to rejoin the condensate at the rear. This leads to the condensate moving slowly around the system in the opposite direction to the direction of particles. This behaviour is very similar to the slinky motion of the non-Markovian ZRP discussed in section 2.5, but with a critical density of zero, i.e. no background fluid.

Using a mean-field like assumption we derived an approximation to the saturation level of the mean of T, $\bar{T}$, and W, $\bar{W}$. Fitting $\bar{T}$ seen in simulations to aL^b we saw that the predicted $\bar{T}$ seemed to have the correct exponent b, but that the prefactor a could be orders of magnitude out. Using a self-consistent sampling method we found that we could dramatically improve the prefactor to allow for

a much more accurate prediction of the saturation level of T. We deduced the L dependence of $\bar{W}$ from $\bar{T}$ and used this to predict how the condensate lifetime $\bar{l}_s$ depends on L. We saw that the predicted lifetime exponent wasn't a bad approximation to the lifetime exponent computed from the simulations, and argued that the discrepancy between the two may be a finite lattice size effect.

Chapter 7

Robustness of condensation

In this chapter we will investigate different physical systems using the non-Markovian TASEP as a baseline. We will see that a random walker in a random force field experiences randomly distributed potential wells, and generates power law distributed waiting times for escape from a well. This is known as the trap model in glassy dynamics. If we restrict the walkers, which interact by mutual exclusion, to move in one discrete spatial dimension we can use the non-Markovian TASEP to generalise the trap model to a number of interacting particles. We will investigate two varieties of the multiple interacting particle trap model: one where particles re-sample their current potential well after every attempted move, and one where particles only re-sample their potential well after a successful move.

We saw in chapter 2 the range of expansions and extensions of the TASEP in order to make it a more realistic minimal model of traffic flow. The generalisation which we will investigate here is allowing particles to move in both directions. The interesting question which arises from this is: once the totally asymmetric condition is relaxed, how robust is the full spatial condensate?

7.1 Asymmetric Exclusion Process

In this section we relax the constraint that particles are restricted to move in a single direction in the non-Markovian ASEP to see if this affects the complete condensation. This is defined mostly the same way as before, there is a one dimensional lattice of L sites containing N particles which interact by mutual exclusion, and can only move to adjacent sites. In the same manner as the

semi-Markov process discussed in chapter 3, we define Markovian transition probabilities between sites, and then draw a waiting time to the next attempted move. Before there only existed a single option, particles always leave a site to the right with probability 1, but now they can leave the site to the right with probability $p \leq 1$, and to the left with probability $1 - p$. The waiting time to that chosen event is then chosen from the waiting time distribution $p_1(t) = (\gamma - 1)t^{-\gamma}\Theta[t - 1]$. We are interested in the effect of allowing transitions in both directions on condensates, and so we choose to perform calculations on the region $\gamma = 2.2$ as this shows the effects of condensation, however it will be difficult to use the brute force simulations.

The fully symmetric Markovian SEP and the Markovian TASEP occupy different universality classes and the crossover between the two has been investigated using a Weakly Asymmetric Simple Exclusion Process (WASEP) where $p - 0.5 \sim L^{-1}$ [25]. In the non-Markovian fully symmetric case we expect there to be no condensation as there is no net drift around the system, so particles will not tend to aggregate. We have shown that there is a condensation effect for the non-Markovian TASEP, and so we expect to see some sort of crossover regime for intermediate values of asymmetry $0.5 < p < 1$.

In principle there are two options for the simulation algorithm of the non-Markovian ASEP; when a particle has attempted to make a move it can choose to pick a direction first and an attempt time second (which we call Asymmetric Model 1), or an attempt time first and a direction second (which we call Asymmetric Model 2). The models are equivalent for the brute force method, as the time drawn by the particle is independent of the direction chosen. For the accelerated method, the waiting time is now dependent on the direction of travel, and we must know that first in order to know if the particle is blocked, hence we can only use the accelerated method in Model 1.

Without substantially altering how the simulation is run the accelerated algorithm is no longer rejection-free, as particles which were not blocked when they chose their waiting times may become so due to particles now being allowed to move in both directions. To use the blocked waiting time distribution we need a value for T, and since failed moves are allowed the blocking particle may fail to move once T has elapsed. We make the choice that T is the waiting time chosen by the blocking particle minus the time elapsed since it last attempted to move, as in the totally asymmetric case. The simulation algorithm for Asymmetric Model 1 is therefore:

- Particle chooses a direction. A random number, u, is drawn uniformly between $(0, 1)$. If $u < p$ the particle moves right, otherwise it moves left.
- If the target site is occupied, T is the time that has yet to elapse until the blocking particle is scheduled to move off, whether that move will turn out to be successful or not.
- The waiting time for the particle is drawn from $p_A(W; T)$ as usual.

In Model 1 we have integrated out a number of attempted moves whilst keeping the direction constant. This implies that we have in effect removed the constraint that both directions have a constant probability, by allowing a particle which is blocked to choose a direction of motion and preferentially choose that same direction for a time. Consider a ribosomal motor whose back leg detaches and moves forward. If this gives the motor a preference to attach that leg to the site in front, rather than re-attach it in its original place and reverse the direction of motion, then Asymmetric Model 1 may be a useful approximation.

7.1.1 Asymmetric Model 1

Since we can use the accelerated algorithm, we will start by investigating Model 1. Once particles are allowed to move in both directions, they will have the option to move away from such a blockage, and so we expect full spatial condensation to rely on the totally asymmetric property. In addition, increasing the symmetry (taking p closer to 0.5) will reduce the bias for particles to make laps of the lattice, and therefore make it more unlikely for a particle to stop for long enough to allow everything to condense behind it.

The result in figure 7.1 seems counter-intuitive, as the full condensate persists at all levels of asymmetry for Asymmetric Model 1, until we realise that we have inadvertently introduced an effective attraction between the particles. To illustrate this effective attraction, consider the case of a particle which is blocked, and suppose that it would take x attempts for the sum of the waiting times to exceed T. In the accelerated routine a particle cannot change its mind about its direction until it has made x attempted moves, however in the brute force routine the probability that a particle does not move in the opposite direction in x picks is $p^x < 1$ unless $p = 1$. For $p < 1$ we have conditioned on particles not moving away from their neighbours if they become blocked by them. This is an effective attraction that explains the unintuitive behaviour of the accelerated

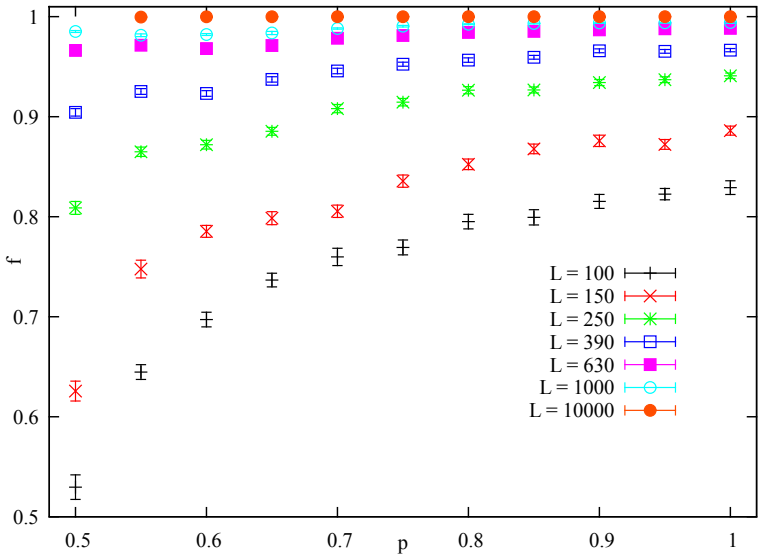

Figure 7.1 *Fraction of time spent in spatially complete condensate, f, for $\gamma = 2.2$, $\rho = 0.1$ for the non-Markovian ASEP using Asymmetric Model 1 and a range of p.*

Asymmetric Model 1. This is an example of the need to choose the correct simulation algorithm for the physics you are trying to investigate, at the risk of studying something subtly different which has substantially different behaviour. The choice of simulation algorithm which correctly accommodates the ability of particles to move in both directions, is one where the waiting time and the direction chosen are independent, i.e. using the brute force method. We discuss this in the next section.

7.1.2 Asymmetric Model 2

We will now use the second choice of simulation mechanism, Asymmetric Model 2, where particles choose a waiting time first and a direction second. This implies that we cannot use the blocked waiting time distribution as discussed above, and we therefore expect the simulations to take significantly longer.

We expect the crossover between the non-Markovian TASEP-like regime and the non-Markovian SEP-like regime nearer to $p = 1$ than $p = 0.5$, as the condensate effects we have so far observed require that a particle be constantly blocked for long enough to choose an exceedingly large waiting time. Once particles are allowed to move in both directions they can simply choose to move freely away from the blockage. This led me to the conclusion that any degree of asymmetry will destabilise the complete condensate. We can use the non-

Markovian TASEP as a baseline to attempt to collapse the curves for different L onto each-other and thereby see if there is a universal trend with increasing p, or if changing L also has an effect. We have a range of L and we know that f increases with increasing L for the non-Markovian TASEP, so we plot the ratio of f to the value of f for the TASEP, i.e. $\frac{f}{f_{p=1}}$. In figure 7.2a we see that the fraction of time spent in the fully condensed state f increases with increasing asymmetry, which is indicative of a crossover much closer to $p = 0.5$. The curves have collapsed down towards each other, however there is still some noticeable dependence on L, especially for higher p, so in figure 7.2b is shown the increase of $\frac{f}{f_{p=1}}$ with L. This increase leads us to the conclusion that $\frac{f}{f_{p=1}}$ will tend to one in the thermodynamic limit. For $p < 0.575$ any increase in $\frac{f}{f_{p=1}}$ is imperceptible over the range of L that we have simulated, which is consistent with a crossover in this region. In this simulation I have not been able to directly observe the crossover, so cannot tell from this data what critical exponent it has.

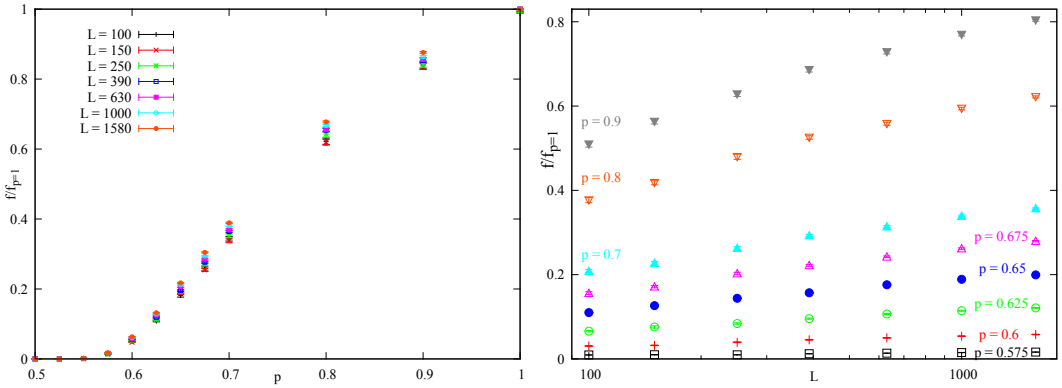

(a) *Range of p* **(b)** *Range of L*

Figure 7.2 *Fraction of time spent in spatially complete condensate, f, over f for TASEP, $f_{p=1}$, for $\gamma = 2.3$, $\rho = 0.1$ for the non-Markovian ASEP using Asymmetric Model 2*

A possible explanation of this result is that any net drift around the system is enough to allow spatially complete condensates to form, albeit with an effectively higher catch-up time C. If the lattice contained only a single particle, it would be a biased random walker. The position distribution of a driftless random walker is a Gaussian which spreads with time. For a random walker with a drift term, the Gaussian moves in the direction of the drift, and so the probability that a particle will be far in the opposite direction to the drift is exponentially suppressed. This implies that for a large enough lattice and $p > 0.5$, the probability that the particle will complete a lap of the lattice to the right (as in the non-Markovian TASEP) is significantly greater than the probability it will complete the lap to

the left. On average we expect particles to drift around the lattice in the same manner as the non-Markovian TASEP, though this will affect the catch-up time C. Consider a particle making n steps: on average we expect np steps forward and $n(1-p)$ steps back, which leads to a net expected forward number of hops of $np - n(1-p) = n(2p-1)$. The net rate of making forward hops is therefore $2p-1$. If a particle has to travel η spaces to traverse the lattice to get round to the back of the condensate, for the asymmetric case we expect it to take $\frac{\eta}{(2p-1)}$ steps. This introduces a prefactor to C, which does not alter the fact that the inter-condensate time grows at a slower rate with L than the condensate lifetime, so we still expect the separation of timescales for all $p \neq 0.5$. Since I only know a mean field approximation of the catch-up time C, exactly how other properties of the system depends on this prefactor is an avenue for possible future work.

Figures 7.2 are compatible with a crossover regime between the regime with full spatial condensation and the regime without, anywhere in the region $p < 0.575$. In order to expand out this region we can use "condensate measure", m. This is a measure of how condensed the system is, and as such, is more sensitive to condensation on the lattice than the fraction of time spent in the full spatial condensate. The "condensate measure", m, is defined as follows

$$m = \frac{2N - e}{2(N-1)} \tag{7.1}$$

where e is the number of "ends" on the system. An end is defined as an allowed particle direction; if a particle is unblocked to the left and the right it has two ends, if it is unblocked in one direction only it has one end, and if a particle is blocked in both directions it has no ends. With this definition the number of ends is equal to the number of domain walls in the system. The condensate measure m, can be considered an order parameter describing the amount of condensation in the system. For a completely un-condensed state where all particles can move in both directions there are $2N$ ends and $m = 0$. In the case where all particles are in a single block, only the rightmost particle can move right, and only the leftmost particle can move left, which implies that $e = 2$ and $m = 1$. We can now create similar graphs using m as opposed to the fraction of time spent in the full spatial condensate f. As useful comparison is with m computed using the assumption that all sites are equally likely to contain a particle, as in the steady state of the Markovian TASEP on a ring, $m_{s.s.}$. This can be computed

quite simply by re-expressing m in the N large limit.

$$\begin{aligned} m &= \frac{2N - e}{2(N-1)} \\ &= \frac{N - \frac{e}{2}}{N-1} \\ &\approx 1 - \frac{e}{2N} \end{aligned}$$

$\frac{e}{N}$ is the number of ends per particle, and this can be computed using equally likely configurations condition. The probability that any particular site contains a particle is ρ so, picking a particle at random, the probability that it is unblocked on both ends is $(1-\rho)^2$ (i.e. has $e = 2$). The probability that it has $e = 1$ is $2\rho(1-\rho)$, and the probability that it is blocked at both ends ($e = 0$) is ρ^2. The probability of a particle having e ends is then

$$p(e) = \begin{cases} (1-\rho)^2 & \text{if } e = 2 \\ 2\rho(1-\rho) & \text{if } e = 1 \\ \rho^2 & \text{if } e = 0 \end{cases} \tag{7.2}$$

The expected number of ends per particle is $\bar{e} = 2(1-\rho)^2 + 2\rho(1-\rho) = 2(1-\rho)$. The expected for the steady state condition $m_{s.s.} \approx 1 - \frac{N\bar{e}}{2N}$ gives the result that

$$m_{s.s.} = \rho \tag{7.3}$$

In figure 7.3a is a plot of m against p, which shows that m increases with p and L. Figure 7.3b shows clearly that for $p = 0.5$ for all L, the mean condensate measure is indistinguishable from the "all configurations are equally likely" steady state $m = \rho$. For all the shown $p > 0.5$ we have an increasing amount of condensation in the system. This is evidence of the crossover region $p < 0.525$. It should be noted here that because I can only see where the crossover is not, and have never measured it directly, I cannot tell whether this is a crossover or a transition with a critical exponent greater than one. It appears that the shape of the m as a function of p is indicative of $m = \rho$ only at $p = 0.5$, and therefore the cross-over between the symmetric and totally asymmetric like regimes of the non-Markovian ASEP is also at $p = 0.5$.

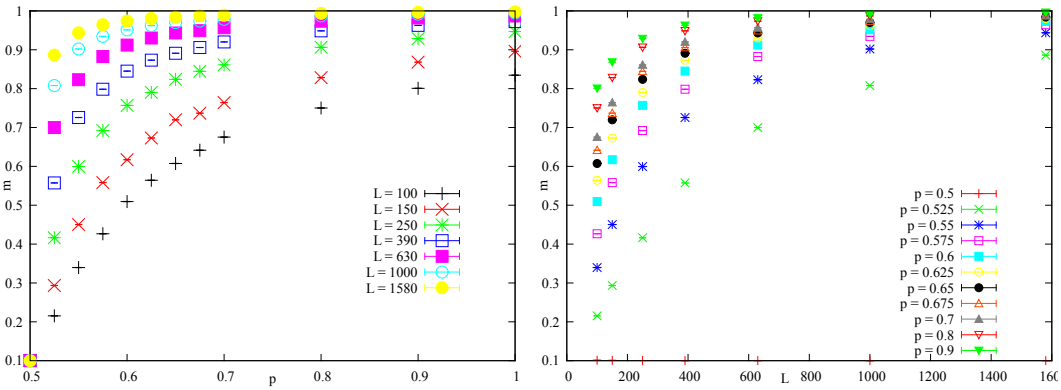

(a) *Range of p* **(b)** *Range of L*

Figure 7.3 *Mean condensate measure m for $\gamma = 2.3$, $\rho = 0.1$ for the non-Markovian ASEP using Asymmetric Model 2*

7.2 Trap model

In this section we discuss how a power law waiting time distribution can arise naturally from underlying physics. Consider, as discussed in [35] and [14], a one dimensional continuous time random walk in a random force field ($RWRF$). It is is governed by a Langevin equation of the form

$$\frac{\mathrm{d}x}{\mathrm{d}t} = -\frac{\partial U}{\partial x} + \eta$$

Where $U(x)$ is the random potential, and η is Gaussian white noise. A random walker in a random potential will experience the large fluctuations of $U(x)$ as potential wells. It can be shown with the method of steepest descent that the distribution of potential wells is exponential [14]. Since particles move about getting stuck in potential wells, this is known as the "trap model".

Consider potential wells which are exponentially distributed $P(E) = \frac{x}{T}\exp[-\frac{xE}{T}]$, where N is a constant, T is the temperature and x is a temperature dependent number. The time trapped in the potential of depth E is $\tau = \tau_0 \exp[\frac{E}{T}]$ by Arrhenius' equation [20]. The distribution of trapping times τ is $\Psi(\tau)$ which we get by using conservation of probability $\Psi(\tau)\mathrm{d}\tau = P(E)\mathrm{d}E$ which implies

$$\Psi(\tau) = \kappa\tau_0^x\tau^{-(x+1)}\Theta[\tau - \tau_0]$$

This is an example of power law waiting times arising naturally from the underlying physics. The random walker in a random potential appears in ageing

phenomena in spin glasses [14] and kink propagation along a dislocation line [35]. Since kink propagation along a dislocation line occurs in 1D, we can model it as a non-Markovian TASEP. For parity with our previous results we will use periodic boundary conditions and a discrete lattice of sites.

The power law waiting time TASEP described in previous chapters can be considered a multi-particle version of the trap model under the condition that the well depth is reset at every attempted move and the particles interact by hard-core exclusion. This is equivalent to a random walker escaping randomly distributed potential wells, but only moving a physical site when it is unblocked. We can therefore investigate this trap picture using slight modifications to the previous simulations. We define the following models.

- Model A: This is the power law TASEP discussed previously.
- Model B: This is a multiple particle trap model with the underlying waiting time probability distribution $p_1(t)$ sampled in two steps. After each attempted move, a particle experiences a new randomly distributed trap. The distribution of expected escape times from this trap is then $p(\tau) = \nu\tau^{-(\nu+1)}$ where the decay parameter $\gamma = \nu + 1$. An escape time τ is drawn from $p(\tau)$ and the particle makes an attempt to escape that trap at a Poisson distributed time with mean τ, $p(t) = \frac{1}{\tau}\exp[-\frac{t}{\tau}]$.
- Model C: This multiple particle trap model differs from Model B in the following regard: a particle only exits a trap once it can move a physical place. This implies that when a particle executes an allowed move it is assigned a new potential well. The particle draws an expected escape time τ from $p(\tau) = \nu\tau^{-(\nu+1)}$ where the decay parameter $\gamma = \nu + 1$, and the particle makes an attempt to escape that trap at a Poisson distributed time with mean τ, $p(t) = \frac{1}{\tau}\exp[-\frac{t}{\tau}]$ as before. Whilst a particle is blocked it makes a number of attempted moves drawn from an exponential distribution with a particular mean. We saw in chapter 5 that this is equivalent to a particle only starting to escape its potential well once it becomes unblocked. We make the simulations of model C rejection-free by assigning it a waiting time $W = T + t$, where T is the time it is blocked for, and t is the time drawn from the exponential decay.

We expect Model B to be equivalent to Model A, as particles are allowed failed moves due to being blocked, and figure 7.4 shows that this is the case. Since the renewal process governing the escape time of a particle in Model C is Markovian,

we do not expect to see the ageing effects from Model A. Models A and B are also indistinguishable in mean time between full condensates, mean time assigned to the front particle of a full condensate and mean lifetime of a full condensate (data not shown). This implies that the particular generalisation of the trap model that is Model B exhibits condensation which is spatiotemporally complete in the thermodynamic limit. Figure 7.4 illustrates that Model C is substantially different to Models A and B, and we will discuss the behaviour of Model C for the remainder of this section.

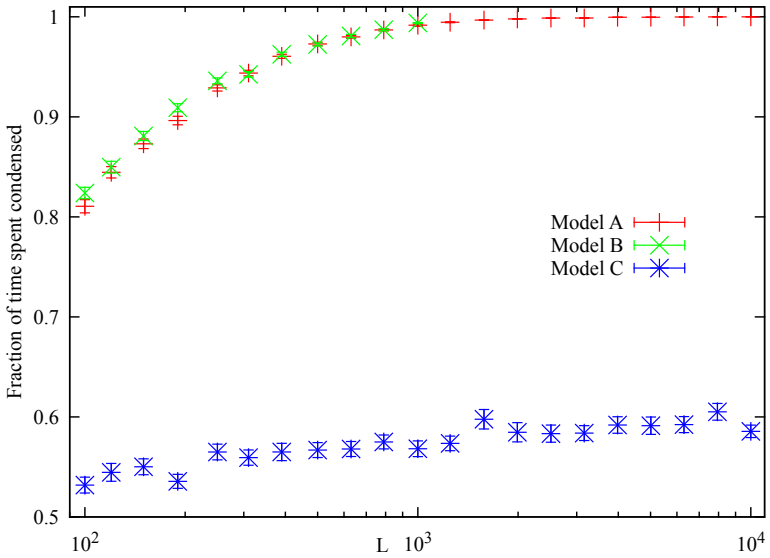

Figure 7.4 *Fraction of time spent in spatially complete condensate for* $\gamma = 2.2$, $\rho = 0.1$ *for Models A, B, C.*

7.2.1 Model C

In figure 7.5a we compare the fraction of time spent fully condensed, f, in Model C for a range of γ and L. The time taken to get a sufficient number of full condensates to ensure proper statistics takes a larger time as γ increases, and we have only had time to extend this graph up to $\gamma = 2.3$. This data suggests that f tends to a finite fraction $0 < f < 1$ in the range $2 < \gamma < 3$. We can use our knowledge of the separation of timescales in the non-Markovian TASEP (section 4.4) to assist us here: If a separation of timescales was to occur between the condensate lifetime and the intercondensate lifetime, we would expect it to be more pronounced at lower γ. We can fit the mean condensate lifetime for the range of L at $\gamma = 2.2$ to the form aL^b and the mean inter-condensate lifetime to cL^d. If $f \to 1$ in the thermodynamic limit we would expect $b > d$, $b < d$ implies

$f \to 0$, and $b \approx d$ implies $f \to$ constant. From the fitting we find $b = 1.69 \pm 0.03$ and $d = 1.60 \pm 0.01$. The condensate lifetime scaling is slightly stronger than the inter-condensate lifetime scaling, but they are significantly closer than we would expect at $\gamma = 2.2$ if there was a separation of timescales.

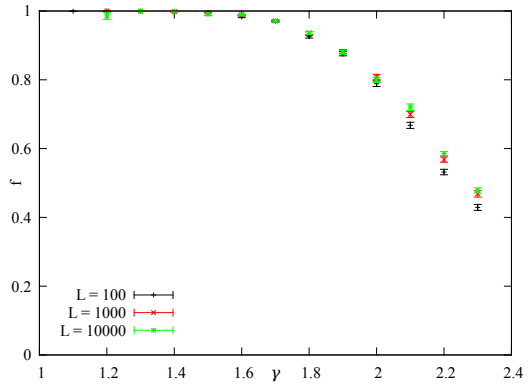

(a) *Fraction of time spend fully condensed for Model C,* $\rho = 0.1$

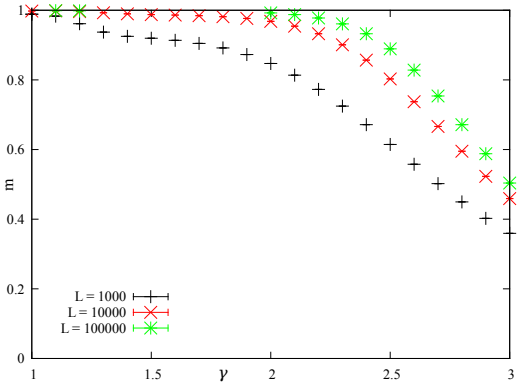

(b) *Mean condensate measure* m *for Model C,* $L = (1000, 10000, 100000)$*,* $\rho = 0.1$

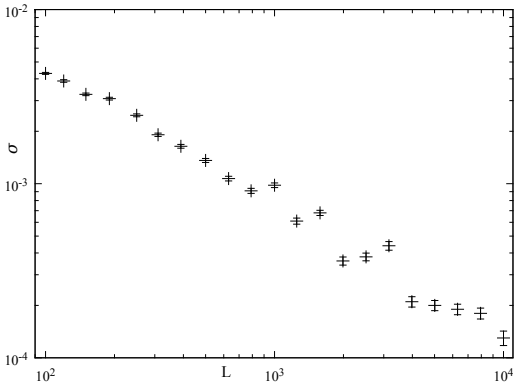

(c) *Fraction of condensates interacting* σ *for Model C,* $\gamma = 2.2$*,* $\rho = 0.1$

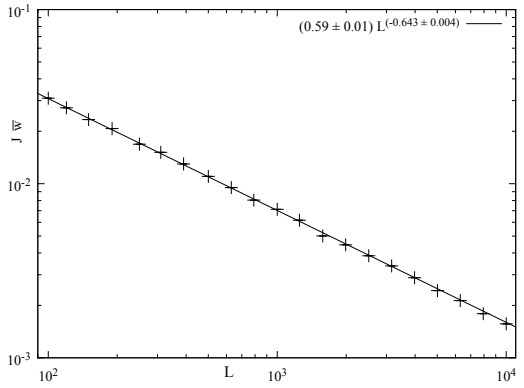

(d) *Flux times* $\langle t \rangle$ *for* $\gamma = 2.2$*,* $\rho = 0.1$

Figure 7.5 *Data for Model C*

A simulation was performed to compute the mean condensate measure m discussed in the previous section. Figure 7.5b shows that m increases with decreasing γ and increasing L. It does not appear that there is a sharp crossover at $\gamma = 3.0$ between the case with increasing m and the constant $m = \rho$ predicted for the Markovian-like configuration. The fact that m appears to increase more slowly with increasing L may be also be indicative of a macroscopic condensate existing for a finite fraction of time.

We can consider Model C to have a blocked waiting time $p(W;T) = (\gamma - 1)W^{-\gamma}\Theta[W - 1]$, and therefore if a particle is blocked, it will not get the re-

enforcement of W due to a number of failed move attempts. We conclude that a full condensate is possible, but that consecutive full condensates are unlikely. In figure 7.5c we can see that the probability that two consecutive condensates interact does indeed decrease.

In the thermodynamic limit consecutive condensates do not form out of the remnants of the preceding condensate. The naive model in section 4.5 assumed that condensate formed out of a fluid state, and dissolved back into it once the condensate broke apart. This is a significantly better approximation for Model C than Model A, and it predicts the thermodynamic limit of f in the range $2 < \gamma < 3$ of $0 < f < 1$. We will briefly reiterate this naive argument here, as a candidate explanation of the behaviour of Model C. The recursive argument in section 4.5 starting from the assumed steady state of the Markovian TASEP gave us $\eta \sim L$ where η is the number of picks made by the last particle in the condensate to travel to its resting place. The weak law of large numbers in section 3.4.3 allows us to write the dominant term in the catch-up time $C \sim \eta\langle t\rangle$, where $\langle t\rangle = \int_{t=0}^{\infty} t p_1(t) \mathrm{d}t$. The probability that on a single pick, a particle draws a time larger than C is $C^{1-\gamma}$. There are ρL particles, so the expected time until any particle picks a time larger than C is $\tau = \frac{\langle t\rangle C^{\gamma-1}}{\rho L}$. The mean time drawn from $p_1(t)$ conditioned on it being larger than C is $\langle t\rangle C$, so the mean pack-leader time $\sim C \sim L$. The fluid phase lifetime $l_f \sim C + \tau \sim L$, and the solid phase lifetime is the difference between the mean pack-leader time and the catch-up time, $l_s \sim C \sim L$. The fraction of time spent in the condensate is therefore a constant, $f = \frac{l_s}{l_f + l_s}$.

7.2.2 Restoration of particle-hole symmetry

As we discussed in chapter 2, the flux is a useful indicator of the presence of condensation in a driven diffusive system. In figure 7.5d we can see a power law decrease in the flux with increasing L. We would expect the flux to tend to a finite value if the system spends a finite fraction of time in the fully condensed state, and the remainder in a free-flowing Markovian-like state. A possible explanation for this result is the fact that the fraction of time spent in the condensate has not yet saturated to the expected constant, as shown in figure 7.4.

The fundamental diagram for Model C (the plot of the flux against the particle density on the system) is shown in figure 7.6. Firstly, and least interestingly, the flux times the mean of $p_1(t)$ is still below the value predicted for the Markovian

TASEP on a ring in the steady state. We also notice that the fundamental diagram for Model C is symmetric about $\rho = 0.5$, which is indicative of particle hole symmetry. This can be understood intuitively in discrete time. In Model A, a particle has a jump probability which is dependent on how long it has occupied its current site. Swapping particles and holes, the particle now has a jump probability which is dependent on how long the adjacent hole has occupied its current site, so clearly Model A breaks particle hole symmetry. In Model C, a particle has a jump probability which is dependent on how long its target site has been a hole. Swapping particles and holes, the particle now has a jump probability dependent on how long the target site has been a hole. Since the particle becomes the neighbour of the hole at the same time the hole becomes the neighbour of the particle, these two times are identical, so the particle-hole symmetry is exact in Model C.

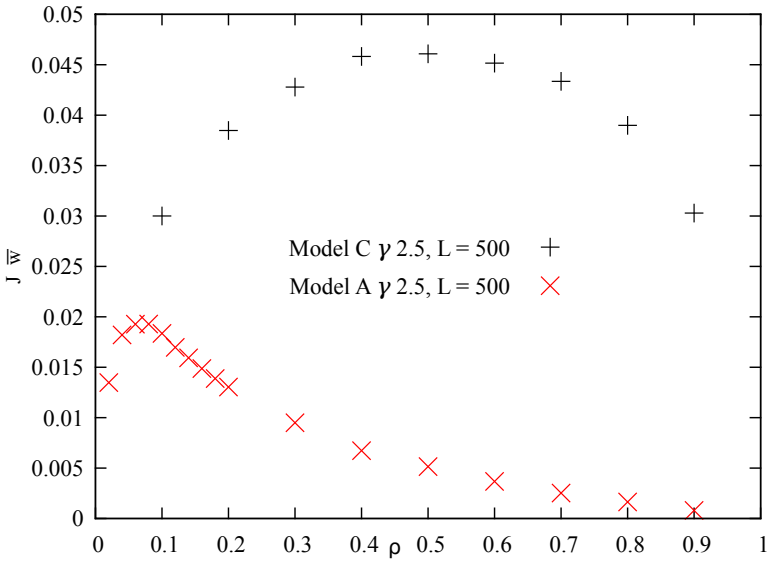

Figure 7.6 *Fundamental diagram for Models A, C, $\gamma = 2.5$, $L = 500$*

7.3 Mapping of Models A and C to non-Markovian ZRPs

In chapter 2 we discussed the mapping between the TASEP and the Zero Range Process (ZRP). In this section we discuss the mappings between the TASEP and the ZRP once the waiting time distributions are non-Markovian. A full spatial condensate in the TASEP corresponds to a site containing all the particles in the ZRP. This differs from the types of condensation seen in the ZRP before as there

is no background fluid of particles. It also has no critical density above which condensation occurs, though that can also be achieved in the Markovian ZRP. The complexity in the mapping results in the dynamics of the particles. I will discuss them in discrete time, as I find it more intuitive.

The TASEP maps to the ZRP by turning particles into sites, and with the number of unoccupied spaces to the right of that TASEP particle being the number of particles on the ZRP site. Moving a particle right in the TASEP corresponds to the equivalent ZRP site attempting to donate a particle to the site to its left, see section 2.4. In the non-Markovian TASEP (Model A), the probability that a particle moves to the right is dependent on the time since it last attempted to move. In the ZRP this corresponds to each site having a counter that records how long since it last attempted to donate a particle to its left. Since in the TASEP a particle attempts to make moves regardless of whether the target site is blocked, the renewal process associated with the times of the particle can be decoupled from the actual location of said particle. In the ZRP this implies that ZRP particles do not reset the counter on the target site, only the exit site, and hence the renewal process is associated with the ZRP sites, and not the ZRP particles. The failed moves of a blocked particle in the TASEP correspond to the failed attempts of an empty site in the ZRP to donate particles to the site to its left. We have shown these failed moves to be important. These are not the usual dynamics for the ZRP, where the transition rate of a particle out of site is dependent on the number of particles in that site and, in principle, the number of particles on the target site. This is a non-Markovian system whereby each site has both a number of particles on it and a counter recording the time since it last attempted to donate a particle to the left. In this case we expect to see a site containing all of the particles on the system, which exists for a fraction of time tending to one in the thermodynamic limit. Since condensates in the TASEP travel backwards around the system as a number of particles chip off from them at the front and rejoin at the back, we also expect to see the condensate moving around the system in the ZRP. We showed in section 6.7 that the fraction of the condensate that chips off the front of the lattice vanishes in the thermodynamic limit, so we also expect the ZRP condensate to move by a vanishing fraction of the size of the lattice, which is reminiscent of the moving condensate discussed in section 2.5. The mapping between chipping in the TASEP and the ZRP is cartooned in figure 7.7.

Model C in the non-Markovian TASEP has a restored particle hole symmetry, in that the probability that a particle moves is dependent how long that particle

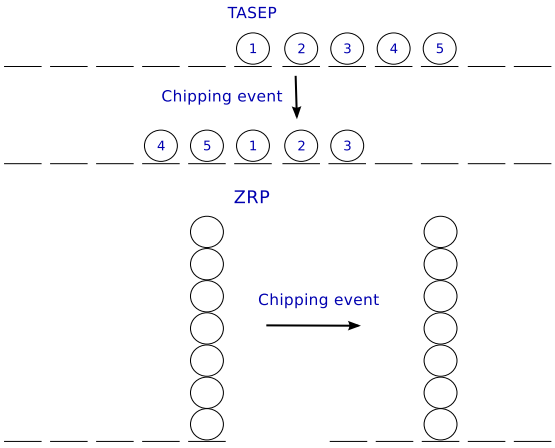

Figure 7.7 *Cartoon of the mapping of condensate chipping between the TASEP and the ZRP. Particles in TASEP are mapped to sites, and in the TASEP they are numbered for convenience.*

has been unblocked on its current site. The dynamics of the ZRP are slightly more complicated: an empty site is inactive and when it receives a particle it becomes active and starts attempting to donate that particle left. The probability that it does so is dependent on how long it has been since the site became active or how long it has been since it last attempted to donate a particle left, whichever is most recent. This can be properly mapped to dynamics of particles. The first particle onto a site resets the counter on that site, and only the most recent particle to arrive on the site is allowed to attempt to move (is active). Thereafter the probability that an active particle moves left is dependent on how long it has been since the counter was reset. A successful move resets the counter of the exit site. The dynamics are properly local, in that it is only the counter on the current site that determines how likely it is for an active particle to move between sites. Model C therefore maps to a slightly unusual non-Markovian ZRP, but the mapping works in terms of the positions of particles, and the dynamics. In this case we expect to see a site containing all of the particles on the system, which exists for a fraction of time tending to a constant $0 < f < 1$ in the thermodynamic limit. Since the condensates in the Model C TASEP do not interact as they do in Model A, we expect the condensates in the ZRP to completely dissolve and reappear on a randomly chosen site.

7.4 Chapter summary

In this chapter we used our knowledge of the non-Markovian TASEP to investigate a number of related physical models. Firstly we extended the TASEP to allow for a range of asymmetry, in order to see the robustness of the condensation effect to increasing symmetry. We concluded that, in the thermodynamic limit, only in the case of perfect symmetry do we not see complete condensation which exists for a fraction of the time approaching one. In using the accelerated algorithm to investigate the ASEP, we did not allow particles to change their direction of motion until they executed a successful move. This made the system even more non-Markovian and introduced an effective interaction between particles, which led to a stabilisation of the condensation effect such that it even occurred in the fully symmetric case. We also proposed a potential application of this modification, when a particle keeps its direction of motion for a number of attempted moves.

We saw that random walkers in random force fields experienced a power law distributed waiting time distribution as a consequence of being trapped in randomly distributed potential wells. If we restrict the particles, which interact by mutual exclusion, to one discrete spatial dimension we can model them using the non-Markovian TASEP. In Model B we allowed particles to escape from their potential well, even if they are blocked on the lattice. This allowed particles to draw a number of power law distributed random waiting times once it becomes blocked, and we showed that this has equivalent behaviour to the non-Markovian TASEP. In Model C we only allowed particles to escape their current potential well on a successful move on the lattice. This made the renewal process governing their blocked waiting times completely Markovian, and resulted in full spatial condensation which exists for a finite fraction of the time in the thermodynamic limit. The consequence of this choice is the restoration of particle-hole symmetry. We then mapped Models A and C to non-Markovian ZRPs. The dynamics of particles in Model A do not map to the dynamics of particles in the related ZRP, but Model C does properly map to non-Markovian ZRP due to the restoration of particle-hole symmetry.

Chapter 8

Conclusions

In this thesis we addressed an interesting open question: what is the effect of relaxing the Markovian constraint in the TASEP, one of the fundamental models of non-equilibrium statistical mechanics? Stochastic processes which are amenable to description by a master equation, or other stochastic differential equation, can be extended to include non-Markovian effects. There are a number of published methods of relaxing the Markovian assumption including: by use of the semi-Markov process described in chapter 3, the non-Markovian master equation [82][15], the generalisation of the linear-noise approximation for the Langevin equation by using non-Poissonian distributions [16], the creation of a non-Markovian fluctuation-dissipation relation [81][11] and/or the solution of non-Markovian problems by the inclusion of extra variables [21]. Systems of many interacting stochastic particles may be described by a set of interacting differential equations [24], and it is the exception rather than the rule that these can be solved in general. There are a number of ways of solving the steady state of driven diffusive systems (see [13] and references therein), however to my knowledge there have been no non-Markovian extensions of these techniques. Unless there is some overarching understanding which can be directly applied, the first forays into uncharted physics are specific exploratory models. Once the specific results are understood, the search can shift to finding general results, techniques and methods which can be used to explain them [86]. In chapter 2 we saw a pair of exploratory models: a non-Markovian extension to the well understood Markovian ZRP, and a non-Markovian extension of the open boundary TASEP. There has also been an exploratory simulation study in a non-Markovian extension to the burnt-bridge exclusion process [75]. In this thesis

we investigated a non-Markovian extension to the closed boundary TASEP, that displays fundamentally different behaviour to other condensation effects seen in these models previously. We found a condensate which forms dynamically and was spatially complete. The condensate displays an interesting ageing effect which we can understand quantitatively, and use to predict the behaviour of the system in the thermodynamic limit. In this limit, the condensate never fully breaks apart, but the front detatches and rejoins the traffic jam at the rear. We extend this model to allow particles to move in both directions and conclude that even the smallest bias in the direction of particles is enough to cause the condensates which are complete in space and time.

In the study of the non-Markovian TASEP we have employed a couple of famous and well used principles. Firstly, we made much headway understanding the behaviour of the thermodynamic limit when we noticed a separation of timescales. Separation of timescales is often encountered in biology, where the short timescale of biochemical reactions is compared to longer timescales in the assembly of long molecules for instance. It can be a problem in glassy dynamics where we wish to investigate emergent properties such as the trapping of particles, which relies intimately on the short term dynamics [39]. Separation of timescales may assist with calculations: in short timescales, longer processes can be considered quasi-static [15], or in longer timescales, short processes can be approximated as instantaneous [62]. The trap model discussed in chapter 7 is an example of integrating out shorter timescales, by replacing its dynamics with the stochastic process of escape from randomly distributed potential wells. We also integrated out unwanted short timescale dynamics in chapter 5, when we made the continuous time Monte Carlo method rejection-free. The second fundamental principle we used in this thesis was the breaking and restoration of particle-hole symmetry. Finding symmetries can result in clever methods for solving problems, as we know from elementary electromagnetism. It is the breaking of symmetries that often provides new physics, as we discussed in chapter 2, when we saw induced phase transitions by the introduction of disorder. We showed in chapter 4 that we had broken particle-hole symmetry in our choice of algorithm for the non-Markovian TASEP, and that there was a correlation between symmetry breaking and the presence of condensation. In chapter 7 we introduced a variant on our non-Markovian TASEP which restored particle-hole symmetry. This allowed us to use the TASEP to ZRP mapping and solve a non-Markovian ZRP for free.

As a minimal model of traffic flow, there have been many extensions to the Markovian TASEP. We investigated the robustness of condensation to the

relaxation of the totally asymmetric constraint, but it would be interesting to see if it is affected by other variations. Extensions to the TASEP are usually motivated by making the model more realistic, and we demonstrated that power law waiting time distributions may arise naturally from underlying physics. Unfortunately, due to our reliance on the infinite variance of the waiting time distribution, the application of our specific exploratory models to real-world systems is an outstanding problem of this work. Since the accelerated algorithm can be used with any waiting time distribution, it would be interesting to know if there are distributions with finite variance that also generate new condensation effects in the thermodynamic limit. As the statistical mechanics of non-Markovian interacting particle systems becomes more explored, I hope that the exploratory models investigated in this thesis will be used to shed light on other problems, and one day contribute to a more fundamental mathematical framework, which is not just an outstanding problem of this work, but of the entire field.

Appendix A

Convolution theorem

One of the reasons that Laplace transforms come up regularly in probability theory is convolution theorem. Consider a pair of independent random variables $x \geq 0, y \geq 0$ which are drawn from the probability distributions $f(x), g(y)$. The random variable which is the sum of the two takes the value t if $x = u$ and $y = t - u$, where $u \in [0, t]$, hence the probability distribution for t is

$$p(t) = \int_0^t f(u)g(t-u)\mathrm{d}u$$

This is the convolution of f and g over the finite range $[0, t]$. We define the convolution notation as follows

$$[f \star g](t) = \int_0^t f(u)g(t-u)\mathrm{d}u \tag{A.1}$$

Now consider the product of the two Laplace transforms $\tilde{f}(s)$, $\tilde{g}(s)$, where the Laplace transform is defined as

$$\mathcal{L}[f(t)] = \mathcal{L}[f(t), t, s] = \tilde{f}(s) = \int_0^\infty \exp[-st]f(t)\mathrm{d}t \tag{A.2}$$

in the usual way.

$$\begin{aligned}
\tilde{f}(s)\tilde{g}(s) &\equiv \mathcal{L}\left[f(t), t, s\right]\mathcal{L}\left[g(t), t, s\right] \\
&= \int_{u=0}^\infty \exp[-su]f(u)\mathrm{d}u \int_{v=0}^\infty \exp[-sv]g(v)\mathrm{d}v \\
&= \int_{u=0}^\infty \int_{v=0}^\infty \exp[-s(v+u)]f(u)g(v)\mathrm{d}v\mathrm{d}u
\end{aligned}$$

Make the change of variable $t = u + v$, $\mathrm{d}t = \mathrm{d}v$, $v = t - u$ and then exchange the order of integration.

$$\begin{aligned}\tilde{f}(s)\tilde{g}(s) &= \int_{u=0}^{\infty}\int_{t=u}^{\infty}\exp[-st]f(u)g(t-u)\mathrm{d}t\mathrm{d}u \\ &= \int_{t=0}^{\infty}\int_{u=0}^{t}\exp[-st]f(u)g(t-u)\mathrm{d}u\mathrm{d}t \\ &= \int_{t=0}^{\infty}\exp[-st]\int_{u=0}^{t}f(u)g(t-u)\mathrm{d}u\mathrm{d}t\end{aligned}$$

This then gives us the convolution theorem, which shows that convolutions are products in Laplace space.

$$\mathcal{L}\left[[f \star g](t), t, s\right] = \tilde{f}(s)\tilde{g}(s) \tag{A.3}$$

Appendix B

Inverse Laplace transforms by contour integration

The formula for the inverse Laplace transform lends itself to being solved by complex contour integration. To do this we need various results which are formally proved in [3]. Cauchy's Theorem states that if a function $f(s)$ is analytic on, and in, a simple closed contour $\mathcal{C}$, then

$$\oint_{\mathcal{C}} f(s)\mathrm{d}s = 0 \tag{B.1}$$

where s is the complex variable.

A Laurent series expansion of a function about a point s_0 takes the form

$$f(s) = \sum_{-\infty}^{\infty} C_n (s - s_0)^n \tag{B.2}$$

where the coefficients C_n are given by

$$C_n = \frac{1}{2\pi i} \oint_{\mathcal{C}} \frac{f(s)\mathrm{d}s}{(s - s_0)^{n+1}} \tag{B.3}$$

and $\mathcal{C}$ is any closed contour in the analytic region surrounding the singularity.

Cauchy Residue Theorem states that if $f(s)$ is analytic on a simple closed contour $\mathcal{C}$, and inside it except at a finite number of isolated singular points

$s_1, s_2, ..., s_N$ then

$$\oint_{\mathcal{C}} f(s)\mathrm{d}s = 2\pi i \sum_{j=1}^{N} a_j \tag{B.4}$$

where a_j is the *residue* of the function $f(s)$ at the j^{th} singularity located at s_j. The residue of a function at s_j is

$$a_j = \frac{1}{2\pi i} \oint_{\mathcal{C}} f(s)\mathrm{d}s \tag{B.5}$$

where $\mathcal{C}$ is a loop around the singularity. Setting $n = -1$ in equation B.3 we find that

$$\begin{aligned} a_j &= \frac{1}{2\pi i} \oint_{\mathcal{C}} f(s)\mathrm{d}s \\ &= C_{-1} \end{aligned} \tag{B.6}$$

Hence by taking the Laurent expansion about all singularities of the function, we can read off the residues a_j from the coefficients of the $(s - s_j)^{-1}$ terms.

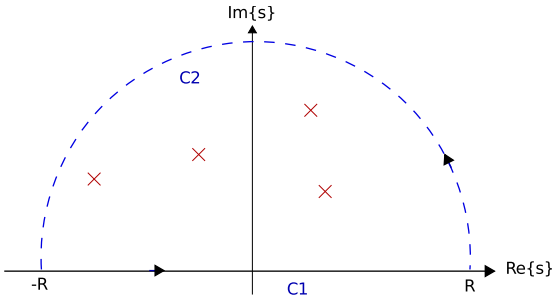

Figure B.1 *Contour integral for $f(s)$, singularities cartooned in red.*

Jordan's Lemma states that on the infinite upper semicircle $\mathcal{C}_R$ (see $\mathcal{C}_2$ in figure B.1)

$$\lim_{R\to\infty} \int_{\mathcal{C}_R} \exp[iks] f(s)\mathrm{d}s = 0 \qquad \text{for } k > 0 \tag{B.7}$$

if $f(s) \to 0$ uniformly as $R \to \infty$, i.e. $|f(s)| \leq K_R$ which depends on R but not $\arg\{s\}$ and $K_R \to 0$ as $R \to \infty$. The proof of this result is intereresting, and shown in appendix C. A similar result can be derived for $k < 0$ where contour is

now the anti-clockwise contour in the bottom half plane, $\mathcal{C}_L$.

$$\lim_{R\to\infty}\int_{\mathcal{C}_L}\exp[iks]f(s)\mathrm{d}s = 0 \qquad \text{for } k<0 \tag{B.8}$$

Jordan's Lemma then implies that we can write integrals of the type $\int_{-\infty}^{\infty}\exp[ikx]f(x)\mathrm{d}x$ as contour integrals as in figure B.1 taking the limit $R\to\infty$.

$$\oint\exp[iks]f(s)\mathrm{d}s = \int_{-\infty}^{\infty}\exp[ikx]f(x)\mathrm{d}x + \int_{\mathcal{C}_2}\exp[iks]f(s)\mathrm{d}s$$

By Jordan's Lemma above $\int_{\mathcal{C}_2}\exp[iks]f(s)\mathrm{d}s = 0$ if $f(s)\to 0$ uniformly as $R\to\infty$, and since there are singularities contained in the contour we can use the Cauchy residue theorem to get

$$\int_{-\infty}^{\infty}\exp[ikx]f(x)\mathrm{d}x = 2\pi i\sum_{j=1}^{N}a_j$$

where a_j are the residues of the function $\exp[iks]f(s)$.

The half-planes in Jordan's Lemma can be rotated by taking $s\to is$. $\mathcal{C}_R$ becomes the infinite left hand semicircle going anticlockwise and $\mathcal{C}_L$ becomes the infinite right hand semicircle going anticlockwise, and can be shown in the same way, to give us

$$\lim_{R\to\infty}\int_{\mathcal{C}_R}\exp[ks]f(s)\mathrm{d}s = 0 \qquad \text{for } k>0 \tag{B.9}$$

$$\lim_{R\to\infty}\int_{\mathcal{C}_L}\exp[ks]f(s)\mathrm{d}s = 0 \qquad \text{for } k<0 \tag{B.10}$$

Furthermore we can introduce an axis shift to the above results which gives a contribution of $\exp[ck]$ to the calculation, but this is a constant and taken care of by the fact that $f(s)$ decreases continuously as $R\to 0$.

We can then do the Bromwich inversion integral by contour integration. For a function with no branch cuts, as illustrated in figure B.2, we can write

$$\frac{1}{2\pi i}\oint\exp[st]\tilde{f}(s)\mathrm{d}s = \frac{1}{2\pi i}\int_{c-i\infty}^{c+i\infty}\exp[st]\tilde{f}(s)\mathrm{d}s + \int_{\mathcal{C}_2}\exp[st]\tilde{f}(s)\mathrm{d}s$$

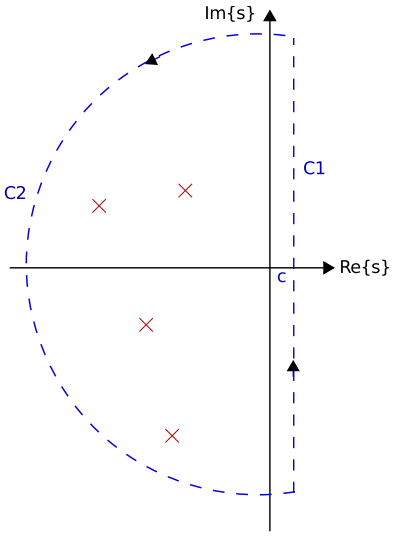

Figure B.2 *Contour integral for* $\exp[st]\tilde{f}(s)$*, C1 is the Bromwich contour integral, singularities cartooned in red.*

By Jordan's Lemma $\int_{\mathcal{C}_2} \exp[st]\tilde{f}(s)\mathrm{d}s = 0$, and so

$$f(t) = \frac{1}{2\pi i}\int_{c-i\infty}^{c+i\infty} \exp[st]\tilde{f}(s)\mathrm{d}s = \sum_{1}^{N} a_j \tag{B.11}$$

where a_j is the residue of the function $\exp[st]\tilde{f}(s)$ at the j^{th} singularity located at s_j. We notice that for a function where $f(t \to \infty) \to 0$, all of the singularities of $\tilde{f}(s)$ must have $\Re[s] \leq 0$.

We can also now see why we have to set c such that it is to the right of all singularities. The Laplace transform is blind to $k < 0$, and loses all information in this region. If however we were to set c such that there was a singularity to the right of it, the Bromwich integral would be closed by $\mathcal{C}_L$ which corresponds to $k < 0$ and the sum of residues would give a non-zero result. This then is a spurious answer and all singularities must be to the left of c. There is another simple reason which is due to the region of validity of the Laplace transform, for instance $\mathcal{L}[\exp[at], t, s] = \frac{1}{s-a}$ has the condition $s > a$, i.e. the Laplace transform is only valid to the right of all singularities.

A multi-valued function is one which does not return to the same value as it makes loops around branch points. A branch cut is a line connecting two branch points, and is introduced to arbitrarily create a single-valued function from a multivalued function, for ease of computation. A contour integral must be deformed to not cross the branch cut, and so there are extra contributions to

it. An example of Laplace transform inversion with a branch cut is explored in the next section.

B.1 Analytic inverse examples

We will illustrate the results of the previous section with a pair of examples, an inverse Laplace transform with a branch cut, and one without. Firstly consider the function function $\tilde{f}(s) = \frac{1}{(s+a)(s+b)^2}$. To invert it we find the residues of the function $\exp[st]\tilde{f}(s)$ at its singularities and use equation B.11. We see that $\exp[st]\tilde{f}(s)$ has a pole of order 1 at $s = -a$ and a pole of order 2 at $s = -b$. The residue of $\exp[st]\tilde{f}(s)$ at a singularity located at s_j is $C_{-1,j}$, the coefficient of the $(s - s_j)^{-1}$ term of the Laurent series expansion. We find the Laurent expansion about the singularity by taking the Taylor series expansion of the part of $\exp[st]\tilde{f}(s)$ which is analytic at the singularity.

At the first order pole, $s = -a$. The analytic part of the function is $\frac{\exp[st]}{(s+b)^2}$, the Taylor expansion of which is

$$\frac{\exp[st]}{(s+b)^2} = \frac{\exp[-at]}{(b-a)^2} + (s+a)\left(-\frac{2\exp[-at]}{(b-a)^3} + \frac{\exp[-at]t}{(b-a)^2}\right) + ...$$

so the Laurent series expansion of $\exp[st]\tilde{f}(s)$ about $s = -a$ is

$$\frac{\exp[st]}{(s+a)(s+b)^2} = \frac{\exp[-at]}{(s+a)(b-a)^2} + \left(-\frac{2\exp[-at]}{(b-a)^3} + \frac{\exp[-at]t}{(b-a)^2}\right) + ...$$

We can read the residue straight off as $\frac{\exp[-at]}{(b-a)^2}$.

We apply the same routine at the second order pole. The analytic part of the function at $s = -b$ is $\frac{\exp[st]}{(s+a)}$. The Taylor series of this about the singularity is

$$\frac{\exp[st]}{(s+a)} = \frac{\exp[-bt]}{(a-b)} + (s+b)\left(-\frac{\exp[-bt]}{(a-b)^2} + \frac{\exp[-bt]t}{a-b}\right) + ...$$

so the Laurent series expansion of $\exp[st]\tilde{f}(s)$ about $s = -b$ is

$$\frac{\exp[st]}{(s+a)(s+b)^2} = \frac{\exp[-bt]}{(s+b)^2(a-b)} + \left(-\frac{\exp[-bt]}{(s+b)(a-b)^2} + \frac{\exp[-bt]t}{(s+b)(a-b)}\right) + ...$$

The residue is therefore $-\frac{\exp[-bt]}{(a-b)^2} + \frac{\exp[-bt]t}{(a-b)}$

Putting this all together we get

$$\mathcal{L}^{-1}\left[\frac{1}{(s+a)(s+b)^2}\right] = \frac{\exp[-at]}{(b-a)^2} + \frac{\exp[-bt]t}{(a-b)} - \frac{\exp[-bt]}{(a-b)^2} \tag{B.12}$$

Now we wish to take the inverse Laplace transform of a function with a branch cut. We choose $\tilde{f}_1(s) = s^{-\frac{1}{2}}$ as it has no singularities, as we already know how to deal with them. We note that $\tilde{f}_1(s)$ has a branch point running from $-\infty \to 0$. We would like to do the Bromwich inversion integral (3.10) which we can think of as a contour integral as shown below.

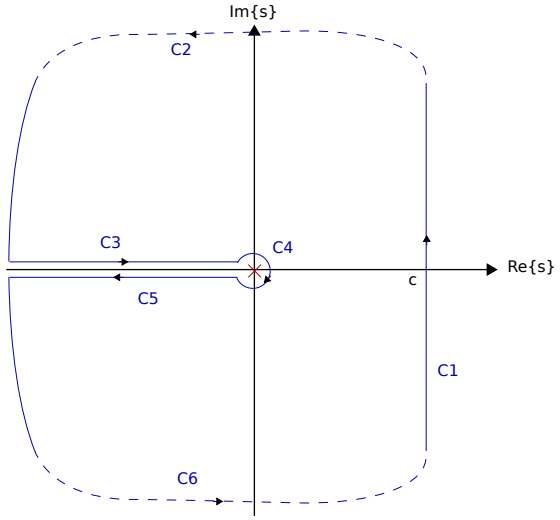

Figure B.3 *Contour integral for $\tilde{f}_1(s)$ split into 6 parts. C2 and C6 are arcs of a circle of radius $R \to \infty$ and C4 is an arc of circle of radius $\epsilon \to 0$*

Noting that there are no enclosed poles in the contour integral in figure B.3 the contour integral

$$\begin{aligned} \oint \tilde{f}_1(s)\mathrm{d}s &= 0 \\ &\Downarrow \\ \oint \exp[st]\tilde{f}_1(s)\mathrm{d}s &= 0 \end{aligned}$$

for $\Re\{s\} < c$, $\exp[st]f_1(s) \to 0$ as $s \to \infty$ the contour integrals along contours 2 and 6 are zero by Jordan's Lemma. The remaining contours are parametrised as follows

$$
\begin{array}{lcll}
\text{C1}: & s & c - i\infty \le s \le c + i\infty \\
\text{C3}: & s = r\exp[i\pi] = -r & -R \le s \le 0 \\
 & & 0 \le r \le R \\
\text{C5}: & s = r\exp[-i\pi] = -r & 0 \le s \le -R \\
 & & R \le r \le 0 \\
\text{C4}: & s = \epsilon\exp[i\theta] & \pi \le \theta \le -\pi
\end{array}
$$

Noting that C1 is the Bromwich inversion integral

$$
\begin{aligned}
0 &= \frac{1}{2\pi i}\left(\oint_{C1} + \oint_{C3} + \oint_{C4} + \oint_{C5}\right)\tilde{f}_1(s)\exp[st]\mathrm{d}s \\
f(t) &= -\frac{1}{2\pi i}\left(\oint_{C3} + \oint_{C4} + \oint_{C5}\right)\tilde{f}_1(s)\exp[st]\mathrm{d}s
\end{aligned}
$$

On C3

$$
\begin{aligned}
\oint_{C3}\tilde{f}_1(s)\exp[st]\mathrm{d}s &= \int_{s=-\infty}^{0}\frac{\exp[st]}{\sqrt{s}}\mathrm{d}s \\
&= \int_{r=\infty}^{0}\frac{\exp[-rt]}{\sqrt{r}\exp[\frac{i\pi}{2}]}(-\mathrm{d}r) \\
&= \int_{r=0}^{\infty}\frac{\exp[-rt]}{i\sqrt{r}}\mathrm{d}r \\
&= -i\int_{r=0}^{\infty}\frac{\exp[-rt]}{\sqrt{r}}\mathrm{d}r
\end{aligned}
$$

On C5

$$
\begin{aligned}
\oint_{C5}\tilde{f}_1(s)\exp[st]\mathrm{d}s &= \int_{s=0}^{-\infty}\frac{\exp[st]}{\sqrt{s}}\mathrm{d}s \\
&= \int_{r=0}^{\infty}\frac{\exp[-rt]}{\sqrt{r}\exp[\frac{-i\pi}{2}]}(-\mathrm{d}r) \\
&= -\int_{r=0}^{\infty}\frac{\exp[-rt]}{-i\sqrt{r}}\mathrm{d}r \\
&= -i\int_{r=0}^{\infty}\frac{\exp[-rt]}{\sqrt{r}}\mathrm{d}r
\end{aligned}
$$

So the contributions re-enforce. On C4

$$\begin{aligned}\oint_{C4} \tilde{f}_1(s)\exp[st]\mathrm{d}s &= \int_{\theta=\pi}^{-\pi} \frac{\exp[t\epsilon\exp[i\theta]]}{\sqrt{\epsilon\exp[i\theta]}}\left(i\epsilon\exp[i\theta]\mathrm{d}\theta\right) \\ &\sim O\{\epsilon^{\frac{1}{2}}\} \\ &\to 0 \text{ as } \epsilon \to 0\end{aligned}$$

Putting it all together

$$\begin{aligned}f(t) &= -\frac{1}{2\pi i}\left(\oint_{C3}+\oint_{C4}+\oint_{C5}\right)\tilde{f}_1(s)\exp[st]\mathrm{d}s \\ &= -\frac{1}{2\pi i}\left(-2i\int_{r=0}^{\infty}\frac{\exp[-rt]}{\sqrt{r}}\mathrm{d}r\right) \\ &= \frac{1}{\pi}\frac{\sqrt{\pi}}{\sqrt{t}} \\ \mathcal{L}^{-1}\left[\frac{1}{\sqrt{s}},s,t\right] &= \frac{1}{\sqrt{\pi t}}\end{aligned}$$

Appendix C

Proof of Jordan's Lemma

Jordan's Lemma states that on the infinite upper semicircle $\mathcal{C}_R$ (see $\mathcal{C}_2$ in figure B.1)

$$\lim_{R\to\infty}\int_{\mathcal{C}_R}\exp[iks]f(s)\mathrm{d}s = 0 \qquad \text{for } k>0 \tag{C.1}$$

if $f(s)\to 0$ uniformly as $R\to\infty$, i.e. $|f(s)|\leq K_R$ which depends on R but not $\arg\{s\}$ and $K_R\to 0$ as $R\to\infty$. A similar result can be derived for $k<0$ where contour is now the anti-clockwise contour in the bottom half plane, $\mathcal{C}_L$.

$$\lim_{R\to\infty}\int_{\mathcal{C}_L}\exp[iks]f(s)\mathrm{d}s = 0 \qquad \text{for } k<0 \tag{C.2}$$

This is shown by parametrising the contour $s=R\exp[i\theta]$, $\theta\in[0,\pi]$ to get

$$\begin{aligned}
&\lim_{R\to\infty}\int_{\mathcal{C}_R}\exp[iks]f(s)\mathrm{d}s\\
&=\lim_{R\to\infty}\int_0^\pi \exp[ikR\exp[i\theta]]f(R\exp[i\theta])Ri\exp[i\theta]\mathrm{d}\theta\\
&\leq\lim_{R\to\infty}\int_0^\pi R\exp[-kR\sin[\theta]]\ \ |f(R\exp[i\theta])|\ \ |i\exp[i\theta]|\ \ |\exp[ikR\cos[\theta]]|\mathrm{d}\theta\\
&=\lim_{R\to\infty}\int_0^\pi \exp[-kR\sin[\theta]]K_R R\mathrm{d}\theta
\end{aligned}$$

$\sin[\theta]$ is symmetric about $\frac{\pi}{2}$ so $\exp[-kR\sin[\theta]]$ is symmetric about $\frac{\pi}{2}$. This implies that

$$\int_0^{\pi} \exp[-kR\sin[\theta]]\mathrm{d}\theta = 2\int_0^{\frac{\pi}{2}} \exp[-kR\sin[\theta]]\mathrm{d}\theta$$

The area under $\sin[\theta]$ between $(0, \frac{\pi}{2})$ is the same as the area under $\cos[\theta]$ in the same region, therefore the area under $\exp[-kR\sin[\theta]]$ equals the area under $\exp[-kR\cos[\theta]]$ in the region $(0, \frac{\pi}{2})$.

$$\int_0^{\frac{\pi}{2}} \exp[-kR\sin[\theta]]\mathrm{d}\theta = \int_0^{\frac{\pi}{2}} \exp[-kR\cos[\theta]]\mathrm{d}\theta$$

This can be split up into two terms.

$$\int_0^{\frac{\pi}{2}} \exp[-kR\cos[\theta]]\mathrm{d}\theta = \int_0^{\frac{\pi}{2}} \cosh[kR\cos[\theta]] - \sinh[kR\cos[\theta]]\mathrm{d}\theta$$

The second term is the integral representation of the modified Struve function $L_0(kR)$ [4] where

$$L_\nu(z) = \frac{2(\frac{z}{2})^\nu}{\sqrt{\pi}\Gamma[\nu + \frac{1}{2}]}\int_0^{\frac{\pi}{2}} \sinh[z\cos[\theta]]\sin^{2\nu}[\theta]\mathrm{d}\theta \quad \Re\{\nu\} > -\frac{1}{2}$$

upto a factor of $\frac{2}{\pi}$. The first term is the integral representation of the modified Bessel function $I_0(kR)$ upto a factor of $\frac{2}{\pi}$. The integral representation of $I_0(z)$ is [4]

$$I_0(z) = \frac{1}{\pi}\int_0^{\pi} \cosh[z\cos[\theta]]\mathrm{d}\theta$$

Cosine is anti-symmetric about $\frac{\pi}{2}$, but $\cosh[x]$ is even, so we can write

$$I_0(z) = \frac{2}{\pi}\int_0^{\frac{\pi}{2}} \cosh[z\cos[\theta]]\mathrm{d}\theta$$

Putting this all together gives

$$\lim_{R\to\infty}\int_{\mathcal{C}_R} \exp[iks]f(s)\mathrm{d}s = \lim_{R\to\infty} \pi K_R R\left(I_0(kR) - L_0(kR)\right)$$

The asymptotic expansion of $I_0(z) - L_0(z)$ as $z \to \infty$ is [4]

$$I_0(z) - L_0(z) \sim \frac{-1}{\pi} \sum_{k=0}^{\infty} \frac{(-1)^{k+1}\Gamma[k+\frac{1}{2}]}{\Gamma[\frac{1}{2}-k](\frac{z}{2})^{2k+1}}$$

So the limit $z \to \infty$ of $I_0(z) - L_0(z)$ is $\frac{2}{\pi z}$. Therefore

$$\begin{aligned} \lim_{R\to\infty} \int_{\mathcal{C}_R} \exp[iks] f(s) \mathrm{d}s &= \lim_{R\to\infty} \pi K_R R \frac{2}{\pi k R} \\ &= 0 \end{aligned}$$

as required.

Appendix D

Laplace transform inversion of a known function

We are warned that singularities and discontinuities in the distribution or its Laplace transform slow down the numerical inversion [79]. As discussed previously, if the Laplace function doesn't oscillate after a certain point, we can use various oscillating sum acceleration techniques, Eulers transformation [4] and Van Wijngaarden's algorithm [66] for instance. The Pareto distribution has a discontinuity (Figure D.1a), and its Laplace transform has persistent oscillations (Figure D.1b).

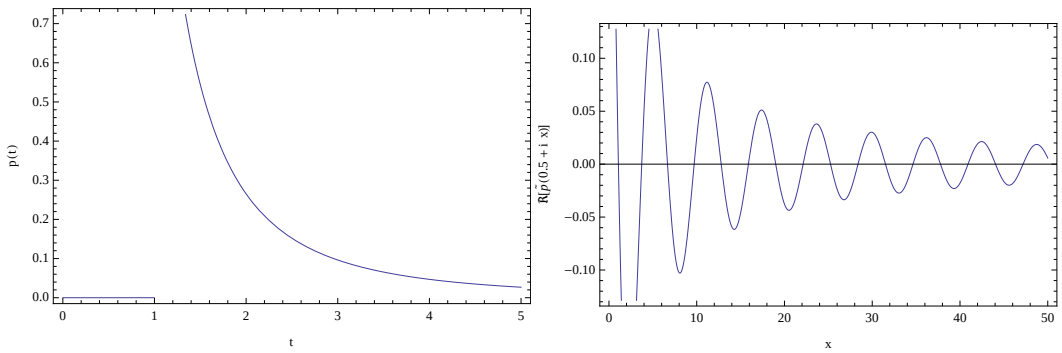

(a) *Pdf* **(b)** *Laplace transform*

Figure D.1 *Pareto distribution* $\gamma = 2.5$

We can define a continuous Pareto function (which I call the *CPareto*) by introducing an essential singularity at the origin (Figure D.2a), which has a much longer oscillation period (Figure D.2b).

$$\text{CPareto}[t,\gamma] \equiv \frac{t^{-\gamma}\exp[-\frac{1}{t}]}{\Gamma[\gamma-1]}$$

$$\mathcal{L}[\text{CPareto}[t,\gamma],t,s] = \frac{2s^{\frac{\gamma-1}{2}}K(\gamma-1,2\sqrt{s})}{\Gamma[\gamma-1]}$$

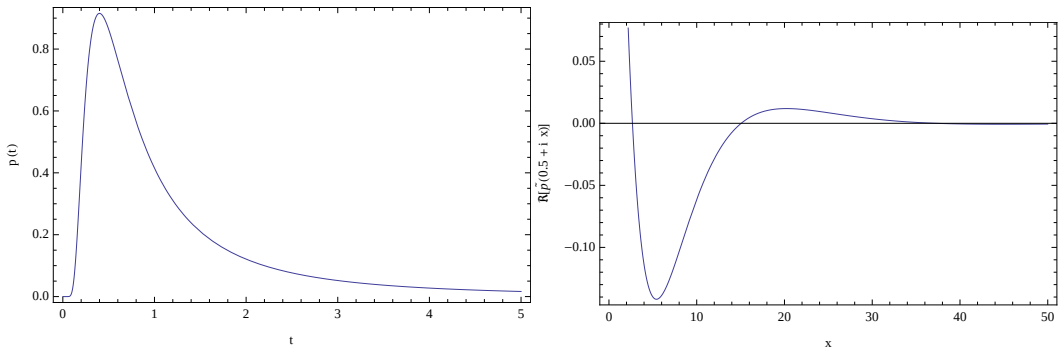

(a) *Pdf* **(b)** *Laplace transform*

Figure D.2 *CPareto distribution for* $\gamma = 2.5$

Even better, we can define a version of the Pareto with a polynomial start (which I will call the *PPareto* here). The Laplace transform of this has only a single crossing of the $\Re[s]$ axis (Figure D.3b).

$$\text{PPareto}[t,\gamma] = \mathcal{N}\left(\left(A(\gamma)t + B(\gamma)t^2 + C(\gamma)t^3\right)\Theta[1-t] + t^{-\gamma}\Theta[t-1]\right)$$

where $\mathcal{N}$ is the normalisation, and $A(\gamma), B(\gamma), C(\gamma)$ are chosen such that at $t = 1$ the function and its first, second and third derivatives are continuous. In this example I will use the PPareto function, though it is perfectly possible to use either of the other two.

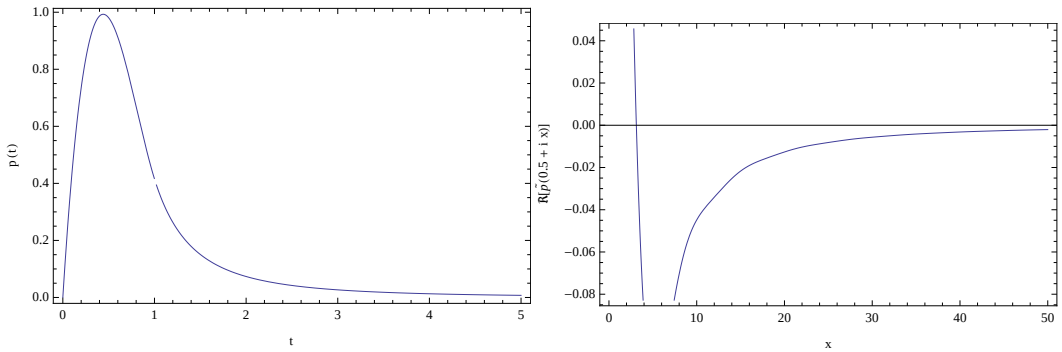

(a) *Pdf* **(b)** *Laplace transform*

Figure D.3 *PPareto distribution for* $\gamma = 2.5$

As we discussed in section 3.5 both c, h control the accuracy, and, as shown below in Figure D.5, also the speed of the inversion. The Laplace transform of the CPareto function is eventually non-oscillatory, and therefore the sum eventually only has a single oscillation in it (see figure D.4). Since the numerical evaluation of the sum computes many terms at once the truncation of the series is done as discussed in sections 3.5 and 3.5.1.

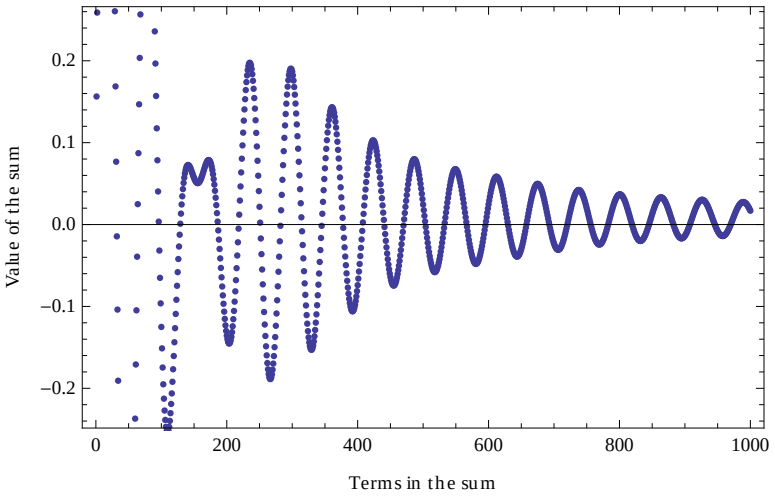

Figure D.4 *The value of an example inversion sum for the CPareto function, for increasing number of terms.*

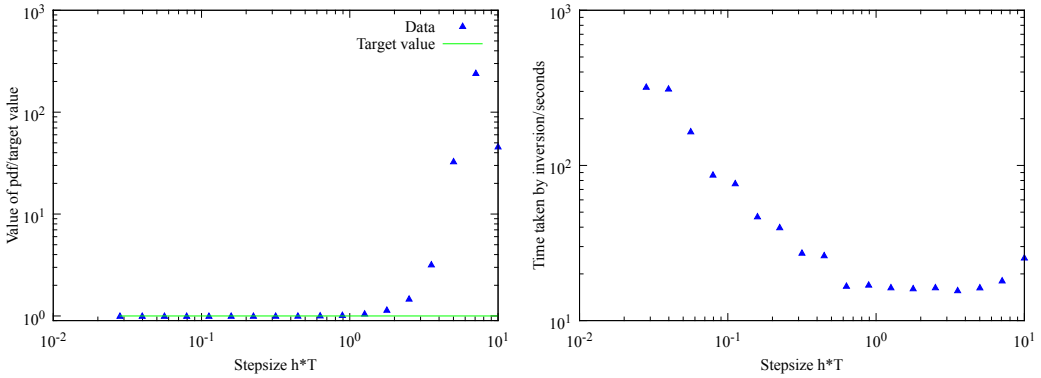

(a) *Inversion tending to true value for decreasing h*

(b) *Time taken by inversion*

Figure D.5 *Data for example Laplace transform inversion, $\gamma = 2.5$, $c = 0.001$*

It is necessary to pick values of c, h that are an acceptable trade off between speed and accuracy. For this particular case, I want an accuracy of $\epsilon = 0.001$ PPareto$[t, \gamma]$. Using equation 3.16 and $h \leq \frac{\pi}{2t}$, we can predict which values of c, h we need. Firstly C is slightly above the maximum value of the pdf (we set $\delta = C -$ maximum value of pdf $= 0.001$). This maximum will be the first turning

point of the polynomial part of the function, which in this case is is

$$C = \text{PPareto}\left(\frac{6 + 8g + 2g^2 - \sqrt{12g + 19g^2 + 8g^3 + g^4}}{3\,(2 + 3g + g^2)}\right) + \delta$$

Setting h at the upper end of the allowed region, $h = t^{-1}$ we get the value of c

$$c = \frac{1}{\pi t} \ln\left(\frac{C}{0.001\ \text{PPareto}[t, \gamma]}\right)$$

In figure D.6a we can see the fractional error on the inverse of the PPareto function (Error $= \frac{\text{Value of inversion} - \text{target value}}{\text{target value}}$) and the time taken by the inversion. Since all these errors are less than 1×10^{-3}, these are consistent with the target accuracy we used to compute c, h

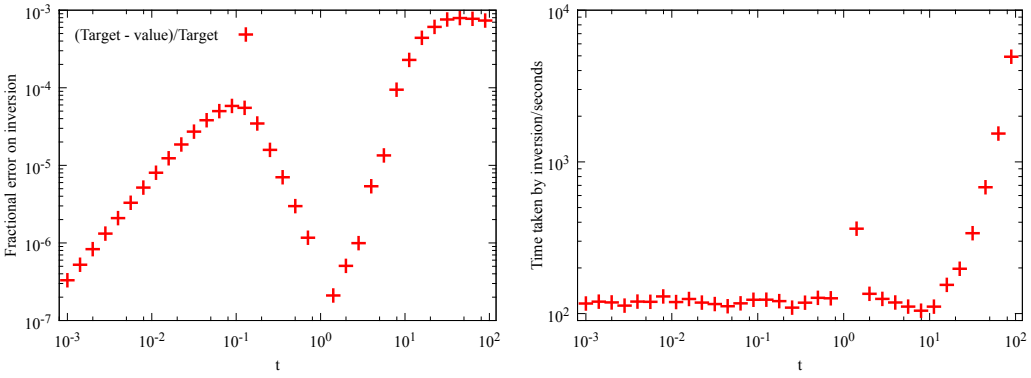

(a) *Fractional error on PPareto inversion*

(b) *Time taken by inversion*

Figure D.6 *Data for example Laplace transform inversion, $\gamma = 2.5$, h, c as above*

For numerical Laplace transform inversion to be truly useful, the form of the inverse must be hard, or impossible, to get analytically. A potential way of predicting the relevant c, h to use would be to use the analytic methods discussed in section 3.3.1 to compute approximations for the inversion in the limits cdf $\to 0$ and cdf $\to 1$. It may also be necessary to compute where the value of the pdf becomes small to properly take account of these regions too. Trial and error may also be used to find appropriate values of c, h as in chapter 5. It should be noted here that the PPareto function was conceived in order to facilitate the

numerical Laplace transform inversion of a function with a power law tail, as at the time I was having difficulty inverting the Pareto function. I attributed the errors and lack of speed to the Heaviside function causing a discontinuity in the Pareto function. I eventually improved my numerical inversion routine such that it could accommodate the Pareto function, and eventually the blocked Pareto function, and the PPareto function was never used.

Appendix E

Statistical Procedures

E.1 The Kolmogorov-Smirnov test

Sheskin [77] notes that very similar goodness-of-fit tests were developed by Kolmogorov in 1933 and Smirnov in 1939 for different purposes. The test developed by Kolmogorov tests the goodness of fit of a sample of a probability distribution to a specific theoretical probability distribution. If the test statistic is small enough (statistical significance of this is discussed below) the sample is consistent with having been generated from the theoretical probability distribution. The Smirnov test compares two sample probability distributions, and if the test statistic is small enough (again statistical significance discussed below) the two samples are consistent with being generated from the same underlying distribution. Due to the similarity in the mathematics behind the tests, they are referred to as Kolmogorov-Smirnov tests, for one sample and two samples respectively.

First some notation. Let $X_1, X_2, ..., X_N$ be N mutually independent random variables with the common cumulative distribution function $F(x)$ and arranged in ascending order. We construct the empirical cumulative distribution function (or sum-polygon) which is a step function (see Feller [38]) defined by

$$S_N(x) = \begin{cases} 0 & \text{for } x < X_1 \\ \frac{k}{N} & \text{for } X_k \leq x \leq X_{k+1} \\ 1 & \text{for } x > X_N \end{cases}$$

E.1.1 Kolmogorov-Smirnov test for two samples

We follow the prescription described in Sheskin [77] but laid out mathematically in Feller [38] and [51]. Let there be two sets of mutually independent random variables with the common cumulative distribution function $F(x)$, $(X_1, X_2, ..., X_n)$ and $(Y_1, Y_2, ..., Y_m)$ from which we create their empirical cumulative distributions $U_n(x)$ and $V_m(x)$, as above. The Kolmogorov-Smirnov test statistic is the maximum distance between the two empirical distributions

$$D_{n,m} = \max|U_n(x) - V_m(x)| \tag{E.1}$$

If at any point the test statistic $D_{n,m}$ is greater than the critical test statistic then the hypothesis that the two distributions are drawn from the same underlying probability distribution is rejected. A table of critical test statistics can be found in the appendix Table 23 of Sheskin [77], and we discuss how these are derived here.

We now define a random walk, on a one dimensional discrete lattice, where at each time step the walker takes a step right with probability $p = \frac{1}{2}$ and left with probability $q = \frac{1}{2}$. We number the lattice sites such that if the particle is sat on site i then it has taken $i = r - l$ where $r =$ the number of right steps taken, and $l =$ the number of left steps taken. We then constrain the walker to start at zero and return to zero at time T. We know that the average position of the walker is at the origin because on average we expect the moves to be distributed evenly between right and left. We can now put in two absorbing boundary conditions at x and $-x$. We can now work out the survival probability of the walker as a function of x and T, $S(x, T)$.

The argument for $S(x, T)$ can be generalised to the case where $p = \frac{n}{T}$, $q = \frac{m}{T}$, $T = n + m$ and the particle is constrained to end up at site $n - m$. The survival function for this case would be written $S(x, n, m)$.

Now lets relate this to the Kolmogorov-Smirnov test. Let us draw $T = n + m$ random samples from the distribution $F(x)$ and assign them to set X with initial probability $p = \frac{n}{n+m}$ and set Y with initial probability $q = \frac{m}{n+m}$, until we have n samples in X and m samples in Y. The probability changes in the same way as sampling without replacement i.e. $p = \frac{r}{n+m-r-l}$ and $q = \frac{l}{n+m-r-l}$ where r and l are the number of X generated so far, and l is the number of Y generated so far. Let us combine the sets and put them in ascending order, and

we would generate a random string of X and Y. Because the events are drawn from the same underlying probability distribution, on average we expect them to be evenly distributed according to their frequencies n and m. This is exactly equivalent to picking a series of right and left steps for the random walker with fixed probabilities p, q and then conditioning on having n right and m left steps at the end.

What we can now do is find the distance x such that, say, 95% of walkers survive, or equivalently, the maximum difference between the number of X and the number of Y (as we generate them from $F(x)$) that 95% of the samples will not exceed. This can be evalutated either numerically or graphically by considering the difference between the empirical cumulative distribution functions.

$$\begin{aligned} D_{n,m} &= \max|U_n(x) - V_m(x)| \\ &= \max|\frac{r}{n} - \frac{l}{m}| \end{aligned}$$

For $n = m$ this measure correctly measures the maximum displacement of the random walker. For $n \neq m$, the KS test statistic would correspond to the maximum distance travelled away from the expected value by a walker in continuous space, where a right step takes you a distance of $\frac{1}{n}$, and left takes you $\frac{1}{m}$. I have not worked out what this survival function looks like, but it was deduced by Smirnov, and its limit function found for $n \to \infty$, $m \to \infty$ where $\frac{n}{m} \to$ constant.

The test statistic gives a measure of whether we should reject the null hypothesis (the two sets are drawn from the common cumulative distribution function $F(x)$). For $S(x, n) = 95\%$, 5% of the samples from the common distribution would exceed x. If the KS test statistic is less than x, this particular sample lies within the 95% and at the p-value 0.05, the null hypothesis is not rejected. If it is outside x, at p-value 0.05 we reject the null hypothesis.

Comparing a dataset with n data points with another containing m data points, each having a single tail (there being some finite lower cuttoff for instance), the critical KS statistic KS_c for $p = 0.05$ is $\mathrm{KS}_c = 1.22\sqrt{\frac{n+m}{nm}}$ [77].

E.1.2 Kolmogorov-Smirnov test for one samples

Let there be a set of mutually independent random variables with the common cumulative distribution function $F(x)$, $(X_1, X_2, ..., X_n)$ from which the empirical cumulative distribution is $U_n(x)$, as above. We wish to compare $U_n(x)$ with an analytic cumulative distribution function $V(x)$

The Kolmogorov-Smirnov test statistic is the maximum distance between the two distributions

$$D = \max|U_n(x) - V(x)| \tag{E.2}$$

Comparing a dataset with n data points, each having a single tail (there being some finite lower cuttoff for instance), the critical KS statistic KS_c for $p = 0.05$ is $\mathrm{KS}_c = \frac{1.22}{\sqrt{n}}$ [77].

E.2 Fitting a power law tail using a Maximum Likelihood Estimator

We follow the techniques laid out in Clauset et al [18] to fit a power law tail to a distribution. The power law distribution function can be written

$$p(x) = \frac{\alpha - 1}{x_m} \left(\frac{x}{x_m} \right)^{-\alpha} \Theta[x - x_m] \tag{E.3}$$

where x_m is the minimum x value, as ensured by the Heaviside Theta function $\Theta[x - x_m]$. The probability that a particular set of data with $x \geq x_m$ with n values is drawn from a power law of the above form is

$$p(\mathrm{Data}|\alpha) = \prod_{i=1}^{n} \frac{\alpha - 1}{x_m} \left(\frac{x_i}{x_m} \right)^{-\alpha} \tag{E.4}$$

where x_i is the i^{th} data point in the set. The minimum of $p(\mathrm{Data}|\alpha)$ occurs at the same point as the minimum of $\log\left(p(\mathrm{Data}|\alpha)\right)$, hence we solve $\frac{\partial \log(p(\mathrm{Data}|\alpha))}{\partial \alpha} = 0$ to find the value of α which gives the maximum likelihood of the data being

drawn from the power law, $\bar{\alpha}$

$$\bar{\alpha} = 1 + n \left(\sum_{i=1}^{n} \log \left(\frac{x_i}{x_m} \right) \right)^{-1} \tag{E.5}$$

This assumes that for a general data set, the value of x_m at which the data is well represented by a power law is known. Clauset et al [18] propose a simple technique to find the best x_m and its associated $\bar{\alpha}$ by computing a range of x_m and then using the values of $x_m, \bar{\alpha}$ which minimises the Kolmogorov Smirnov statistic when comparing the cdf of the data with the predicted cdf. Specifically the KS value that should be minimised is the ratio of the computed value to the target critical value, as then smaller data sets are not automatically favoured. The way I usually implement this is to set x_m to the smallest value of the data set, compute $\bar{\alpha}$ and the KS value, then remove that data point, and repeat until there are only 50 data points remaining. Any fewer than this can lead to problems with small data sets [18].

E.3 Bootstrap technique for estimation of errors

The bootstrap technique is a method of finding the uncertainty on a particular statistic by re-sampling the dataset. In this thesis I follow the following routine for implementing the bootstrap. For a dataset with n entries a sample statistic (the mean, or KS statistic for instance) can be computed. The uncertainty on the sample statistic can be measured by creating a number, N, of extra datasets of n entries by sampling the original dataset with replacement. The sample statistic can be computed for each dataset, the standard deviation of the sample statistics is then a measure of the uncertainty of the original sample statistic. For a more in depth discussion of the Bootstrap technique for estimation of errors, see [30][31].

Bibliography

[1] J. Abate and W. Whitt. The fourier-series method for inverting transforms of probability distributions. *Queueing Systems*, 10:5–88, 1992.

[2] J. Abate and W. Whitt. A united framework for numerically inverting laplace transforms. *INFORMS Journal on Computing*, 18:408–421, 2006.

[3] M. J. Ablowitz and A. S. Fokas. *Complex Variables, Introduction and Applications*. Cambridge University Press, 2nd edition, 2003.

[4] M. Abramowitz and I. A. Stegun. *Handbook of Mathematical Functions*. Dover Publications Inc., 1972.

[5] M. H. Anderson, J. R. Ensher, M. R. Matthews, C. E. Wieman, and E. A. Cornell. Observation of bose-einstein condensation in a dilute atomic vapor. *Science*, 269:198–201, 1995.

[6] M.A. Aziz-Alaoui and C. Bertelle, editors. *Emergent Properties in Natural and Artificial Dynamical Systems*. Springer Berlin Heidelberg, 2006.

[7] A. Basu and D. Chowdhury. Traffic of interacting ribosomes: Effects of single-machine mechanochemistry on protein synthesis. *Phys. Rev. E*, 75: 021902, 2007.

[8] A. Basu and D. Chowdhury. Modeling protein synthesis from a physicist's perspective: A toy model. *Am. J. Phys.*, 75:931, 2007.

[9] O. G. Berg. A model for the statistical fluctuations of protein numbers in a microbial population. *J. Theor. Biol.*, 71:587–603, 1978.

[10] P. Bialas, Z. Burda, and D. Johnston. Condensation in the backgammon model. *Nuclear Physics B*, 493:505–516, 1997.

[11] M. Bianucci and P. Grigolini. Nonlinear and non[U+2010]markovian fluctuation–dissipation processes: A fokker–planck treatment. *J. Chem. Phys.*, 96:6138–6148, 1992.

[12] M. Blum. On the sums of independently distributed pareto variables. *SIAM Journal on Applied Mathematics*, 19:191–198, 1970.

[13] R. A. Blythe and M. R. Evans. Nonequilibrium steady states of matrix-product form: a solver's guide. *J. Phys. A*, 40:R333–R441, 2007.

[14] J. P. Bouchaud. Weak ergodicity breaking and aging in disordered systems. *J. Phys. I France*, 2:1705–1713, 1992.

[15] D. Bratsun, D. Volfson, L. S. Tsimring, and J. Hasty. Delay-induced stochastic oscillations in gene regulation. *PNAS*, 102:14593–14598, 2005.

[16] T. Brett and T. Galla. Stochastic processes with distributed delays: chemical langevin equation and linear-noise approximation. *Phys Rev Lett*, 110: 250601, 2013.

[17] Z. Burda, D. Johnston, J. Jurkiewicz, M. Kaminski, M. A. Nowak, G. Papp, and I. Zahed. Wealth condensation in pareto macroeconomies. *Phys. Rev. E*, 65:026102, 2002.

[18] A. Clauset, C. R. Shalizi, and M. E. J. Newman. Power-law distributions in empirical data. *SIAM Review*, 51:661–703, 2009.

[19] A. M. Cohen. *Numerical Methods for Laplace Transform Inversion*. Springer, 2007.

[20] K. A. Connors. *Chemical Kinetics: The Study of Reaction Rates in Solution*. Wiley-VCH, 1990.

[21] D. R. Cox. The analysis of non-markovian stochastic processes by the inclusion of supplementary variables. *Proc. Camb. Phil. Soc.*, 51:433–441, 1955.

[22] J. D. Cutnell and K. W. Johnson. *Physics*. John Wiley and Sons, Inc., 3rd edition, 1995.

[23] P. J. Davis and P. Rabinowitz. *Methods of Numerical Integration*. Academic Press, Inc., 1984.

[24] B. Derrida. An exactly soluble non-equilibrium system: The asymmetric simple exclusion process. *Physics Reports*, 301:65–83, 1998.

[25] B. Derrida and K. Mallick. Exact diffusion constant for the one-dimensional partially asymmetric exclusion model. *J. Phys. A*, 30:1031–1046, 1997.

[26] B. Derrida, S. A. Janowsky, J. L. Lebowitz, and E. R. Speer. Exact solution of the totally asymmetric simple exclusion process: Shock profiles. *Journal of Statistical Physics*, 73:813–842, 1993.

[27] L. Devroye. *Non-Uniform Random Variate Generation*. Springer-Verlag, 1986.

[28] S. N. Dorogovtsev and J. F. F. Mendes. *Evolution of networks : from biological nets to the Internet and WWW*. Oxford University Press, 2003.

[29] H. Dubner and J. Abate. Numerical inversion of laplace transforms by relating them to the finite fourier cosine transform. *Journal of the Association for Computing Machinery*, 15:115–123, 1968.

[30] B. Effron. Bootstrap methods: another look at the jackknife. *The annals of Statistics*, 7:1–26, 1979.

[31] B. Efron and R. J. Tibshirani. *An Introduction to the Bootstrap*. Chapman & Hall, 1993.

[32] M. R. Evans. Exact steady states of disordered hopping particle models with parallel and ordered sequential dynamics. *J. Phys. A*, 30(16):5669, 1997.

[33] M. R. Evans and T. Hanney. Nonequilibrium statistical mechanics of the zero-range process and related models. *J. Phys. A*, 38(19):195–240, May 13 2005. ISSN 0305-4470.

[34] M. R. Evans, S. N. Majumdar, and R. K. P. Zia. Canonical analysis of condensation in factorised steady states. *Journal of Statistical Physics*, 123: 357–390, 2008.

[35] M. V. Feigel'man and V. M. Vinokur. On the stochastic transport in disordered systems. *J. Phys. France*, 49:1731–1736, 1988.

[36] W. Feller. *An Introduction to Probability Theory and Its Applications*, volume 2. Wiley, 2nd edition, 1971.

[37] W. Feller. *An Introduction to Probability Theory and Its Applications*, volume 1. Wiley, 2nd edition, 1971.

[38] W. Feller. On the kolmogorov-smirnov limit theorems for empirical distributions. *Annals of Mathematical Statistics*, 19(2):177–189, 1948. ISSN 0003-4851. doi: 10.1214/aoms/1177730243.

[39] S. M. Fielding and P. Sollich. Equivalence of driven and ageing fluctuation-dissipation relations in the trap model. *Phys Rev E*, 67:011101, 2003.

[40] J. Galambos. *The Asymptotic Theory of Extreme Order Statistics*. Wiley, 1978.

[41] C. Godreche and J. M. Luck. Dynamics of the condensate in zero-range processes. *J. Phys. A*, 38:7215–7237, 2005.

[42] M. Gorissen and C. Vanderzande. Ribosome dwell times and the protein copy number distribution. *J. Stat. Phys.*, 148:627–635, 2012.

[43] P. Greulich, A. Garai, K. Nishinari, A. Schadschneider, and D. Chowdhury. Intracellular transport by single-headed kinesin KIF1A: Effects of single-motor mechanochemistry and steric interactions. *Phys. Rev. E*, 75(4), 2007. ISSN 1539-3755.

[44] S. Grosskinsky, G.M. Schuetz, and H. Spohn. Condensation in the zero range process: stationary and dynamical properties. *J. Stat. Phys*, 113(3-4), Nov 2003.

[45] D. L. Hartl and A. G. Clark. *Principles of Population Genetics*. Sinauer, 3rd edition, 1997.

[46] O. Hirschberg, D. Mukamel, and G.M. Schuetz. Condensation in temporally correlated zero-range dynamics. *Physical Review Letters*, 103, 2009. ISSN 0031-9007.

[47] O. Hirschberg, D. Mukamel, and G. M. Schutz. Motion of condensates in non-markovian zero-range dynamics. *Journal of Statistical Mechanics*, 2012: 08014, 2012.

[48] J. Howard. *Mechanics of Motor Proteins and the Cytoskeleton*. Sinauer Associates, Inc., 2001.

[49] R. A. Howard. *Dynamic Probabilistic Systems*, volume 1. John Wiley and Sons, Inc., 1971.

[50] R. A. Howard. *Dynamic Probabilistic Systems*, volume 2. John Wiley and Sons, Inc., 1971.

[51] Jr. J. L. Hodges. The significance probability of the smirnov two-sample test. *Arkiv för Matematik*, 3:469–486, 1957.

[52] R. Jiang, M. Hu, Y. Wu, and Q. Wu. Weak and strong coupling in a two-lane asymmetric exclusion process. *Phys. Rev. E*, 77:041128, 2008.

[53] A. John, A. Schadschneider, D. Chowdhury, and K. Nishinari. Trafficlike collective movement of ants on trails: absence of jammed phase. *Phys Rev Lett*, 102:108001, 2009.

[54] F. P. Kelly. *Reversibility and stochastic networks*. Cambridge University Press, 1979.

[55] J. Krug and P. A. Ferrari. Phase transitions in driven diffusive systems with random rates. *J. Phys. A*, 29:1911–1926, 1996.

[56] J. L. Lebowitz, E. Presutti, and H. Spohn. Microscopic models of hydrodynamic behavior. *J. Stat. Phys.*, 51:841–862, 1998.

[57] C.T. MacDonald, J.H. Gibbs, and A.C. Piplin. Kinetics of biopolymerization on nucleic acid templates. *Biopolymers*, 6(1):1–25, 1968.

[58] R. Mahnke, J. Kaupuzs, and I. Lubashevsky. Probabilistic description of traffic flow. *Phys. Rep.*, 408, 2005. ISSN 0370-1573.

[59] S. N. Majumdar, A. Rosso, and A. Zoia. Time at which the maximum of a random acceleration process is reached. *J. Phys. A*, 43(11), 2010.

[60] K. Mallick. Shocks in the asymmetry exclusion model with an impurity. *J. Phys. A*, 29:5375–5386, 1996.

[61] K. Motegi, K. Sakai, and J. Sato. Exact relaxation dynamics in the totally asymmetric simple exclusion process. *Phys. Rev. E*, 85:042105, 2012.

[62] J. D. Murray. *Mathematical Biology*. Springer-Verlag, 1989.

[63] K. Nagel and M. Schreckenberg. A cellular automaton model for freeway traffic. *Journal de Physique I*, 2:2221–2229, 1992.

[64] R. M. Nisbet and W. S. C. Gurney. *Modelling Fluctuating Populations*. Wiley, 1982.

[65] A. Parmeggiani, T. Franosch, and E. Frey. Phase coexistence in driven one dimensional transport. *Phys. Rev. Lett.*, 90:086601, 2003.

[66] W. H. Press, S. A. Teukolsky, W. T. Vetterling, and B. P. Flannery. *Numerical Recipes in C*. Cambridge University Press, 2nd edition, 1992.

[67] S. Prolhac, M. R. Evans, and K. Mallick. The matrix product solution of the multispecies partially asymmetric exclusion process. *J. Phys. A*, 42:165004, 2009.

[68] T. Reichenbach, T. Franosch, and E. Frey. Exclusion processes with internal states. *Phys Rev Lett*, 97:050603, 2006.

[69] M. S. Ridout. Generating random numbers from a distribution specified by its laplace transform. *Statistics and Computing*, 19:439–450, 2009.

[70] G. E. Roberts and H. Kaufman. *Table of Laplace Transforms*. W. B. Saunders Company, 1966.

[71] B. Roehner and P. Winiwarter. Aggregation of independent paretian random variables. *Advances in Applied Probability*, 17:465–469, 1985.

[72] A. K. Saxena. *An Introduction to Thermodynamics and Statistical Mechanics*. Alpha Science International Ltd., 2010.

[73] B. Schmittmann and R.K.P. Zia. *Statistical Mechanics of Driven Diffusive Systems*, volume 17 of *Phase Transitions and Critical Phenomena*. Academic Press Inc, 1995.

[74] Y. A. Schreider. *The Monte Carlo Method*. Pergamon Press, 1966.

[75] J. H. P. Schulz, A. B. Kolomeisky, and E. Frey. Current reversal and exclusion processes with hitory-dependent random walks. *Europhysics Letters*, 74: 031906, 2011.

[76] L. B. Shaw, R. K. P. Zia, and K. H. Lee. The totally asymmetric exclusion process with extended objects, a model for protein synthesis. *Phys. Rev. E*, 68:021910, 2003.

[77] D. J. Sheskin. *Handbook of Parametric and Nonparametric Statistical Procedures*. CRC Press, 5 edition, 2011.

[78] J. F. Shortle, M. J. Fischer, D. Gross, and D. M. B. Masi. Using the transform approximation method to analyze queues with heavy-tailed service. *Journal of Probability and Statistical Science*, 1:15–27, 2003.

[79] J. F. Shortle, P. H. Brill, M. J. Fishcer, D. Gross, and D. M. B. Masi. An algorithm to compute the waiting time distribution for the M/G/1 queue. *INFORMS Journal on Computing*, 16:152–161, 2004.

[80] F. Spitzer. Interaction of markov processes. *Advances in Mathematics*, 5(2), 1970. ISSN 0001-8708.

[81] R. L. Stratonovich. Derivation of the linear and nonlinear non-markov fluctuation-dissipation relations of the first kind for a dynamical model. *Journal of Statistical Physics*, 53:5–18, 1988.

[82] M. Tokuyama and H. Mori. Statistical-mechanical theory of random frequency modulations and generalized brownian motions. *Progress of Theoretical Physics*, 55:411–429, 1976.

[83] R.C. Tolman. *The Principles of Statistical Mechanics*. Oxford University Press, 1938.

[84] G. Tripathy and M. Barma. Driven lattice gases with quenched disorder: Exact results and different macroscopic regimes. *Phys. Rev. E*, 58:1911–1926, Aug 1998.

[85] K. van der Weele, D. van der Meer, M. Versluis, and D. Lohse. Hysteretic clustering in granular gas. *Europhys. Lett.*, 53:328–334, 2001.

[86] J. von Neumann and O. Morgenstern. *Theory of Games and Economic Behavior*. Wiley, 1967.

[87] B. Waclaw and M. R. Evans. Explosive condensation in a mass transport model. *Phys Rev Lett*, 108:070601, 2012.